AD A119297

Research and Development Technical Report
DELET-TR-81-0378-F

AMBIENT TEMPERATURE RECHARGEABLE LITHIUM BATTERY

K. M. Abraham
D. L. Natwig
P. B. Harris
J. W. Avery

EIC Laboratories, Inc.
67 Chapel Street
Newton, MA 02158

August 1982

Final Report for Period 1 March 1981 – 28 February 1982

DTIC
ELECTE
SEP 16 1982
S D
B

Prepared for:
US ARMY ELECTRONICS TECHNOLOGY AND DEVICES LABORATORY

DTIC FILE COPY

ERADCOM

82 00 018

US ARMY ELECTRONICS RESEARCH AND DEVELOPMENT COMMAND
FORT MONMOUTH, NEW JERSEY 07703

NOTICES

Disclaimers

The citation of trade names and names of manufacturers in
this report is not to be construed as official Government
indorsement or approval of commercial products or services
referenced herein.

Disposition

Destroy this report when it is no longer needed. Do not
return it to the originator.

REPORT DOCUMENTATION PAGE		READ INSTRUCTIONS BEFORE COMPLETING FORM
1. REPORT NUMBER DELET-TR-81-0378-F	2. GOVT ACCESSION NO. AD·A119297	3. RECIPIENT'S CATALOG NUMBER
4. TITLE (and Subtitle) AMBIENT TEMPERATURE RECHARGEABLE LITHIUM BATTERY		5. TYPE OF REPORT & PERIOD COVERED FINAL REPORT 3/1/81-2/28/82
		6. PERFORMING ORG. REPORT NUMBER C-655
7. AUTHOR(s) K. M. Abraham, D. L. Natwig, P. B. Harris and J. W. Avery		8. CONTRACT OR GRANT NUMBER(s) DAAK20-81-C-0378
9. PERFORMING ORGANIZATION NAME AND ADDRESS EIC Laboratories, Inc. 67 Chapel Street Newton, Massachusetts 02158		10. PROGRAM ELEMENT, PROJECT, TASK AREA & WORK UNIT NUMBERS 1L162705AH94 11 771
11. CONTROLLING OFFICE NAME AND ADDRESS U.S. Army Electronic Technology & Devices Lab. Attn: DELET-PR Fort Monmouth, New Jersey 07703		12. REPORT DATE August 1982
		13. NUMBER OF PAGES
14. MONITORING AGENCY NAME & ADDRESS(if different from Controlling Office)		15. SECURITY CLASS. (of this report) UNCLASSIFIED
		15a. DECLASSIFICATION/DOWNGRADING SCHEDULE

16. DISTRIBUTION STATEMENT (of this Report)

Approved for Public Release; distribution unlimited.

17. DISTRIBUTION STATEMENT (of the abstract entered in Block 20, if different from Report)

18. SUPPLEMENTARY NOTES

19. KEY WORDS (Continue on reverse side if necessary and identify by block number)

Rechargeable lithium battery, $Cr_{0.5}V_{0.5}S_2$ positive electrode, 2Me-THF/LiAsF$_6$, cell cycling, hermetically sealed 20 Ah cells.

20. ABSTRACT (Continue on reverse side if necessary and identify by block number)

$Cr_{0.5}V_{0.5}S_2$ has been characterized as a useful positive electrode material for rechargeable Li cells. The positive electrode reaction involves intercalation of Li during discharge and deintercalation of Li during recharge. A discharge capacity equivalent to nearly $1e^-/Cr_{0.5}V_{0.5}S_2$ has been obtained in early cycles at low rates. The average capacity which could be realized in long-term cycling appears to be $0.7-0.8 e^-/Cr_{0.5}V_{0.5}S_2$. Laboratory cells exceeded 200 deep discharge cycles.

DD $_{1\ JAN\ 73}^{FORM}$ 1473   EDITION OF 1 NOV 65 IS OBSOLETE

Abstract (continued)

Although $Cr_{0.5}V_{0.5}S_2$ and its Li intercalates are good electronic conductors, optimum rate and rechargeability were found in electrodes with 15-20 weight percent carbon. Because of this relatively large amount of carbon, the volumetric energy density achieved in cells has been significantly lower than what was anticipated at the outset of the program. It now appears that for the ERADCOM battery, $Cr_{0.5}V_{0.5}S_2$ may not offer any particular advantage over TiS_2. However, $Cr_{0.5}V_{0.5}S_2$ provides higher cell voltages. The mid-discharge voltage of $Li/Cr_{0.5}V_{0.5}S_2$ cells is 2.3V; while that of Li/TiS_2 cells is 2.1V.

The major objective of the program, development of a technology base for the construction of large rechargeable Li cells, has been accomplished. Cells with theoretical capacities of 10 and 20 Ah have been constructed and tested. In limited cycle tests, these large cells performed as well as laboratory test cells.

Preliminary work carried out in this program indicated that the low temperature performance of $2Me-THF/LiAsF_6$(1.4M) could be improved by blending this solution with ethers such as THF. A useful solution appears to be 50:50 $THF:2Me-THF/LiAsF_6$(1.5M). However, further work is needed to fully explore the practical potential of this new area of study.

TABLE OF CONTENTS

TABLE OF CONTENTS
(continued)

LIST OF ILLUSTRATIONS

LIST OF ILLUSTRATIONS
(continued)

LIST OF ILLUSTRATIONS
(continued)

LIST OF TABLES

1.0 INTRODUCTION

Recent advances (1-3) in ambient temperature rechargeable Li cell technology have made it possible to consider potential applications for these cells. Some of the recent noteworthy developments include: identification of desirable electrolyte systems such as 2Me-THF/LiAsF$_6$ (4), demonstration of high Li electrode rechargeability in 2Me-THF/LiAsF$_6$ with typical cycling efficiencies of 96-97.5% at Li charge densities of 7-10 mAh/cm^2 (5,6), and construction and testing of Li/TiS$_2$, Li/V$_6$O$_{13}$ and Li/MoS$_3$ cells with capacities of 0.65 to 20 Ah (5-8).

The present study has been directed toward the development of a rechargeable Li battery for military use. The required specifications of this battery are:

Voltage	–	24V average, 20V cutoff
Capacity	–	15 Ah
Weight energy density	–	70 Wh/kg
Volume energy density	–	0.19 Wh/cm^3
Power density	–	25 W/kg
Operating temperature	–	-40 to +160°F
Cycle life	–	1000 cycles target at 60% of DOD.

The approach has been to initiate development of a battery based on existing technology. However, some of the specifications of the battery, particularly its cycle life and low temperature performance, could not be adequately met by existing technology. Therefore, a parallel effort involved development of electrolytes with improved performance characteristics.

The present electrolyte of choice is 2Me-THF/LiAsF$_6$. Among the numerous potentially useful positive electrodes, only TiS$_2$ (6,7) and V$_6$O$_{13}$ (5) have received any significant development effort. The energy densities achieved in 5-6 Ah, prismatic Li/TiS$_2$ and Li/V$_6$O$_{13}$ cells (based on limited number of cycles) are given in Table 1. The required volumetric energy density of the battery under consideration can more or less be achieved in the Li/TiS$_2$ system. The weight energy density required by the battery can be achieved in both the Li/TiS$_2$ and Li/V$_6$O$_{13}$ systems.

An interesting positive electrode material worthy of consideration, but which has received only limited attention so far, is Cr$_{0.5}$V$_{0.5}$S$_2$ (9). This material apparently has structure and properties similar to those of TiS$_2$. Based on limited results with 0.5 Ah cells (9), Cr$_{0.5}$V$_{0.5}$S$_2$ is potentially capable of outperforming TiS$_2$ by 10-20% in both volumetric and grav-

Table 1

Energy Densities Achieved in 5-6 Ah Prismatic Cells

Cell Type	OCV	MDV	Cell Capacity Ah	Gravimetric Energy Density[a], Whr/kg	Volumetric Energy Density, Whr/cm^3
Li/TiS$_2$ (First discharge)	2.45	2.1	6.0	105 (194)	0.197
Li/TiS$_2$ (Tenth discharge)	-	2.1	5.2	90 (168)	0.170
Li/V$_6$O$_{13}$ (NS) First discharge	2.80	2.3	5.04	102 (193)	0.181
Li/V$_6$O$_{13}$ (NS) Tenth discharge	-	2.3	3.66	73 (140)	0.131
Li/V$_6$O$_{13}$ (S)	2.80	2.4	3.0	60 (120)	0.112

[a]The higher values in parenthesis have been obtained by excluding the weight of can and cover.

2

imetric energy densities at low to medium rate (10-20 hr rate) discharges. This significant difference results from its higher cell voltage; an OCV of ~2.7V and a mid-discharge voltage of ~2.4V at the 10-20 hr rate. However, cells with this material had not been optimized with respect to rate or rechargeability.

In this report we present the results of a one man-year study of the Li/2Me-THF, $LiAsF_6/Cr_{0.5}V_{0.5}S_2$ system. The various aspects of the study have been: synthesis and characterization of $Cr_{0.5}V_{0.5}S_2$; optimization of practical cathodes with respect to rate and rechargeability; improvement of low temperature performance of the cells; and construction and testing of large, 10 and 20 Ah theoretical capacity, flat plate cells.

2.0   SYNTHESIS AND CHARACTERIZATION OF $Cr_{0.5}V_{0.5}S_2$

The synthesis of $Cr_{0.5}V_{0.5}S_2$ was accomplished according to the reactions depicted in equations 1 and 2.

$$Li_2CO_3 + 0.5Cr_2O_3 + 0.5V_2O_5 \xrightarrow[700^{\circ}C]{H_2S} 2LiCr_{0.5}V_{0.5}S_2 + \quad\quad (1)$$
$$\text{(volatile products)}*$$

$$2LiCr_{0.5}V_{0.5}S_2 + I_2 \xrightarrow{CH_3CN} Cr_{0.5}V_{0.5}S_2 + 2LiI \quad\quad (2)$$
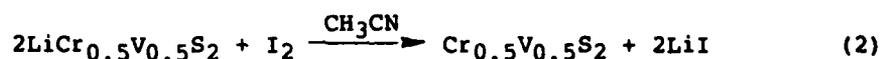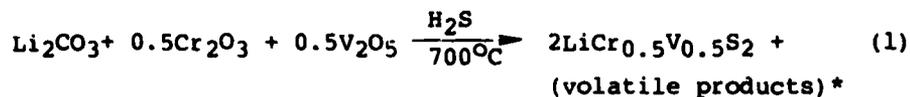
It was characterized by X-ray, SEM and conductivity data.

2.1   Synthesis of $Cr_{0.5}V_{0.5}S_2$

In a preparation, a well ground mixture consisting of 9.5g (0.052 mole) V_2O_5, 7.9g (0.052 mole) Cr_2O_3 and 7.7g (0.104 mole) Li_2CO_3 was placed in a graphite boat which in turn was introduced into a quartz tube. While maintaining a H_2S flow (~25 cc/min) over the oxide mixture, the quartz tube was heated at $700^{\circ}C$ for ~16 hr. The air sensitive $LiCr_{0.5}V_{0.5}S_2$ was obtained as a black powder. The material was delithiated by treatment with an excess of $0.4N$ I_2/CH_3CN solution for 24 hrs. The delithiated product was washed several times with CH_3CN and dried in vacuum initially at $25^{\circ}C$ and then at $160^{\circ}C$.

2.2   X-Ray Analysis of $Cr_{0.5}V_{0.5}S_2$ and $Li_xCr_{0.5}V_{0.5}S_2$

The Debye-Sherrer X-ray diffraction patterns of the relevant materials are given in Tables 2 and 3.

The X-ray data of $Cr_{0.5}V_{0.5}S_2$ are consistent with a layered 1T CdI_2-type structure with $a_o = 3.2$ Å and $C_o = 5.71$ Å. The lithiated products, prepared either by the high temperature reaction according to equation 1 or electrochemically in Li cells, both exhibit X-ray patterns indicative of Li intercalates.

Practically all the Li in $LiCr_{0.5}V_{0.5}S_2$ can be removed either by treatment with a CH_3CN/I_2 solution or by electrochemical oxidation to 3V versus Li^+/Li (vide infra). The cathode reactions involve intercalation-deintercalation processes as depicted in equation 3.

$$Cr_{0.5}V_{0.5}S_2 + Li^+ + e^- \underset{\text{charge}}{\overset{\text{discharge}}{\rightleftharpoons}} LiCr_{0.5}V_{0.5}S_2 \quad\quad (3)$$

---
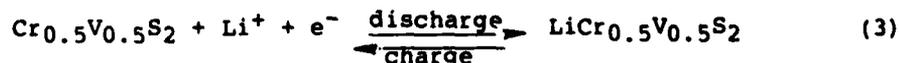
*The volatile products have not been characterized; hence the unbalanced equation. However, the stoichiometric reaction may be, $Li_2CO_3 + 0.5Cr_2O_3 + 0.5V_2O_5 + 5H_2S \rightarrow 2LiCr_{0.5}V_{0.5}S_2 + CO_2 + 5H_2O + S$.

Table 2

Debye-Sherrer X-Ray Pattern of $Cr_{0.5}V_{0.5}S_2$

$d_{(obs)}$, Å	(obs)	hkl
5.71	70	001
2.49	100	101
1.99	90	102
1.58	30	110
1.35	20	201
1.26	20	202
1.12	10	203

A_O = 3.2 Å; C_O = 5.71 Å.

Table 3

X-Ray Diffraction Data for $Li_xCr_{0.5}V_{0.5}S_2$

$LiCr_{0.5}V_{0.5}S_2$ [1]			$Li_{0.77}Cr_{0.5}V_{0.5}S_2$ [2]		
d, Å	I (obs)	hkl	d, Å	I (obs)	hkl
6.06	100	001	6.04	90	001
2.98	10	100	2.98	8	100
2.65	80	101	2.65	100	101
2.11	70	102	2.13	90	102
2.06	5	−	1.73	40	110
1.79	5	−	1.67	40	103
1.73	50	110	1.45	5	201
1.67	50	111	1.34	5	202
			1.20	5	203
			1.14	10	--

[1] The high temperature material.
[2] An electrochemically prepared sample.

Fig. 1.   The SEM of $LiCr_{0.5}V_{0.5}V_2$.   Magnification 10,000X.
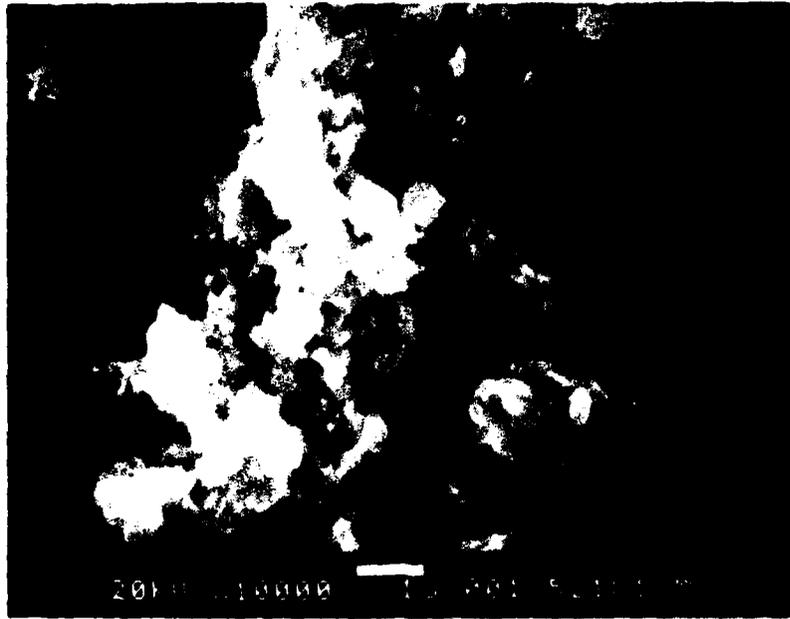
Fig. 2. The SEM of $Cr_{0.5}V_{0.5}S_2$. Magnification 10,000X.

8

2.3 SEM Analysis

Scanning electron micrographs of $LiCr_{0.5}V_{0.5}S_2$ (prepared as in equation 1) and $Cr_{0.5}V_{0.5}S_2$ are shown in Figures 1 and 2. The $LiCr_{0.5}V_{0.5}S_2$ is composed of relatively large and somewhat porous particles which upon delithiation with CH_3CN/I_2 is converted to the very small crystals of $Cr_{0.5}V_{0.5}S_2$. The latter appears to have an average particle size of 1-2 μm.

2.4 Electronic Conductivity of $Cr_{0.5}V_{0.5}S_2$ and $Li_xCr_{0.5}V_{0.5}S_2$

We have determined the electronic conductivities of $Cr_{0.5}V_{0.5}S_2$ and $Li_xCr_{0.5}V_{0.5}S_2$, where x = 1 and 0.77, and their various mixtures with C (Shawinigan 50% compressed) and/or Teflon by a four-point-probe method. The samples were fabricated into pressed pellets of 3.2 mm diameter and 1-1.5 mm thickness by pressing the material in a stainless steel die at a pressure of ~900,000 psi. The resistivities were obtained from the slope of least-square fitted current-potential curves of the type shown in Figure 3, after applying a correction factor for the thickness of the pellet. The data for the various samples are given in Table 4. The conductivity of $Cr_{0.5}V_{0.5}S_2$ is 10.64 $(ohm\ cm)^{-1}$, showing that the material is a good electronic conductor. This conductivity is of the same order as that found in TiS_2. The conductivity of the sample containing 10 w/o Teflon is slightly lower, i.e., 7.5 $(ohm\ cm)^{-1}$. Furthermore, the conductivities of samples with increasing amounts of carbon decrease slightly and reach a minimum in the sample containing 70 w/o $Cr_{0.5}V_{0.5}S_2$, 20 w/o C and 10 w/o T (Fig. 4). This latter effect is probably due to increasing pellet porosities and/or creation of more grain boundaries with increasing amounts of carbon.

The conductivity data seem to indicate that the $Cr_{0.5}V_{0.5}S_2$ cathode, in principle, should exhibit acceptable electrochemical behavior without conductivity enhancing additives. However, the data presented later in this report would show that about 15-20 w/o carbon in the cathode matrix is required for optimum rate and rechargeability characteristics.
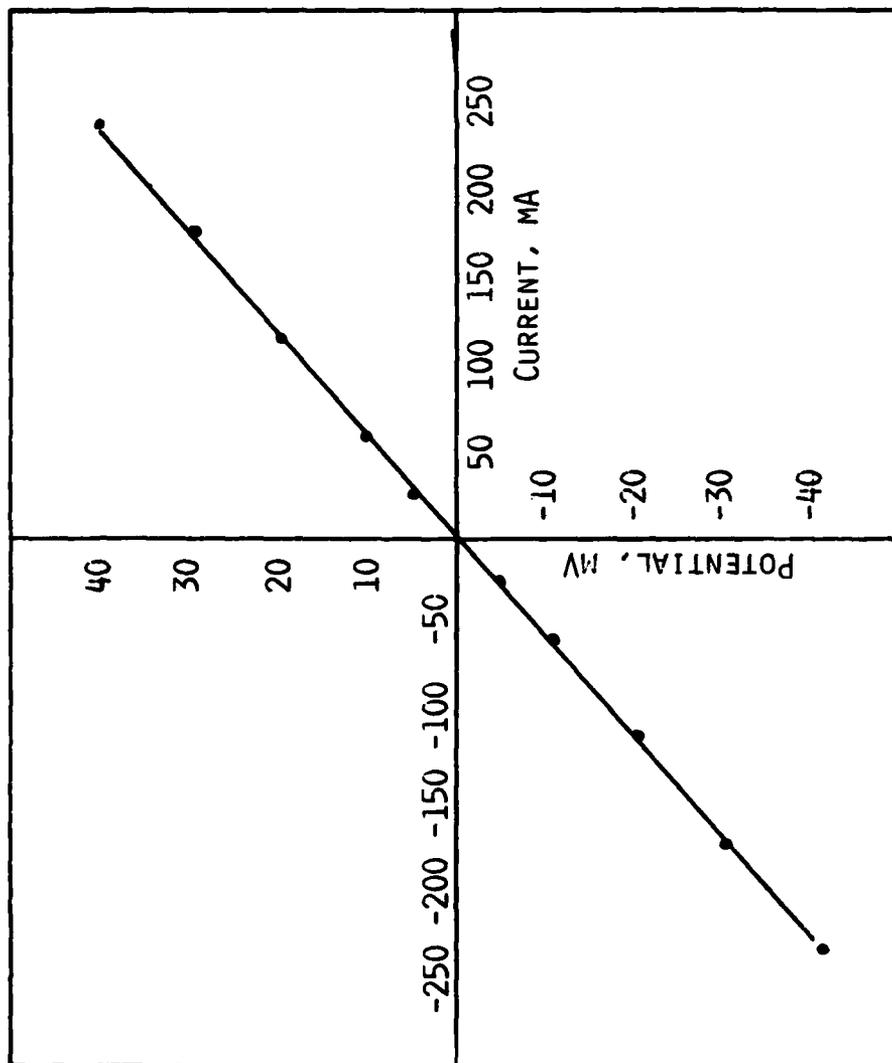
Fig. 3. Least squares plot of current-potential for the $Cr_{0.5}V_{0.5}S_2$ pellet.

Table 4

Electronic Conductivity Data

Sample	Resistivity (ohm-cm)	Specific Conductivity (ohm-cm)$^{-1}$
$Cr_{0.5}V_{0.5}S_2$ (CVS)	0.094	10.64
90 w/o CVS, 10 w/o Teflon (T)	0.134	7.46
80 w/o CVS, 10 w/o C, 10 w/o T	0.291	3.44
70 w/o CVS, 20 w/o C, 10 w/o T	0.357	2.80
60 w/o CVS, 30 w/o C, 10 w/o T	0.338	2.96
$LiCr_{0.5}V_{0.5}S_2$ (LCVS)	0.175	5.71
90 w/o LCVS, 10 w/o T	0.262	3.82
80 w/o LCVS, 10 w/o C, 10 w/o T	0.340	2.94
70 w/o LCVS, 20 w/o C, 10 w/o T	0.397	2.52
90 w/o $Li_{0.77}Cr_{0.5}V_{0.5}S_2$, 10 w/o T*	0.642	1.56
70 w/o CVS, 10 w/o TiS_2, 10 w/o C, 10 w/o T	0.111	9.01

*Electrode from a cell after the first discharge to 1.6V.
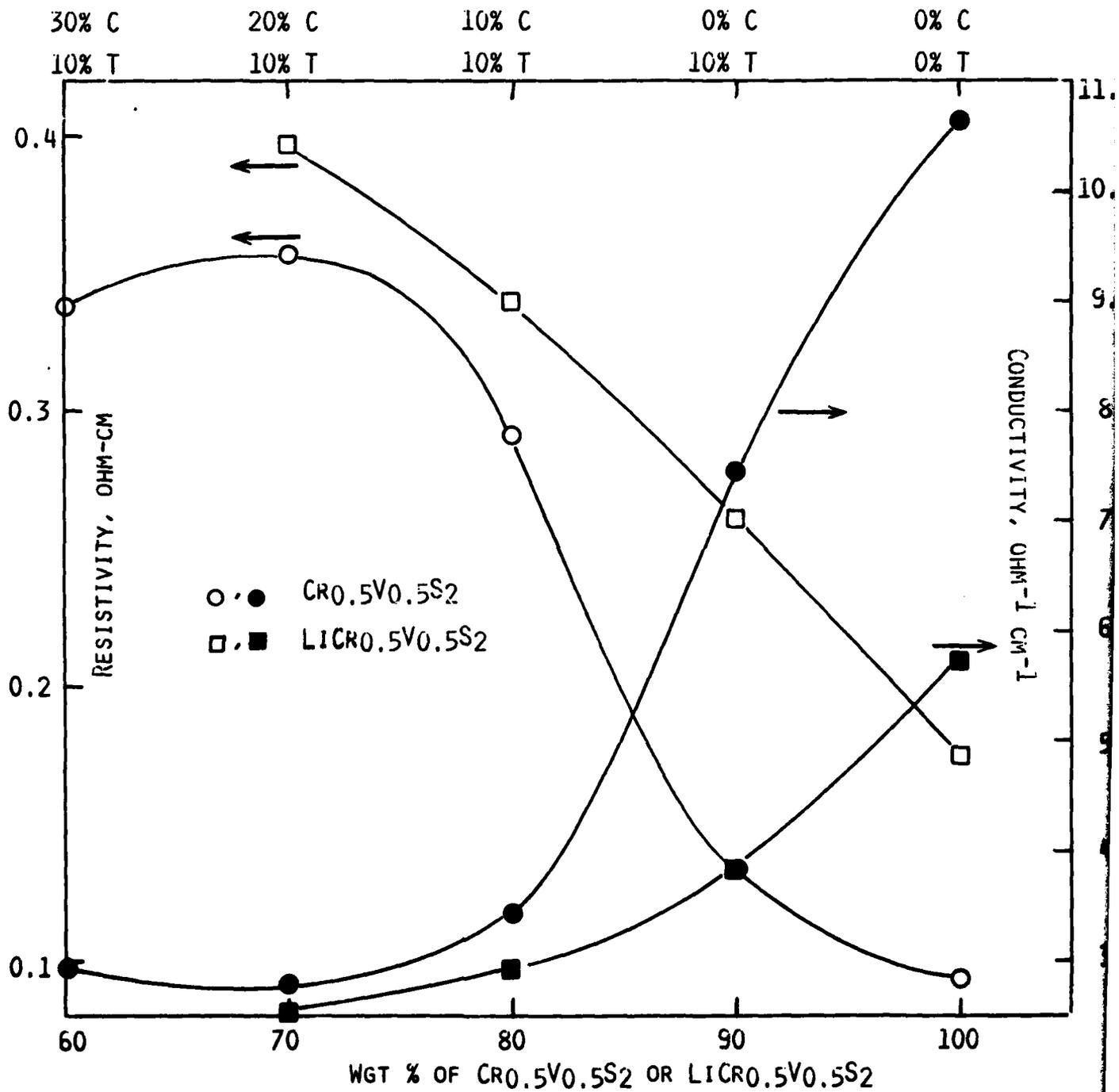
Fig. 4. Resistivity vs. weight-percent of $Cr_{0.5}V_{0.5}S_2$ or $LiCr_{0.5}V_{0.5}S_2$ for pressed pellets.

12

3.0 Li/$Cr_{0.5}V_{0.5}S_2$ CELL STUDIES

The cathodic behavior, including rate, rechargeability and low temperature performance, of $Cr_{0.5}V_{0.5}S_2$ was evaluated in cells of the type,

$$Li/Organic\ electrolyte/Cr_{0.5}V_{0.5}S_2,\ C$$

Typically, the electrolyte was 2-methyl-tetrahydrofuran (2Me-THF)/LiAsF$_6$(1.4M). However, because of the limited low temperature capability of 2Me-THF/LiAsF$_6$ (1.4M) (6), potentially useful alternatives with *improved low temperature* capabilities have been explored. Cells with two such electrolyte systems are discussed later in this report.

3.1 General Experimental

3.1.1 Preparation of Electrolyte

2-methyl tetrahydrofuran, obtained from Aldrich Chemical Company, was distilled over CaH_2 on a spinning band fractionating column (Perkin-Elmer 251) in an Argon atmosphere at a 5:1 reflux ratio. The middle 70% fraction was collected. A 1.4M LiAsF$_6$ electrolyte was prepared by adding an appropriate amount of LiAsF$_6$ (U.S. Steel Agri-Chemicals, electrochemical grade) to cooled ($<0^{\circ}$C) 2Me-THF. The cooling is necessary to minimize possible decomposition (5). The electrolyte was further purified by the APA procedure (4). Typically, the electrolyte prepared in this manner exhibited thin plate (1 coul/cm^2) Li cycling efficiencies of 95-96%.

3.1.2 Cathode Preparation

Cathodes were prepared as pressed powder electrodes. An intimate mixture of $Cr_{0.5}V_{0.5}S_2$, carbon (Shawinigan, 50% compressed) and 10 w/o Teflon was prepared in a blender. The ratio of the disulfide to carbon was varied in the optimization studies. The optimized cathodes contained 15-20 w/o carbon and 10 w/o Teflon. The mixture was pressed on either side of an expanded Ni screen (Exmet Corporation, 5Ni 7-4/0) at a pressure of ~2000 lbs/in^2. The electrodes typically had a thickness of 1-1.25 mm.

3.1.3 Test Cells

Most of the experiments were carried out in a laboratory test cell, packaged in soft-sealed D-size cell cans. In these cells, the electrode package comprised one cathode flanked on either side by a Li electrode. The cathode was wrapped in two layers of Celgard-2400 (Celanese Corporation) polypropylene separators and the separator was heat-sealed on the periphery

of the electrode to form a bag. The Li electrode was fabricated usually from a 15 mil thick Li foil obtained from Foote Mineral Company and pressing the foil on one side of an expanded Ni screen. Each electrode had an area of 9.4 cm^2 (2.5 x 3.75 cm) per side. The total cathode area per cell was ~19 cm^2. A polyethylene disk 1.250" dia x 0.005" thick, is placed at the bottom of the Ni plated cold rolled can for electrical insulation. The electrode package is sandwiched between two Teflon hemi-cylinders and this assembly is inserted into the can with both electrode leads projecting upward. A stainless steel shim is wedged between one hemi-cylinder and the inside wall of the can such that maximum compression is applied to the electrode pack by the spring action of the shim. The electrode leads are then spot welded to the tab connections on the cover assembly. The cell was completed with an appropriate amount of 2Me-THF/LiAsF$_6$ (1.3-1.5M). The cell was sealed by means of an O-ring between the cover and the lip of the can. Electrical leads were taken through a Conax-fitting on the cover assembly. A schematic of the assembled cell is shown in Figure 5.

In some cases, the cells were hermetically sealed. Electrolyte filling of such cells was achieved through the glass-metal sealed fill-tube on the cover assembly by vacuum techniques.

We have also built 10 and 20 Ah theoretical capacity cells. Details of these cells are given in Section 4.

3.2 Cathodic Behavior of $Cr_{0.5}V_{0.5}S_2$

Initial studies of the discharge and cycling behavior of $Cr_{0.5}V_{0.5}S_2$ were carried out with cathodes of the composition 80 w/o $Cr_{0.5}V_{0.5}S_2$, 10 w/o (Shawinigan) C and 10 w/o Teflon. This cathode composition was arbitrarily chosen. The specifications of the cell employed in these studies are given in Table 5.

3.2.1 Low Rate Galvanostatic Cycling of $Li/Cr_{0.5}V_{0.5}S_2$ Cells

Typical cycles of Cell No. TB-5-CVS obtained at 0.5 mA/cm^2 are shown in Figure 6. The voltage limits are 1.6V for discharge and 3.0V for charge. The discharge and charge show gradually sloping potential profiles. There are no breaks in the discharge/charge curves indicative of more than one $Li_xCr_{0.5}V_{0.5}S_2$ ternary phase. The first discharge corresponds to a cathode utilization of 0.8 $Li/Cr_{0.5}V_{0.5}S_2$. The recharge to 3.0V is 100% efficient. There are no significant changes in the cathode utilization in the first five cycles, performed at 0.5 mA/cm^2. The cathode utilization and cycling behavior, especially at higher current densities, depend on the amount of carbon in the cathode maxtrix (see later).
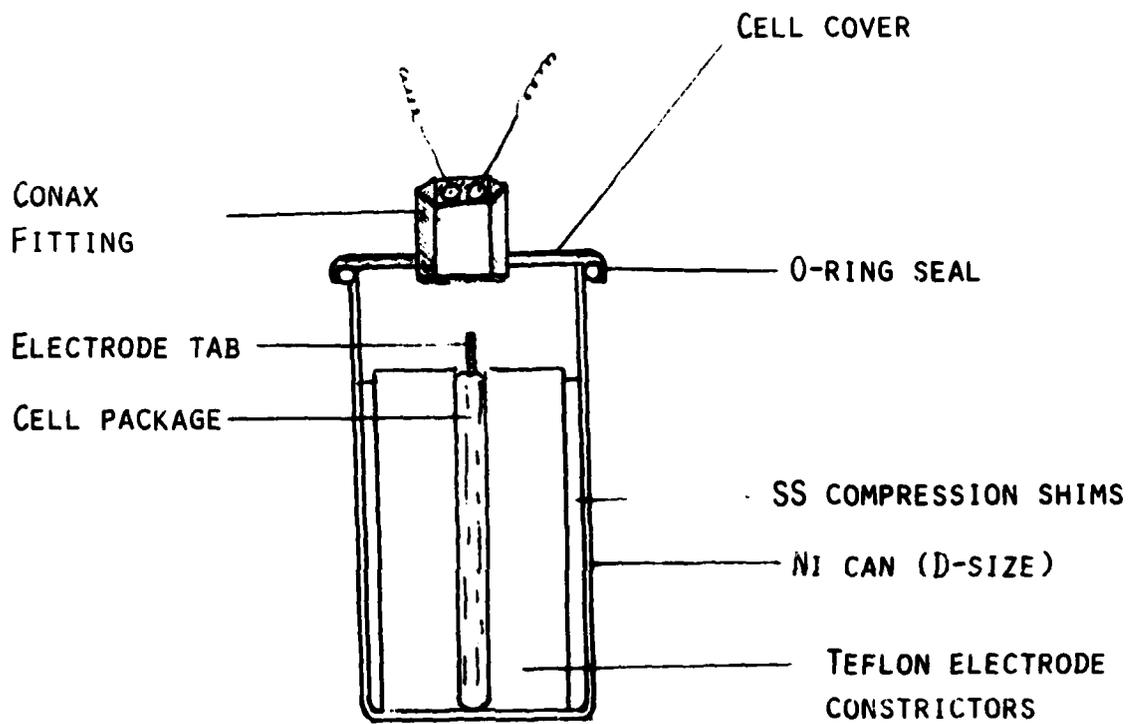
Fig. 5. Schematic representation of soft-sealed laboratory test cell.

Table 5

Specifications of Li/$Cr_{0.5}V_{0.5}S_2$ Cells

Cell No.	Electrolyte 2Me-THF/1.3M $LiAsF_6$ (ml)	Cathode[1]		Anode		Celgard 2400 Separator Thickness (mm)	Cell Package	
		1e⁻ Capacity (mAh)	Thickness (mm)	Capacity (mAh)	Thickness[2] (mm)		Thickness (mm)	Volume (cc)
TB-4-CVS	8.5	260	1.168	2 x 828	2 x .432	2 x (2 x .0254)	2.134	1.985
TB-5-CVS	8.5	241	1.168	2 x 828	2 x .432	2 x (2 x .0254)	2.134	1.985

[1] The cathode area is 9.4 cm²/side.
[2] Measured after pressing the Li onto the Exmet Ni screen.

16
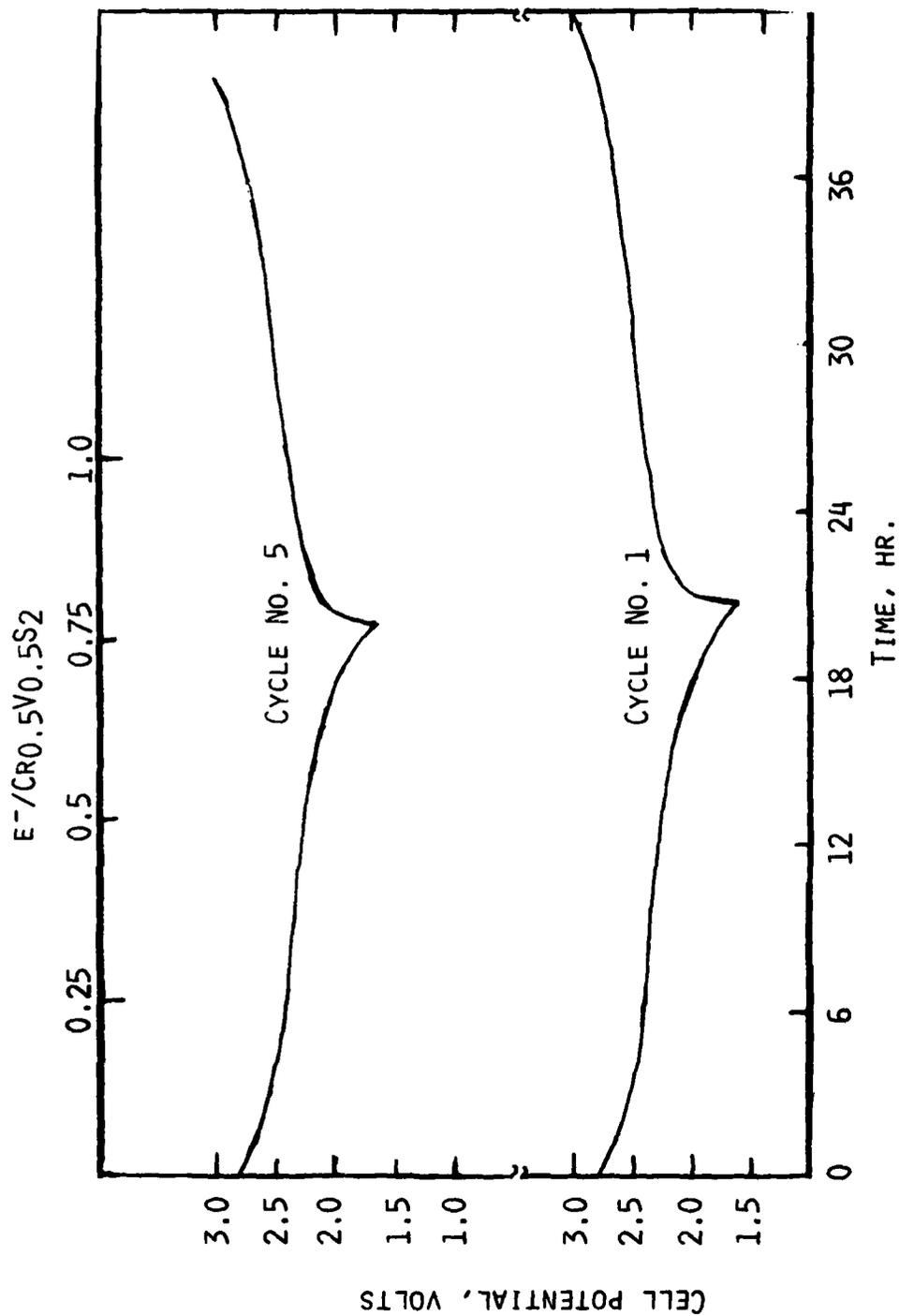
Fig. 6. Typical cycles of a Li/Cr$_{0.5}$V$_{0.5}$S$_2$ cell with 2Me-THF/LiAsF$_6$(1.3M) at 0.5 mA/cm^2. Voltage limits: 1.6-3.1V. Cathode composition: 80 w/o Cr$_{0.5}$V$_{0.5}$S$_2$, 10 w/o C, 10 w/o Teflon.

17

3.2.2 Rate/Capacity Behavior

Preliminary studies of the rate/capacity behavior of $Cr_{0.5}V_{0.5}S_2$ was evaluated potentiostatically with Cell No. TB-4-CVS. The potential for discharge was 1.8V and for charge 3.0V. The potentiostatic cycling data are shown in Figure 7, plotted as capacity versus current density. The data show that capacities greater than 0.5 Li per $Cr_{0.5}V_{0.5}S_2$ are possible at current densities <4 mA/cm^2. However, there is a noticeable difference in the rates of discharge and recharge. The recharge rate capability apparently is lower than that of the discharge.

The cathode utilizations (Fig. 8) achieved galvanostatically in the two cells in Table 5 at current densities between 0.25 and 2.0 mA/cm^2 are in agreement with the potentiostatic data. However, the data presented later will show that the utilizations which can be achieved at current densities >2 mA/cm^2 depend upon the amount of carbon in the cathode.

3.3 Cathode Optimization Studies

Cells were built with cathodes containing various amounts of carbon. The specifications of these cells are given in Table 6. Two cells were built also with 10 and 30 weight-percent of TiS_2. The latter was done on the basis of a recent report from Exxon Corporation (10) showing improved rate capabilities for low rate intercalation cathodes such as MoS_3 in the presence of small quantities of TiS_2.

The capacities obtained as a function of current density for each cathode composition were used as the criterion for selecting the optimum cathode composition for further studies.

3.3.1 Room Temperature Rate-Capacity Behavior of Li/$Cr_{0.5}V_{0.5}S_2$ Cells Versus Cathode Composition

Room temperature discharge capacities of each cell were evaluated at current densities between 0.5 and 4 mA/cm^2. The data were obtained by discharging the cell successively at the current densities of 0.5, 1, 2, 3 and 4 mA/cm^2 with each discharge followed by a charge at 0.5 mA/cm^2. All cells utilized 2Me-THF/1.3M LiAsF$_6$. There were two wraps of the separator between each electrode. The effects of electrolyte conductivity and separator thickness on rate/capacity behavior are discussed in the next section.

Plots of capacity versus current density for the various cells are given in Figure 9. The related discharge curves for cells TB-8-CVS through TB-12-CVS are given in Figures 10 to 14.

Fig. 7. Cathode utilization vs current density data obtained from potentiostatic cycling of Cell No. TB-4-CVS.
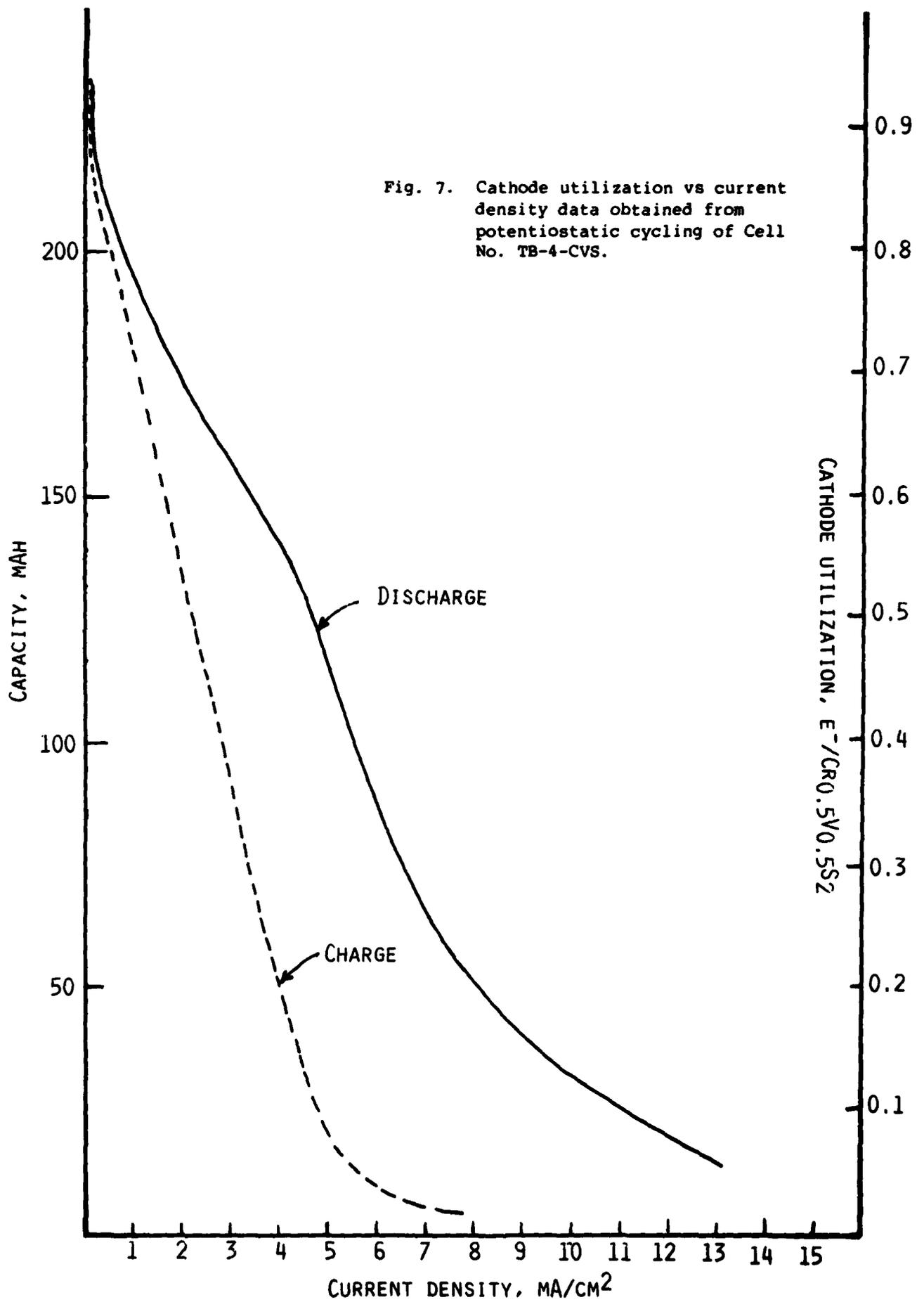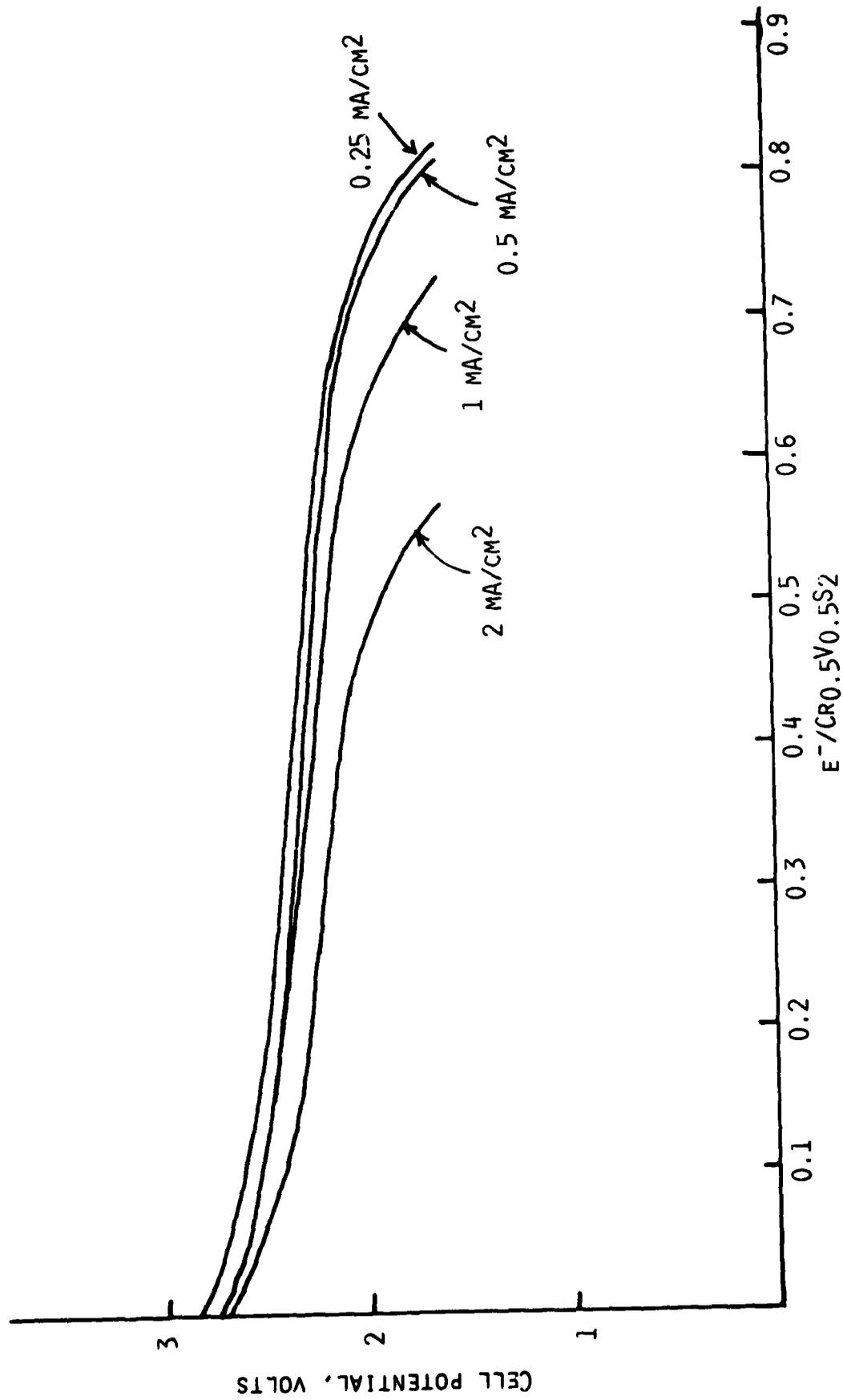
Fig. 8. Galvanostatic discharges of Li/Cr$_{0.5}$V$_{0.5}$S$_2$ cells at various current densities obtained from Cells TB-4-CVS and TB-5-CVS.

Table 6

Specifications of Li/Cr$_{0.5}$V$_{0.5}$S$_2$ Cells

Cell No.	Electrolyte 2Me-THF/1.3M LiAsF$_6$ (ml)	Cathode Composition[1]	Cathode 1e$^-$ Capacity (mAh)	Cathode Thick. (mm)	Anode Capacity (mAh)	Anode Thickness (mm)	Celgard 2400 Separator Thick. (mm)	Cell Package Thick. (mm)	Cell Package Volume (cc)	OCV (V)
TB-7-CVS	9.5	90 w/o CVS 10 w/o T	280	1.168	2 x 828	2 x .432	2 x (2 x .0254)	2.134	1.985	2.930
TB-8-CVS	9.5	80 w/o CVS 10 w/o C 10 w/o T	248	1.295	2 x 828	2 x .432	2 x (2 x .0254)	2.261	2.103	2.959
TB-9-CVS	9.5	70 w/o CVS 20 w/o C 10 w/o T	230	1.371	2 x 828	2 x .432	2 x (2 x .0254)	2.337	2.174	2.962
TB-10-CVS	9.5	60 w/o CVS 30 w/o C 10 w/o T	179	1.574	2 x 828	2 x .432	2 x (2 x .0254)	2.540	2.363	2.970
TB-11-CVS	9.5	50 w/o CVS 30 w/o TiS$_2$ 10 w/o C 10 w/o T	267 (165 CVS + 102 TiS$_2$)	1.371	2 x 828	2 x .432	2 x (2 x .0254)	2.337	2.174	3.012
TB-12-CVS	9.5	70 w/o CVS 10 w/o TiS$_2$ 10 w/o C 10 w/o T	276 (240 CVS + 36 TiS$_2$)	1.218	2 x 828	2 x .432	2 x (2 x .0254)	2.184	2.032	2.987

[1]where CVS = Cr$_{0.5}$V$_{0.5}$S$_2$, C = Shawinigan carbon, T = Teflon.
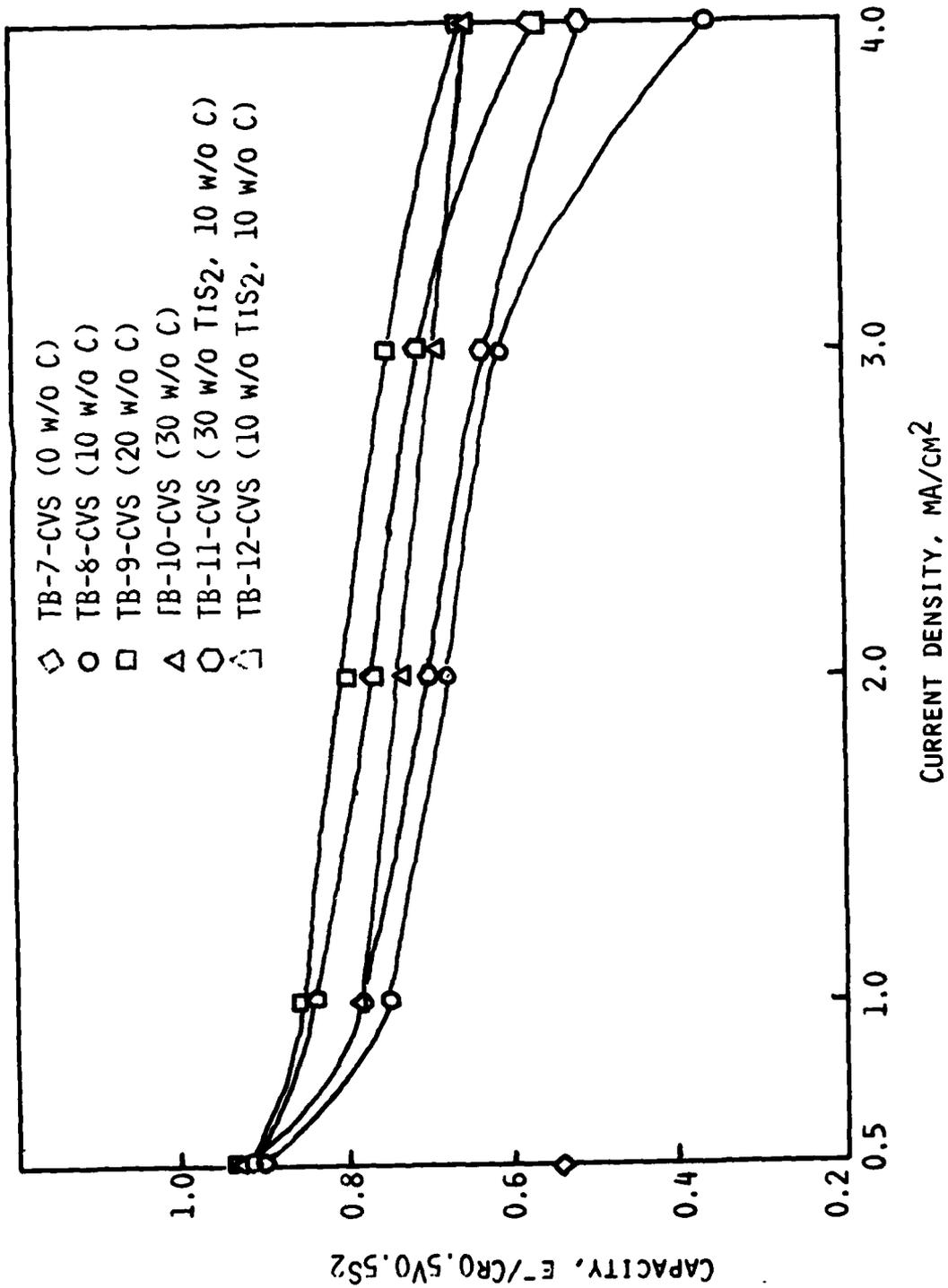
Fig. 9. Capacity versus current density for Li/Cr$_{0.5}$V$_{0.5}$S$_2$ cells.
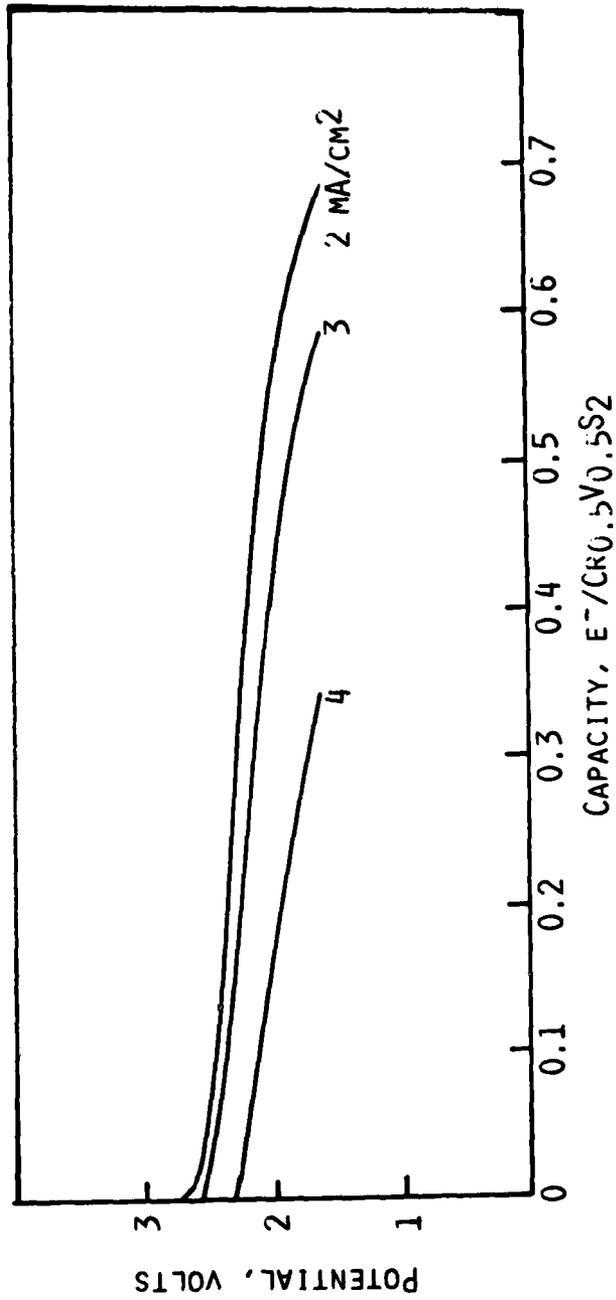
Fig. 10. Discharge curves of Cell TB-8-CVS at various current densities.
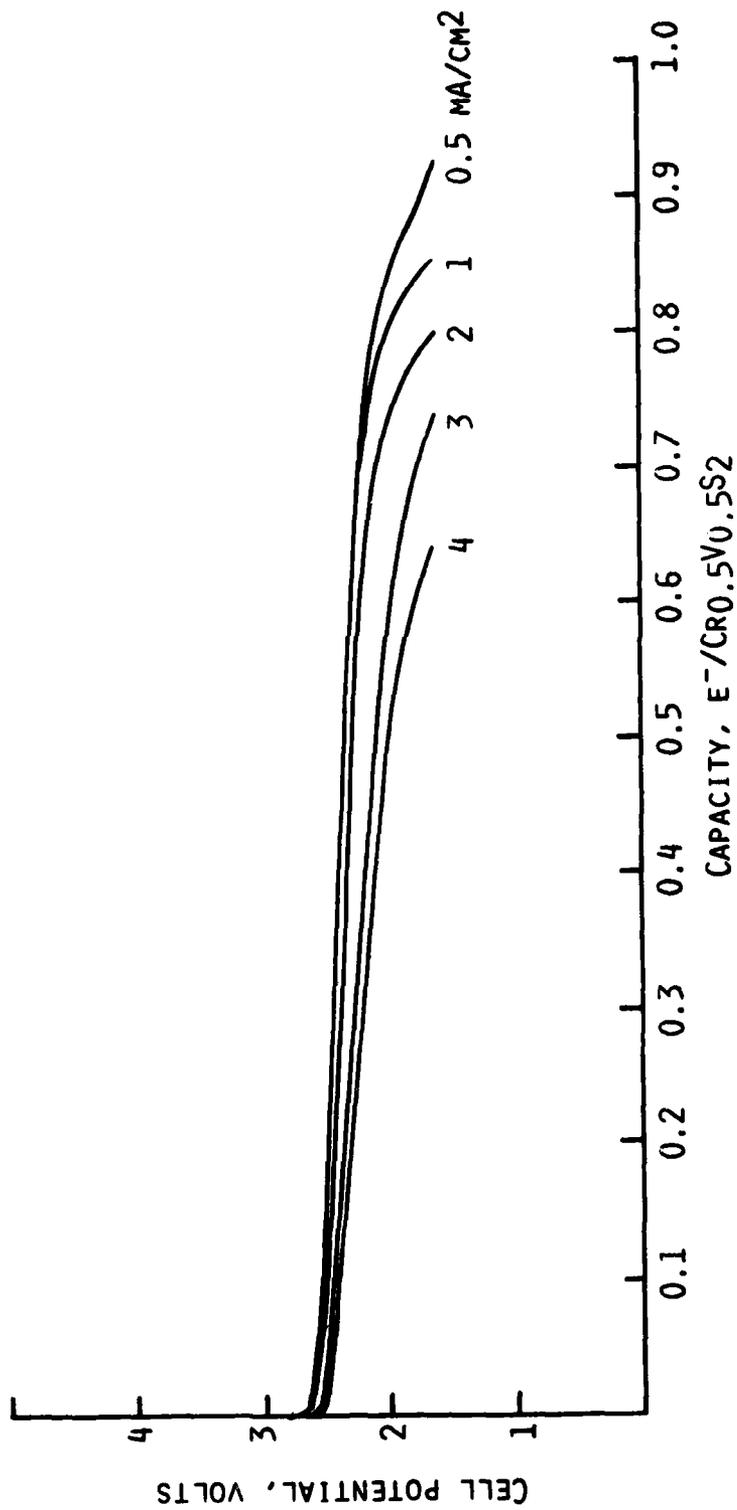
Fig. 11. Discharge curves of Cell TB-9-CVS at various current densities.
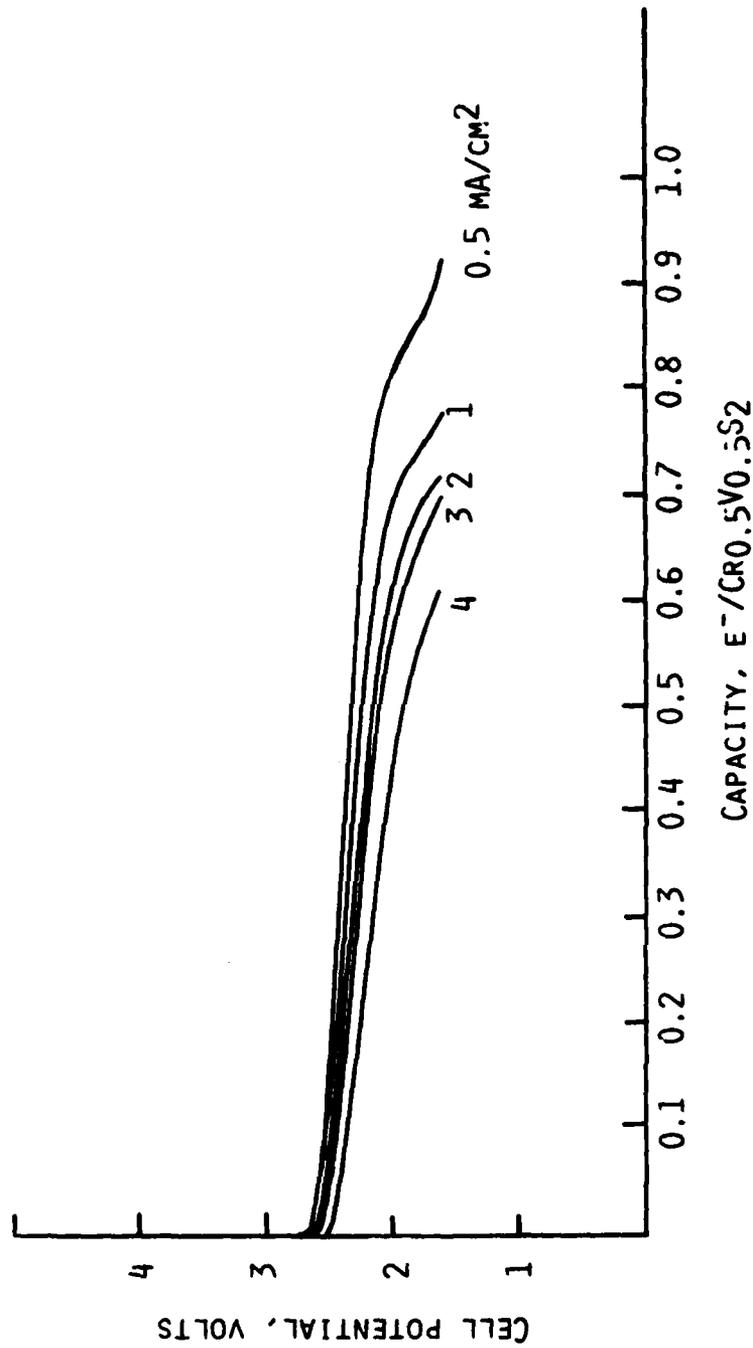
Fig. 12. Discharge curves of Cell TB-10-CVS at various current densities.

CAPACITY, E⁻/CR0.5V0.5S2

0.5 MA/CM²

CELL POTENTIAL, VOLTS
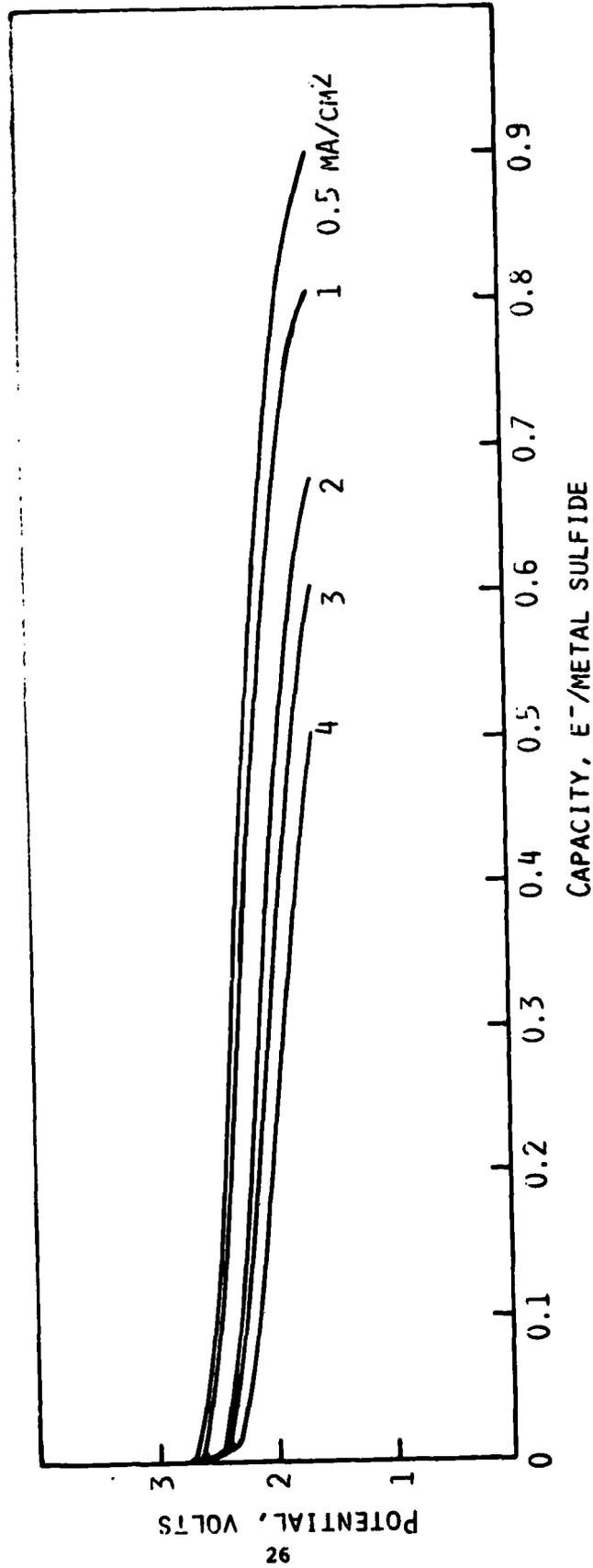
Fig. 13. Discharge curves for Cell TB-11-CVS at various current densities.
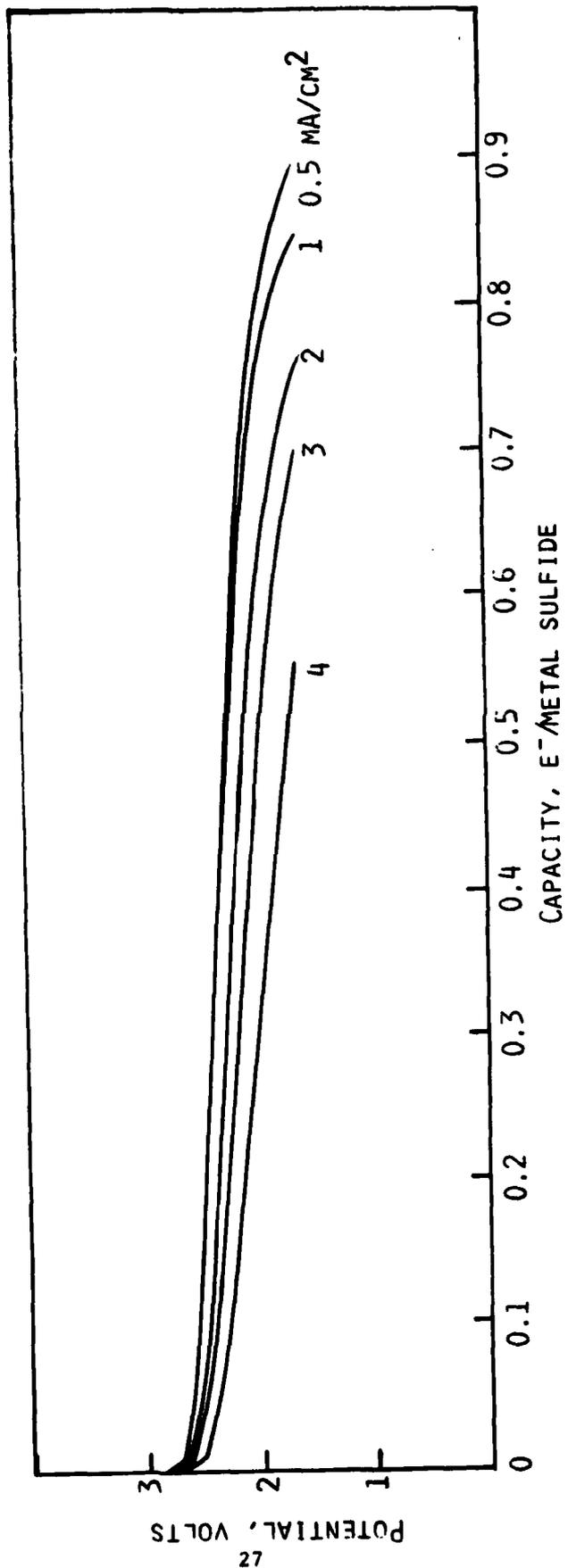
Fig. 14. Discharge curves of Cell TB-12-CVS at various current densities.

There is a remarkable effect of carbon content on $Cr_{0.5}V_{0.5}S_2$ utilization. In Cell TB-7-CVS without any carbon in the electrode matrix, a utilization equivalent to only 0.6 $Li/Cr_{0.5}V_{0.5}S_2$ has been obtained at 0.5 mA/cm^2. Moreover, at higher current densities, capacities in this cell were practically non-existent.

Cathode utilizations, especially at higher current densities, increase with increasing amounts of carbon. However, an amount equivalent to 20 w/o appears to be the optimum required. The highest utilization at all the four current densities has been found in the cell with 20 w/o carbon.

The cells with TiS_2, although they contained only 10 w/o C, have performed better than the one with 10 w/o C alone. However, at 4 mA/cm^2, the performance of the cells with TiS_2 is somewhat inferior to that of the cell with 20 w/o carbon. In addition, extended cycling studies (see later) showed that cells with 10 w/o TiS_2 do not perform as well as those with 20 w/o carbon.

The electronic conductivity data presented earlier show that $Cr_{0.5}V_{0.5}S_2$ is sufficiently conductive to perform well without a conductive additive such as carbon in the cathode. Furthermore, $LiCr_{0.5}V_{0.5}S_2$ and $Li_{0.77}Cr_{0.5}V_{0.5}S_2$ are nearly as conducting as $Cr_{0.5}V_{0.5}S_2$. Actually, electrodes with 20 w/o C and 10 w/o Teflon have slightly lower conductivity than that of either $Cr_{0.5}V_{0.5}S_2$ or the 90 w/o $Cr_{0.5}V_{0.5}S_2$/10 w/o Teflon mixture. At the same time, electrodes with 20 w/o carbon and 10 w/o Teflon perform better than those without C. It seems that the effect of carbon on the performance of the cathodes is not related to electronic conductivity. The major effects probably are associated with: (1) higher electrode porosity and (2) increased particle to particle contact.

3.3.2 Effects of Separator Thickness, Temperature and Electrolyte Conductivity on Rate-Capacity of $Li/Cr_{0.5}V_{0.5}S_2$ Cells

These studies have been carried out with Cells TB-18-CVS and TB-19-CVS. The specifications of these cells are given in Table 7. The cathodes in these cells comprise 70 w/o $Cr_{0.5}V_{0.5}S_2$, 20 w/o C and 10 w/o T, the optimized composition. Both of the cells utilize only one layer of the Celgard 2400 separator between each anode and cathode. In Cell TB-18-CVS, the electrolyte is 2Me-THF/1.3M $LiAsF_6$; in Cell TB-19-CVS, it is a solution of $LiAsF_6$(1.5M) in a 50:50 THF:2Me-THF mixture. The latter electrolyte has a conductivity of 1×10^{-2} $(ohm-cm)^{-1}$ at $25°C$, whereas the conductivity of the 1.3M $LiAsF_6$/2Me-THF solution at $25°C$ is 0.35×10^{-2} $(ohm.cm)^{-1}$. The results with these two cells compare the effect of electrolyte conductivity on the rate/capacity behavior; while, the results with TB-18-CVS and TB-9-CVS (Table 6) compare the effect of separator thickness.

Table 7

Specifications of Li/Cr$_{0.5}$V$_{0.5}$S$_2$ Cells

Cell No.	Electrolyte 2Me-THF/1.3M LiAsF$_6$ (ml)	Cathode Composition[1]	Cathode 1e⁻ Capacity (mAh)	Cathode Thick. (mm)	Anode Capacity (mAh)	Anode Thickness (mm)	Celgard 2400 Separator Thick. (mm)	Cell Package Thick. (mm)	Cell Package Volume (cc)	OCV (V)
TB-18-CVS	9.5	70 w/o CVS 20 w/o C 10 w/o T	240	1.575	2 x 828	2 x .432	1 x .0254	2.490	2.316	2.967
TB-19-CVS	9.5[2]	70 w/o CVS 20 w/o C 10 w/o T	213	1.447	2 x 828	2 x .432	1 x .0254	2.362	2.197	2.963

[1]Where CVS = Cr$_{0.5}$V$_{0.5}$S$_2$, C = Shawinigan carbon, T = Teflon.
[2]Electrolyte is 50:50 THF/2Me-THF(1.5M LiAsF$_6$).

The relevant data plotted as percent cathode utilization versus current density, are shown in Figure 15. The room temperature discharge curves for TB-18-CVS and TB-19-CVS at the various current densities are given in Figures 16 and 17. The low temperature (-10 and -30°C) discharge curves of TB-18-CVS and TB-19-CVS are given in Figures 18 and 19.

At 25°C, the three cells exhibit practically similar cathode utilizations at current densities between 0.5 and 4 mA/cm^2. It appears that at 25°C, the cathode utilizations at current densities of 0.5-4 mA/cm^2 are not affected by varying the separator thickness from 1 mil (1 layer) to 2 mil. Similarly, the higher conductivity of the blended electrolyte does not appear to have an effect on cathode utilizations at current densities up to 4 mA/cm^2. It should, however, be noted that the mid-discharge voltages of the cell with one layer of the separator is slightly higher (e.g., 150 mV at 2 mA/cm^2) than those of the cell with two separator layers.

The performance of Cells TB-18-CVS and TB-19-CVS was evaluated also at -10°C and -30°C. Cell TB-18-CVS utilizing 2Me-THF/LiAsF$_6$ (1.3M) exhibited capacities of 0.72 and 0.45 e$^-$/Cr$_{0.5}$V$_{0.5}$S$_2$ at -10°C at current densities of 0.5 and 1 mA/cm^2 respectively. At 2 mA/cm^2, the capacity was a poor 0.14 e$^-$/Cr$_{0.5}$V$_{0.5}$S$_2$. Moreover, this cell exhibited practically no capacity at -30°C, even at current densities as low as 0.1 mA/cm^2.

The performance of Cell TB-19-CVS containing the THF/2Me-THF blend was considerably better at -10°C. Thus, a capacity of about 0.7 e$^-$/Cr$_{0.5}$V$_{0.5}$S$_2$ was obtained at current densities of 1 and 2 mA/cm^2 and 0.43 e$^-$/Cr$_{0.5}$V$_{0.5}$S$_2$ at 3 mA/cm^2. Furthermore, at -30°C, the cell exhibited a capacity of 0.64 e$^-$/Cr$_{0.5}$V$_{0.5}$S$_2$ at 0.25 mA/cm^2. These results indicate that Cr$_{0.5}$V$_{0.5}$S$_2$ itself is capable of discharges at practically useful rates down to -30°C. We attribute the poor low temperature performance of cells with 2Me-THF/LiAsF$_6$(1.3-1.5M) to the crystallizaton from solution of a solvate of LiAsF$_6$. In the 50:50 THF/2Me-THF blended solution, crystallization of the salt-solvent complexes does not appear to occur even at -30°C. In general, cells with 2Me-THF/LiAsF$_6$(1.3-1.5M) appear to be of limited rate capabilities at temperatures below 0°C.

3.4 Long-Term Cycling of Cells

In addition to some of the cells shown in Table 6 and both of the cells in Table 7, the cells described in Table 8 have been used for long term cycling studies.

3.4.1 Cells TB-18-CVS, TB-19-CVS and TB-20-CVS

These three cells have identical cathode compositions. But while cells TB-18-CVS and TB-20-CVS utilize 2Me-THF/LiAsF$_6$(1.3M), Cell TB-19-CVS utilizes 50:50 THF/2Me-THF/LiAsF$_6$(1.5M). Furthermore, Cell TB-20-CVS has two layers of the Celgard-2400 separator between each anode and the cathode, while the other cells have only one layer of the separator.
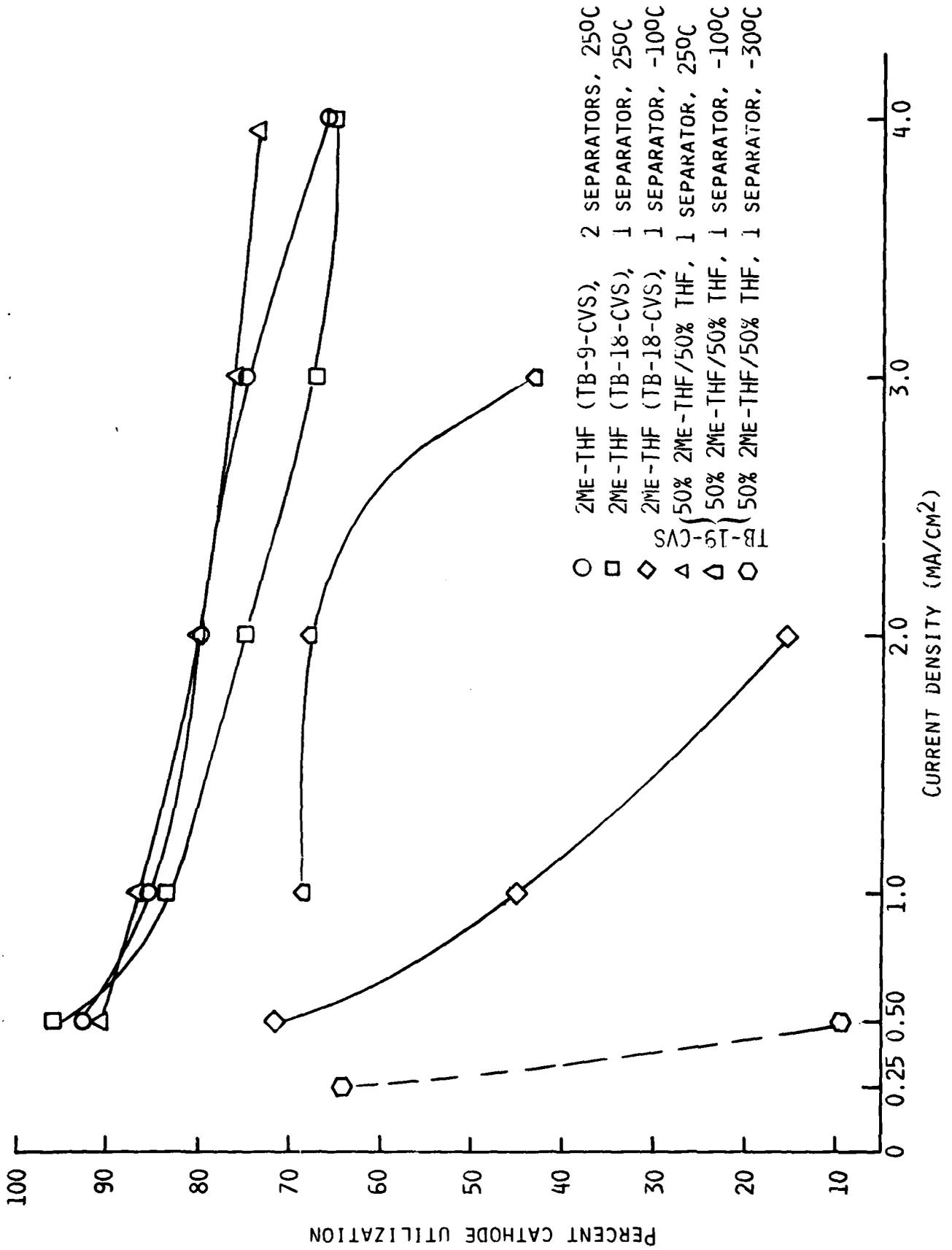
Fig. 15. Cathode utilization vs current density of Li/Cr$_{0.5}$V$_{0.5}$S$_2$ cells.

Legend:

	2ME-THF (TB-9-CVS),	2 SEPARATORS, 25°C
○	2ME-THF (TB-18-CVS),	1 SEPARATOR, 25°C
□	2ME-THF (TB-18-CVS),	1 SEPARATOR, -10°C
◇	50% 2ME-THF/50% THF,	1 SEPARATOR, 25°C
△	50% 2ME-THF/50% THF,	1 SEPARATOR, -10°C
◁	50% 2ME-THF/50% THF,	1 SEPARATOR, -30°C

TB-19-CVS

CURRENT DENSITY (MA/CM²)

PERCENT CATHODE UTILIZATION

31
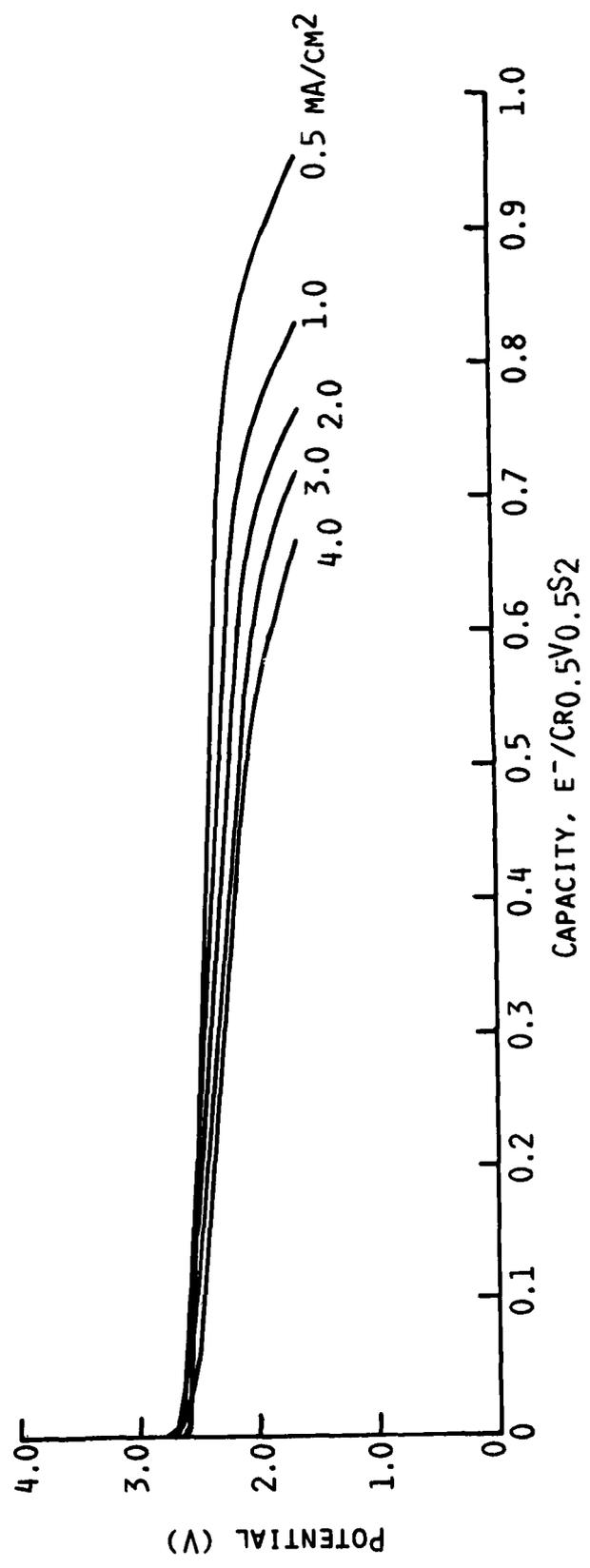
Fig. 16. Discharge curves of Cell TB-18-CVS at 25°C at various current densities.

32
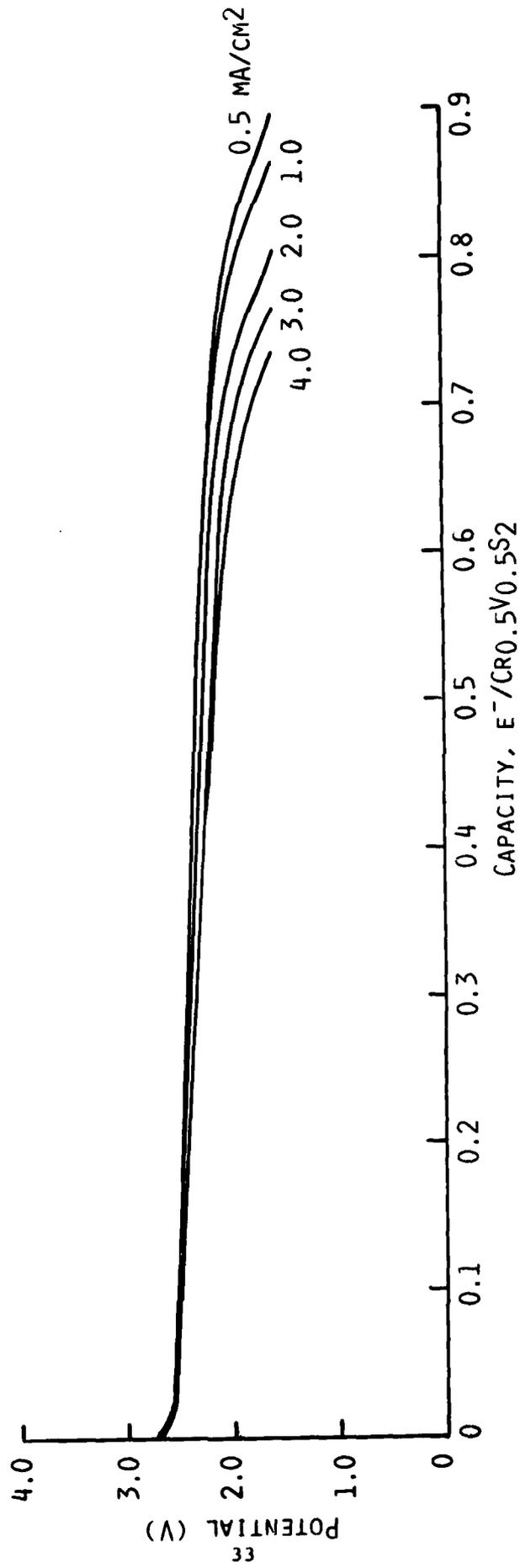
Fig. 17. Discharge curves for Cell TB-19-CVS at 25°C at various current densities.
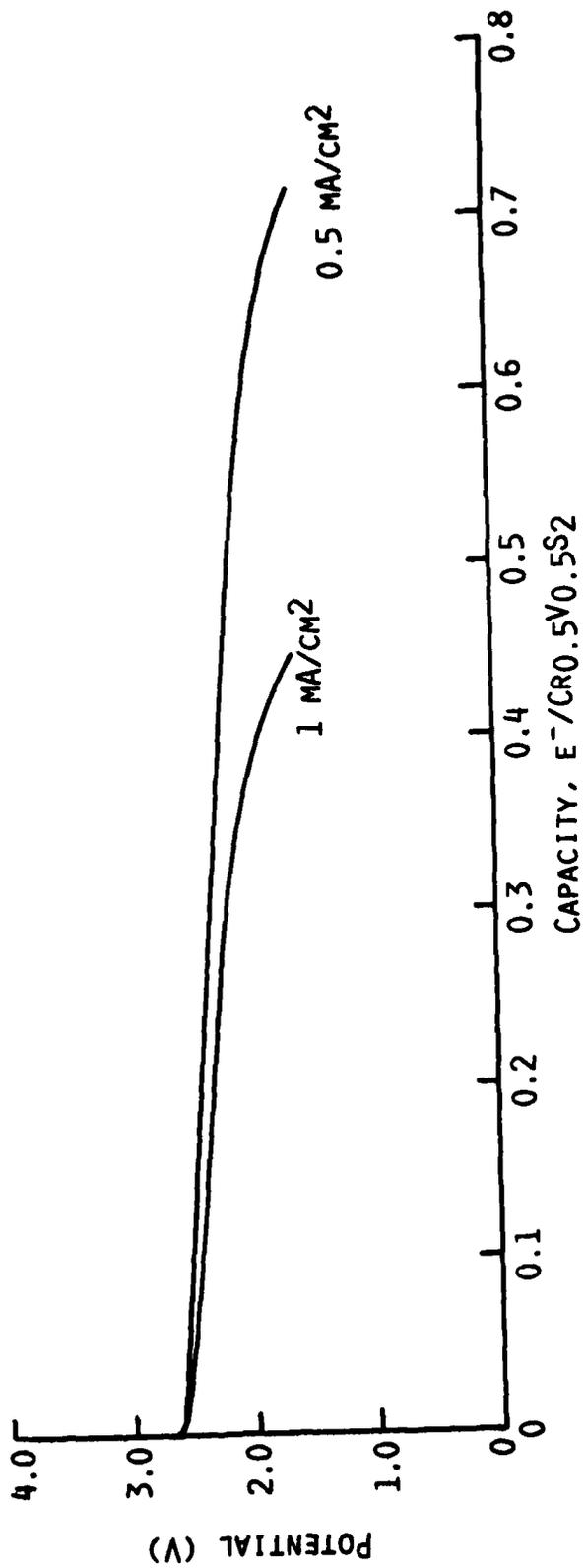
Fig. 18. Discharge curves of Cell TB-18-CVS at -10°C at various current densities.
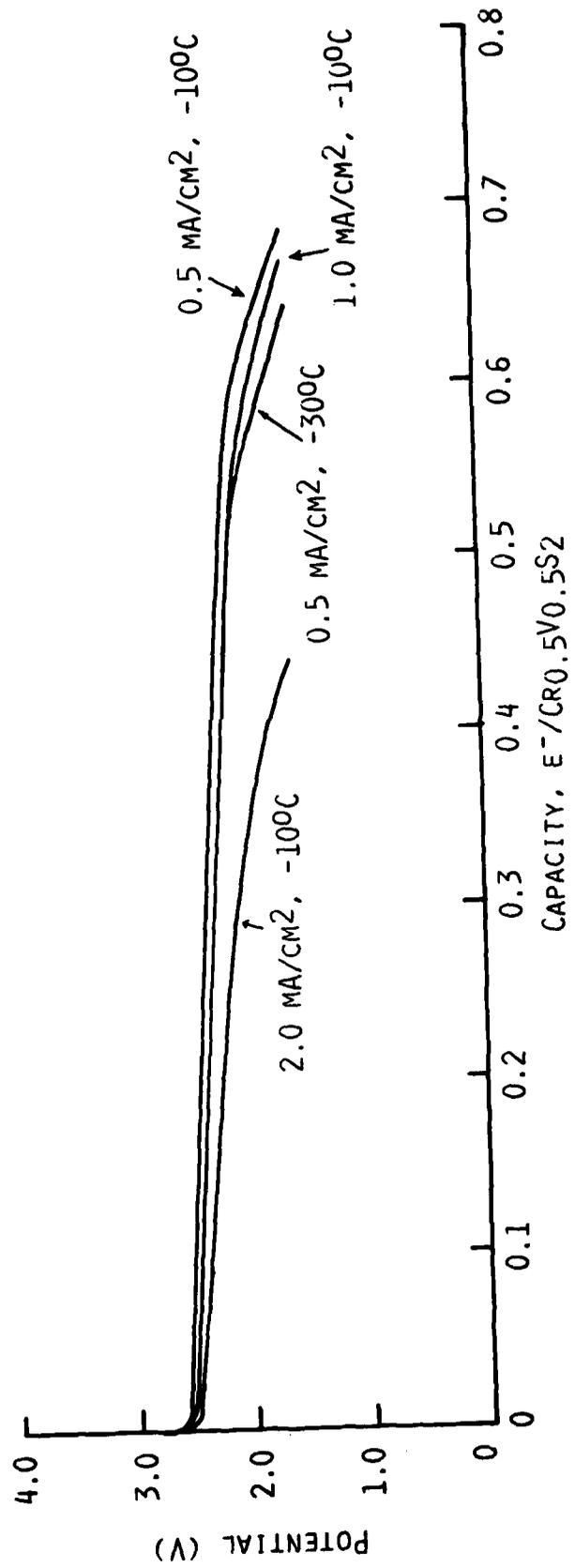
Fig. 19. Discharge curves of Cell TB-19-CVS at -10°C and -30°C at various current densities.

Table 8

Specifications of Li/$Cr_{0.5}V_{0.5}S_2$ Cells

Cell No.	Electrolyte 2Me-THF/1.3M LiAsF$_6$ (ml)	Cathode Composition[1]	le⁻ Capacity (mAh)	Thick. (mm)	Anode Capacity (mAh)	Thickness (mm)	Celgard 2400 Separator Thick. (mm)	Cell Package Thick. (mm)	Volume (cc)	OCV (V)
TB-20-CVS	9.5	70 w/o CVS / 20 w/o C / 10 w/o T	211	1.269	2 x 828	2 x 0.432	2 x (2x0.0254)	2.235	2.079	3.2
TB-21-CVS	9.5	75 w/o CVS / 15 w/o C / 10 w/o T	250	1.549	2 x 828	2 x 0.432	2 x (2x0.0254)	2.515	2.339	3.2
TB-22-CVS	9.5	70 w/o CVS / 10 w/o TiS$_2$ / 10 w/o C / 10 w/o T	260 (CVS = 227, TiS$_2$ = 33)	1.219	2 x 828	2 x 0.432	2 x (2x0.0254)	2.184	2.031	3.2

[1]Where CVS = $Cr_{0.5}V_{0.5}S_2$, C = Shawinigan carbon, T = Teflon.

The long-term cycling of Cell TB-18-CVS began after the rate/capacity studies, at 25 and $-10^{\circ}C$, discussed in the previous section. The cell was cycled between limits of 1.6 and 3.1 volts at current densities of 2 mA/cm^2 for discharge and 1 mA/cm^2 for charge. A plot of cathode utilization versus cycle number is given in Figure 20. Typical cycles are shown in Figure 21. The early cathode utilization of 60% decreased to ~40% by the 95th cycle. However, when the current density was reduced to 0.25 mA/cm^2 at the 96th cycle, the cathode utilization increased to 64%, showing that the decreasing cathode utilization with continued cycling at the higher rate was probably due to cathode structural factors or increasing cell resistance rather than any degradation of $Cr_{0.5}V_{0.5}S_2$.

Cell TB-19-CVS had also been subjected to rate/capacity studies at 25, -10 and $-30^{\circ}C$ as discussed in the previous section. The extended cycling was performed between voltage limits 1.6 and 3.1 volts at a current density of 2 mA/cm^2 for both discharge and charge. The cathode utilization versus cycle number plot is given in Figure 20. Typical cycles are depicted in Figure 22. The performance of the cell was somewhat superior to that of Cell TB-18-CVS. Even at the higher charge rate of 2 mA/cm^2, the rate of decrease in capacity with cycle number was less than that in TB-18-CVS. This is probably due to the higher conductivity of the 2Me-THF:THF(50:50) /$LiAsF_6$ solution. Cathode utilizations of 50 and 40% have been obtained at the 100th and 170th cycles, respectively. Moreover, when the current density at the 177th cycle was reduced to 0.5 mA/cm^2, the utilization increased to nearly 58% and remained fairly steady at this value in the next several cycles. As in the previous cell, increasing the current density to 2 mA/cm^2 after the low rate cycling resulted in a lower utilization of the same level as in the high rate discharges prior to the low rate cycles.

A noteworthy aspect of the results from Cell TB-14-CVS is that a respectable cycling efficiency for the Li electrode has been achieved in the 50:50 2Me-THF/THF ($LiAsF_6$, 1.5M) electrolyte. The Li cycling efficiency was 93%.

Cell TB-20-CVS ran 152 deep discharge cycles before being terminated. The data, plotted as percent utilization versus cycle number, are given in Figure 23. The cycling was performed at 1.5 mA/cm^2 for both discharge and charge between limits 1.6 and 3.1 volts. In cycles 79 and 80, the 0.5 mA/cm^2 capacity was evaluated. Furthermore, at cycle 134 the current density was reduced to 0.5 mA/cm^2 and the rest of the cycling was performed at this rate. A few cycles of this cell are given in Figure 24.

The very high cathode utilization of nearly 90 percent obtained in the first discharge declines fairly rapidly in the first ten cycles. The capacity faded at a rate of ~2% per cycle. Subsequent capacity loss is more gradual and occurred at a rate of ~0.4% per cycle between the 10th and 50th cycle. The capacity loss rate becomes even less subsequently. The 0.5 mA/cm^2 utilization in the 80th cycle is 65%, identical to that in the 20th cycle, obtained at the higher rate. In fact, the 0.5 mA/cm^2 utilization even in the 135th cycle is 61%.

37
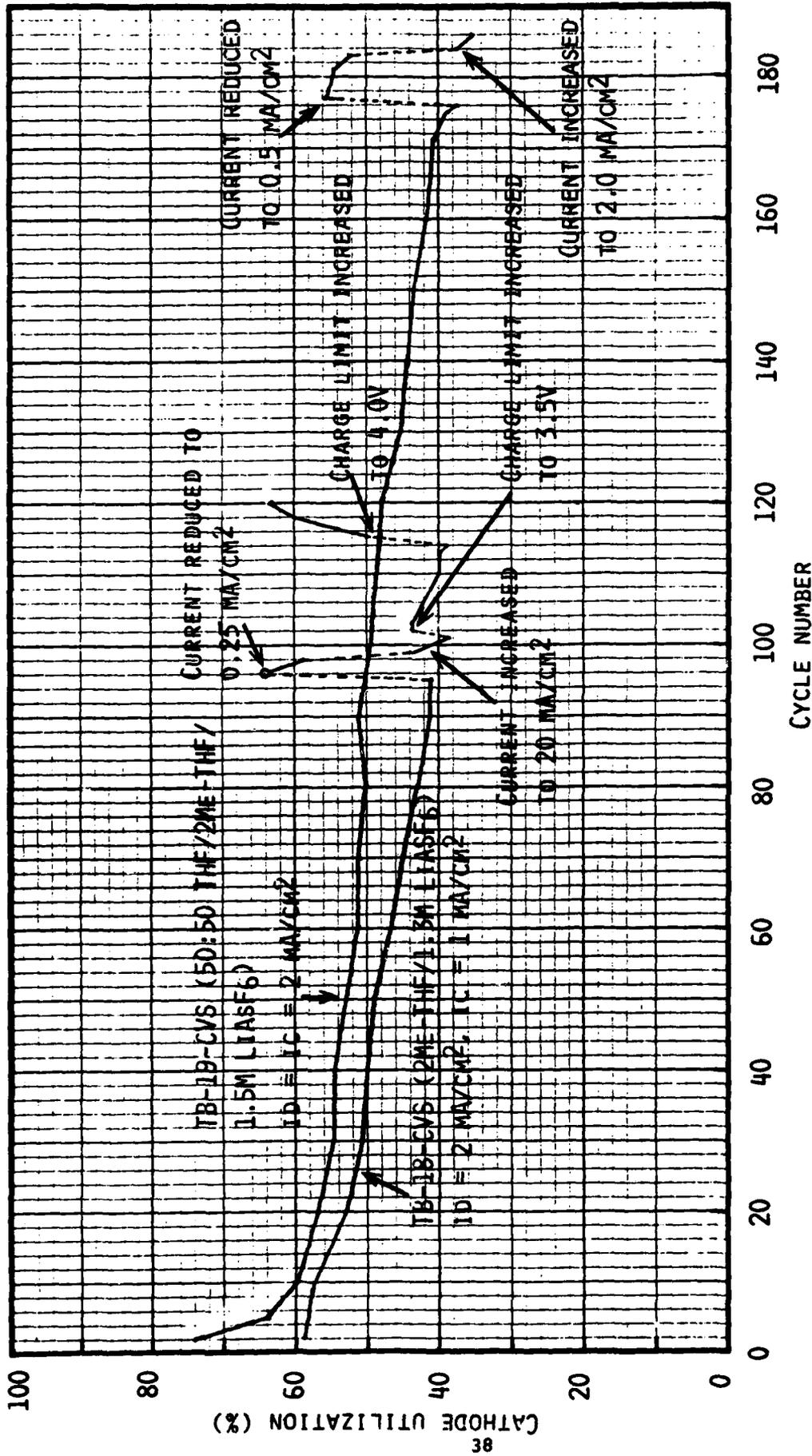
Fig. 20. Percent cathode utilization vs cycle number for cells TB-18-CVS and TB-19-CVS.

38
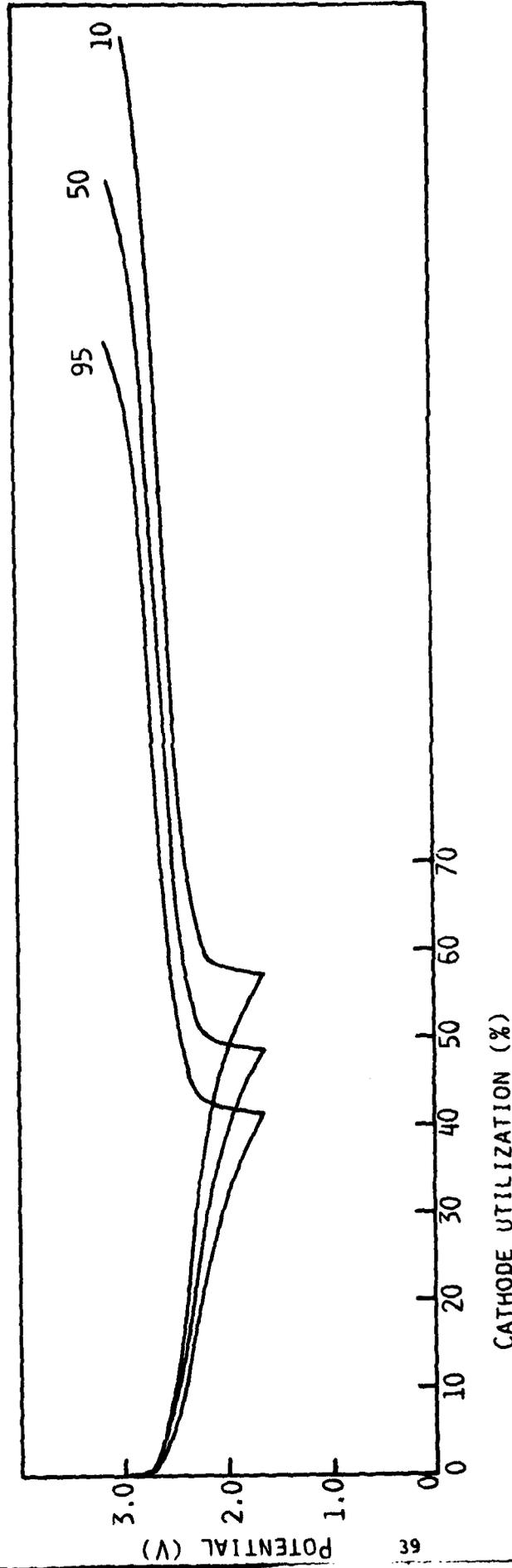
Fig. 21. Typical cycles for Cell TB-18-CVS (2Me-THF/1.3M LiAsF$_6$). Cycling limits: 1.6-3.1 volts. id = 2mA/cm^2, ic = mA/cm^2.
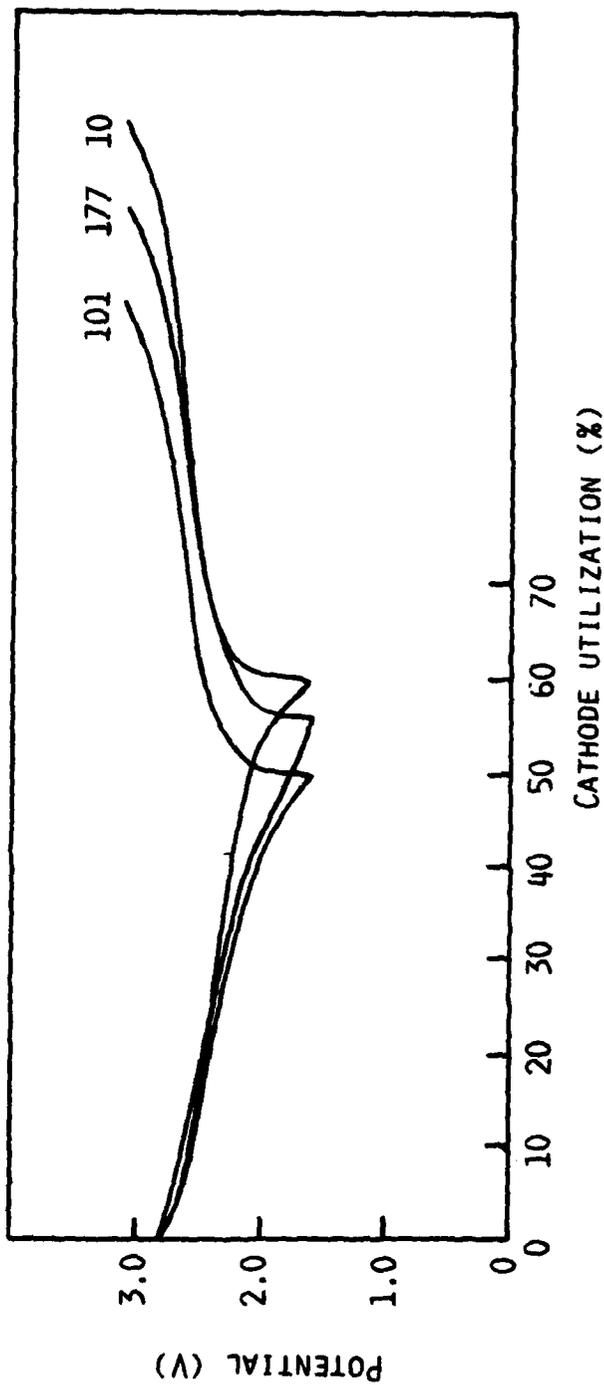
Fig. 22. Typical cycles for Cell TB-19-CVS (50:50 THF/2Me-THF/1.5M LiAsF$_6$)

id = ic = 2 mA/cm^2 for cycles 10 and 101
id = ic = 0.5 mA/cm^2 for cycle 177
Cycling limits: 1.6-3.1 volts
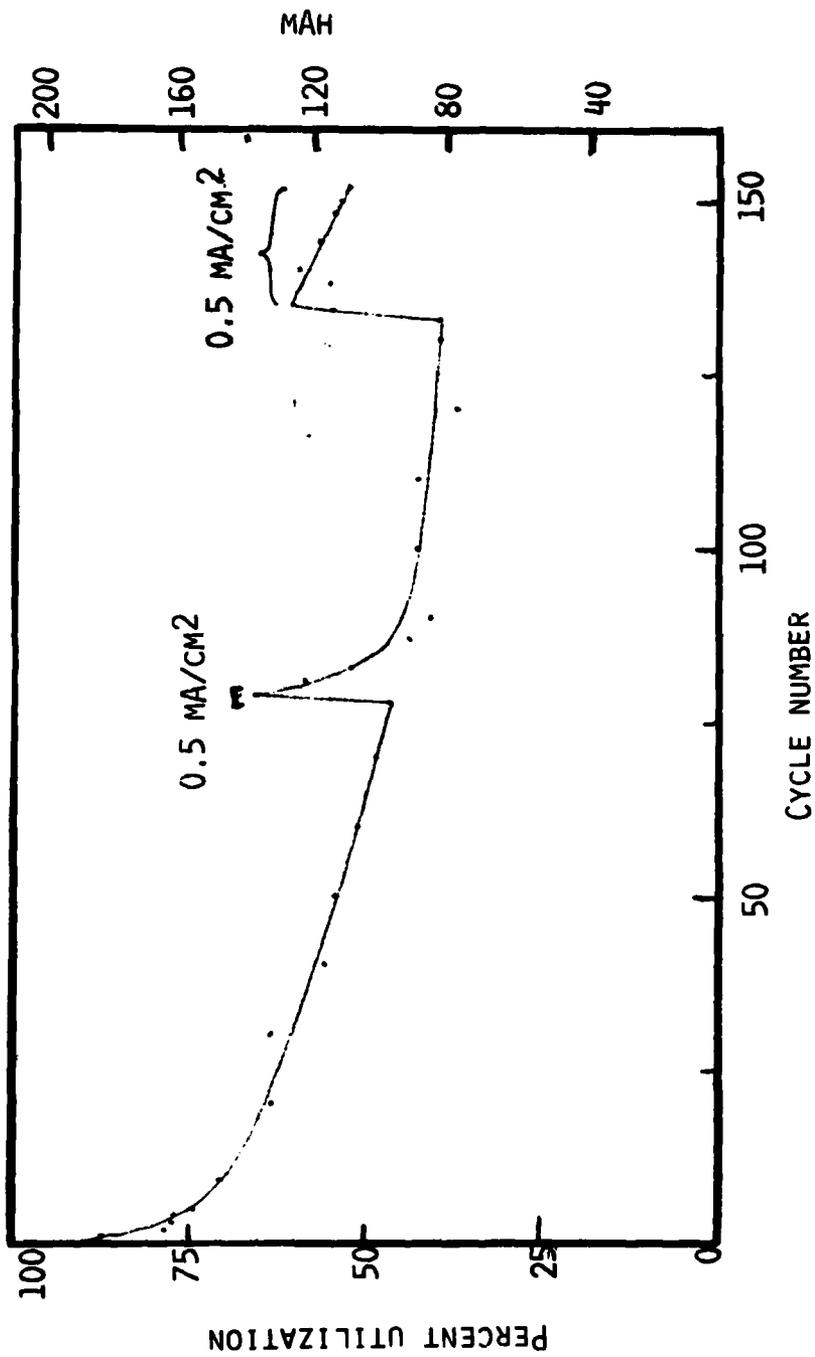
Fig. 23. Capacity versus cycle number for Cell TB-20-CVS. Except where noted, id = ic = 1.5 mA/cm². Voltage limits, 1.6-3.1V.

41
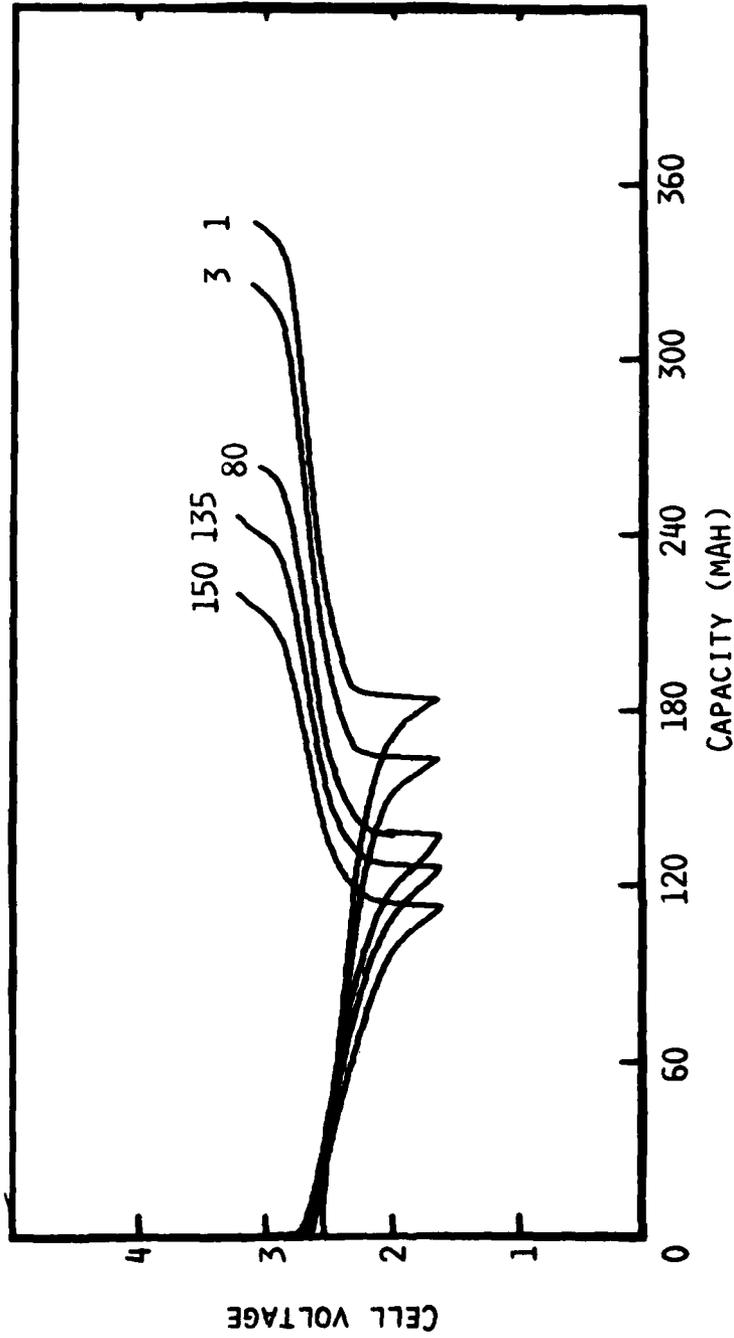
Fig. 24. Some cycles of Cell TB-20-CVS. Current density: Cycles 1 and 3, 1.5 mA/cm^2, others 0.5 mA/cm^2. Theoretical cathode capacity 210 mAh.

3.4.2 Detailed Analysis of the Cycling Data of TB-18-CVS, TB-19-CVS and TB-20-CVS

In order to gain further insight into the causes of capacity loss with cycling, a detailed analysis of the first fifty cycles of the three cells was carried out. For cycles beginning with the second cycle of each cell, the cathode utilization was calculated as percentage of the recharge capacity in the preceeding charge half-cycle. In the first fifty cycles of all three cells, this utilization is a nearly constant 100%. This shows that the apparent loss in cathode utilization with cycling is related to the difficulty in recharging a fraction of the capacity discharged in each cycle. Evidently, the discharge rate capability of the cathode material remains unchanged with cycling. On the other hand, a fraction of the discharged material is not recharged, especially in the early cycles. The results show that the presently employed mode of recharge of these cells is not ideal.

The observed behavior can be explained as follows. Discharge of $Cr_{0.5}V_{0.5}S_2$ results in an expansion of the cathode. Upon recharge, the disulfide lattice contracts, but the shape acquired by the electrode at the end of discharge may not change. Towards the end of charge, a fraction of the material loses particle-to-particle or particle-to-grid contact and becomes electrically isolated. In the next discharge, however, the particles regain contact because of the lattice expansion. Thus, the discharge rate capability remains unchanged.

It should, however, be noted that the utilization calculated as percent of recharge does show decreases with extended cycling, i.e., >100 cycles, suggesting that extensive physical changes of the electrode with repeated cycling affect the discharge rate also. Another factor affecting the later discharge rate capability may be limitations at the Li electrode, such as the formation of resistive films, as well as increases in cell resistance.

3.4.3 Cells TB-9-CVS and TB-10-CVS

The specifications of these cells have already been given in Table 6. The first five cycles of these cells correspond to the rate/capacity studies discussed in Section 3.3.1. Extended cycling of these cells began with cycle No. 6.

Beginning with cycle 6, Cell TB-9-CVS was cycled at 3 mA/cm^2 for both discharge and charge. The capacity as seen in Figure 25 rapidly declined with cycling, diminishing to ~20% of the theoretical by the 15th cycle. There was no further change until the 19th cycle. The current density for recharge was then reduced to 1 mA/cm^2. As a result, the cathode utilization as a result increased to 0.56 Li/$Cr_{0.5}V_{0.5}S_2$. The capacity
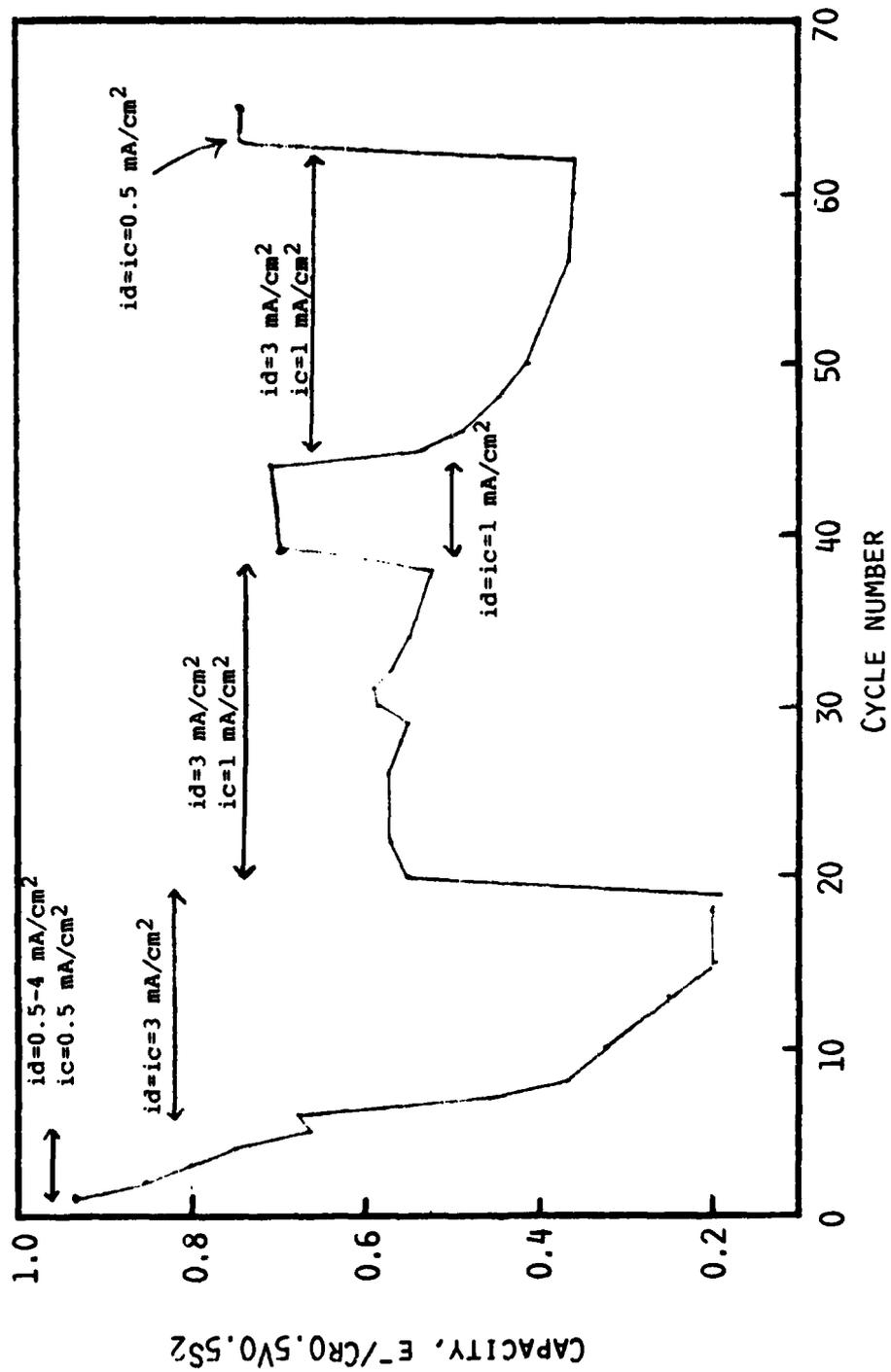
Fig. 25. Capacity versus cycle number of Cell TB-9-CVS. Voltage limits: 1.6-3.2v.

44

remained steady at this value for the next 18 cycles. Cycles 39-44 were obtained at 1 mA/cm^2 for both discharge and charge. The cathode utilization was a steady 0.72 Li/Cr$_{0.5}$V$_{0.5}$S$_2$. Further cycling at rates of 3 mA/cm^2 for discharge and 1 mA/cm^2 for charge led to decreasing cathode utilizations. Nevertheless, a capacity of 0.74 Li/Cr$_{0.5}$V$_{0.5}$S$_2$ was obtained at the 63rd discharge when the current density was reduced to 0.5 mA/cm^2 for both discharge and charge.

The results with Cell TB-9-CVS reinforce the conclusions presented in the previous section. Li/Cr$_{0.5}$V$_{0.5}$S$_2$ cells with ~20 w/o carbon in the cathode can be discharged at relatively high rates with good utilizations. However, the recharge rates have to be relatively low in order to maintain these capacities over a large number of cycles.

The cycling data for Cell TB-10-CVS, containing 30 w/o carbon in the positive electrode, are presented in Figure 26. The cell was cycled at 2 mA/cm^2 for both discharge and charge between voltage limits of 1.6 and 3.2V. The results are quite similar to that obtained with Cell TB-18-CVS. It is apparent that the utilizations during long-term cycling in a cathode with 30 w/o carbon is not better than those achieved in cathodes with 20 w/o C.

3.4.4 Cycling of Cells TB-21-CVS and TB-22-CVS

The cathode in Cell TB-21-CVS had only 15 w/o C. The cell was initially cycled between voltage limits of 1.6 and 3.1V, at current densities of 2 and 1.5 mA/cm^2 respectively for discharge and charge. As seen in Figure 27, the performance of the cell is inferior to that of Cell TB-18-CVS containing 20 w/o carbon in the cathode. After 62 cycles, the current density was reduced to 0.5 mA/cm^2 which resulted in an increase in the utilization to nearly 70% of the theoretical. Beginning with the 68th discharge, the effect of overdischarge on cycling was evaluated (see later).

In Cell TB-22-CVS the effect of 10 w/o TiS$_2$, instead of the same amount of carbon in the cathode matrix, on the cycling of Cr$_{0.5}$V$_{0.5}$S$_2$ was evaluated. The cell had a theoretical capacity of 260 mAh (227 mAh Cr$_{0.5}$V$_{0.5}$S$_2$ and 33 mAh TiS$_2$). It was initially cycled at 2 mA/cm^2 for both discharge and charge, between limits of 1.6 and 3.2 volts. The cycling data are shown in Figure 28. Typical cycles of the cell are depicted in Figure 29. The initial cathode utilization was 90% of the theoretical which is similar to that normally obtained with a cathode containing 20 w/o C. In the early stages of cycling the capacity decreased relatively rapidly so that by the 17th cycle the utilization was ~60% of the theoretical. Beginning with the 18th cycle the charge current density was reduced to 1.5 mA/cm^2. This resulted in a temporary increase in the discharge capacity, manifested by a utilization of 70% in the 18th discharge. The utilization in the 19th discharge was 63%. Subsequent to this, the capacity fade rate was more gradual. Cathode utilization of 50% and 45% were obtained in the
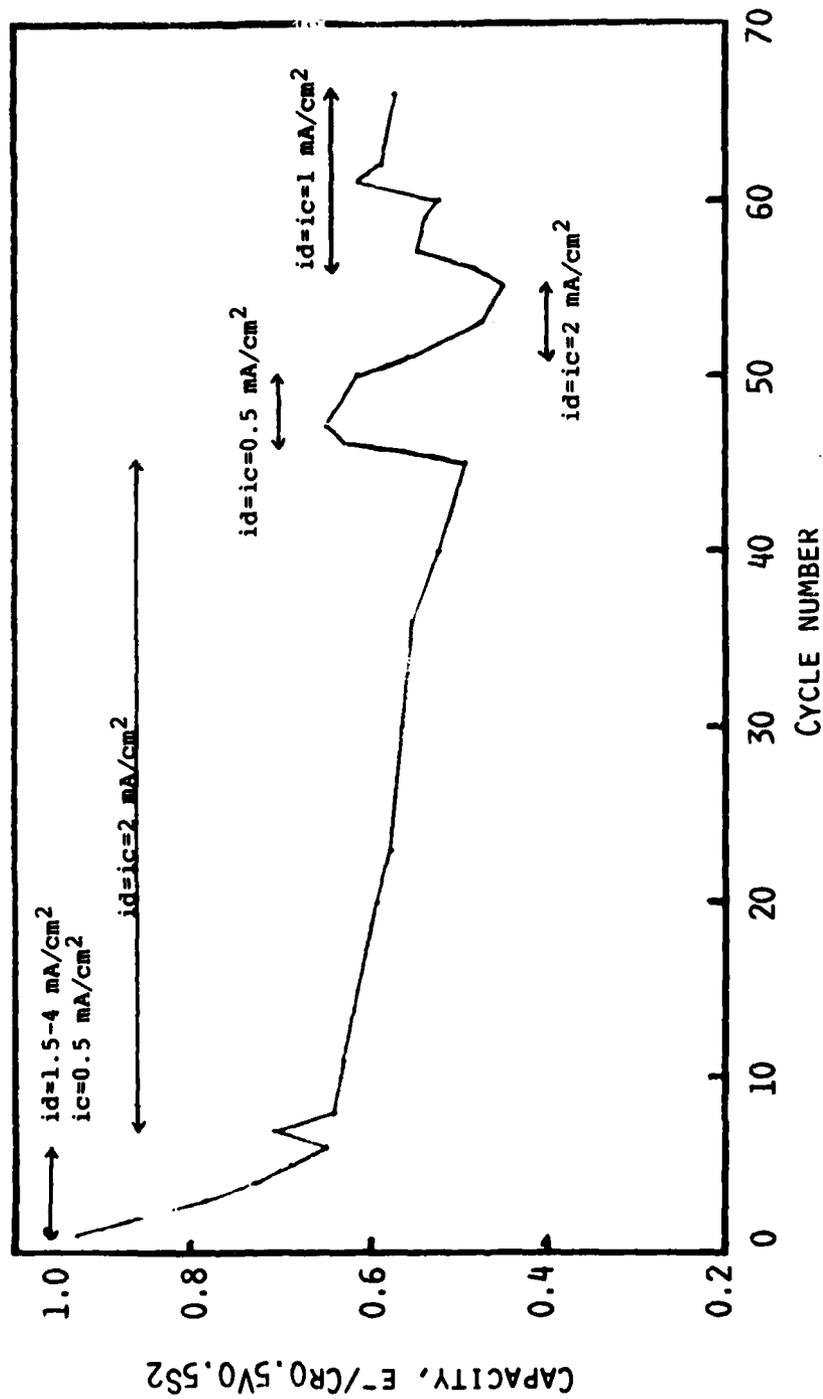
Fig. 26. Capacity versus cycle number of Cell TB-10-CVS. Voltage limits: 1.6-3.2v.

46
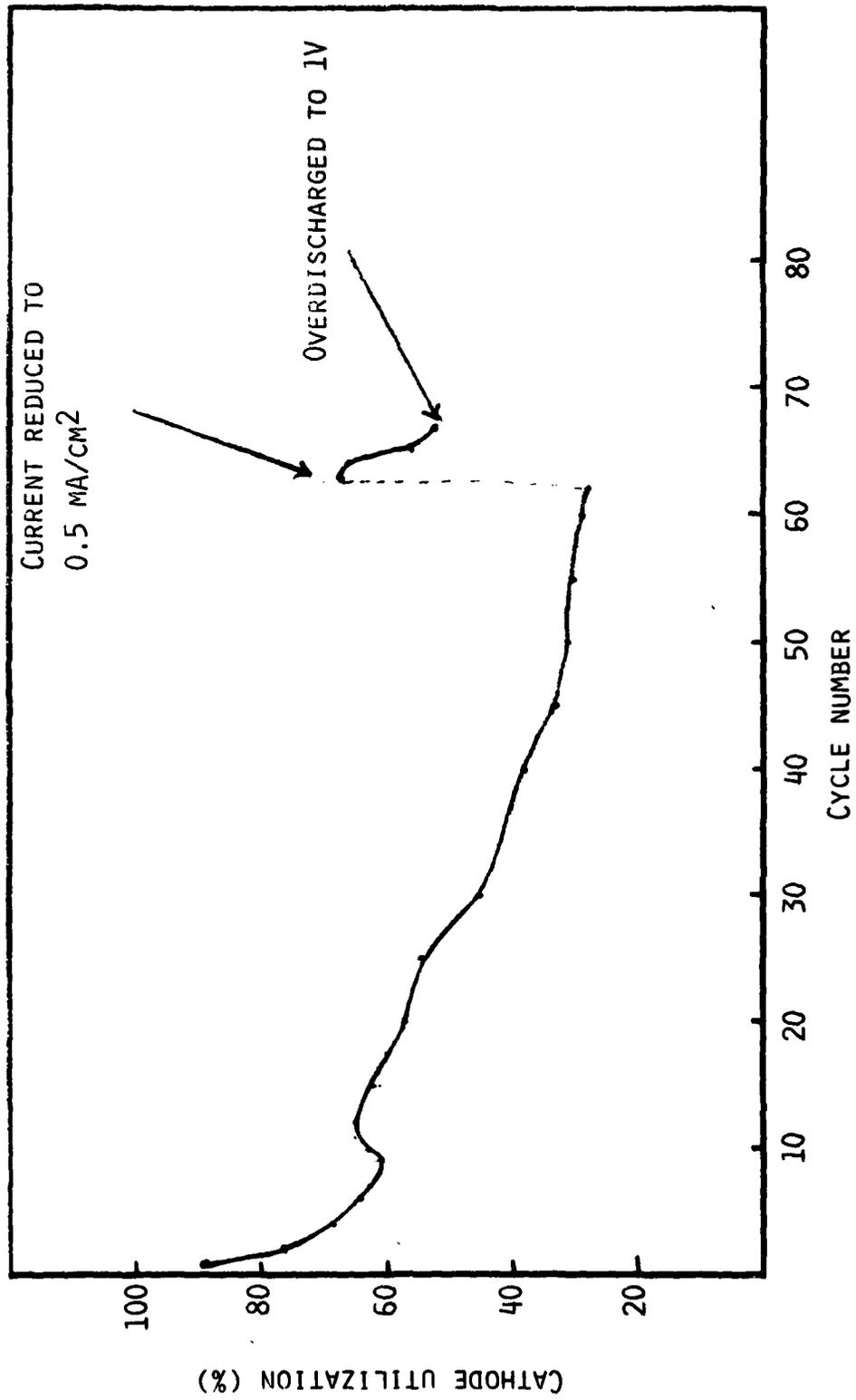
Fig. 27. Cycling data for Cell TB-21-CVS. Current, i_d = 2 mA/cm^2, i_c = 1.5 mA/cm^2 except where noted. Voltage limits 1.6-3.1V.

CURRENT REDUCED TO 0.5 MA/CM^2

OVERDISCHARGED TO 1V

CYCLE NUMBER

CATHODE UTILIZATION (%)
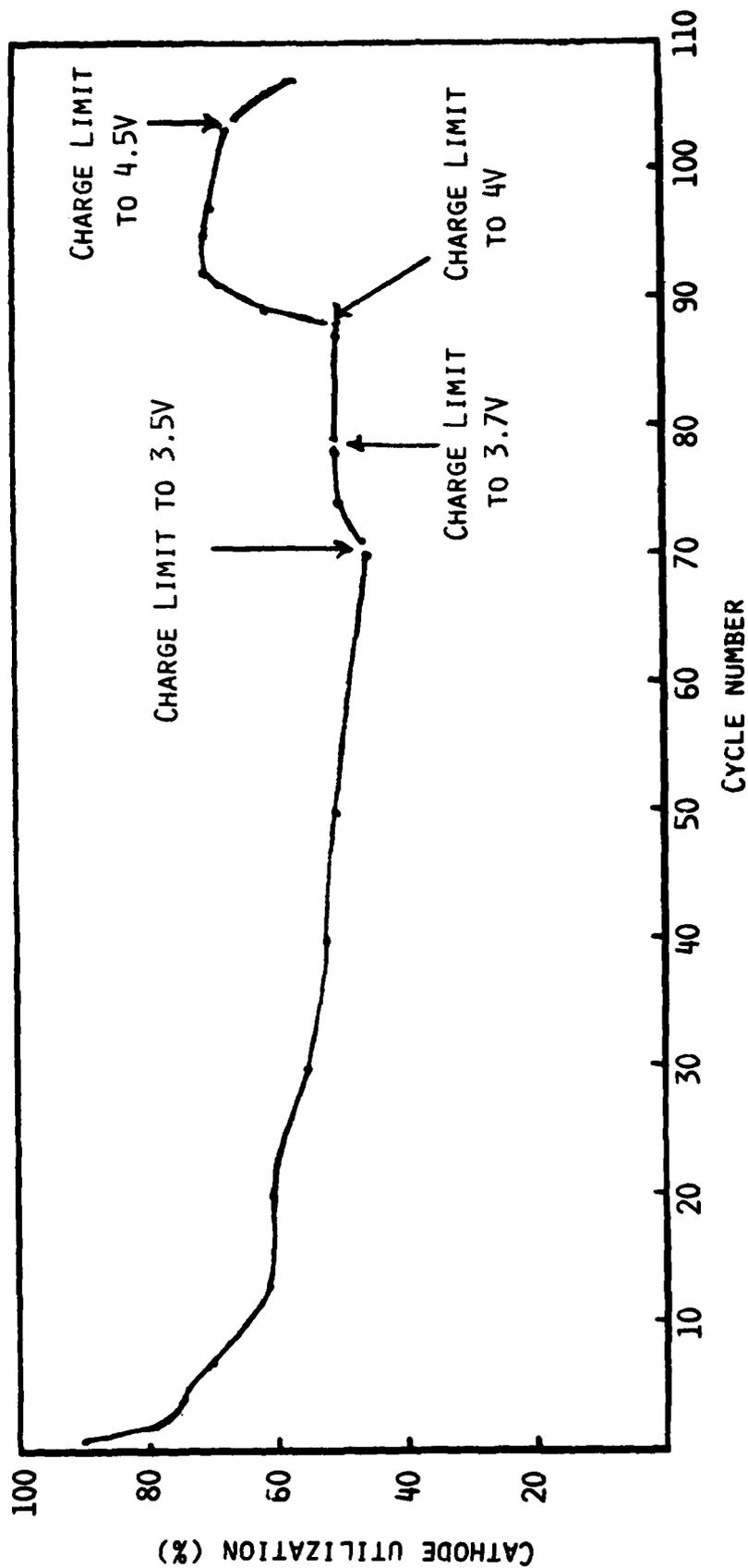
Fig. 28. Cycling data for Cell TB-22-CVS. Cycles 1-17, id = ic = 2 mA/cm^2; from Cycle 18 id = 2 mA/cm^2, ic = 1.5 mA/cm^2. All discharges to 1.6V.
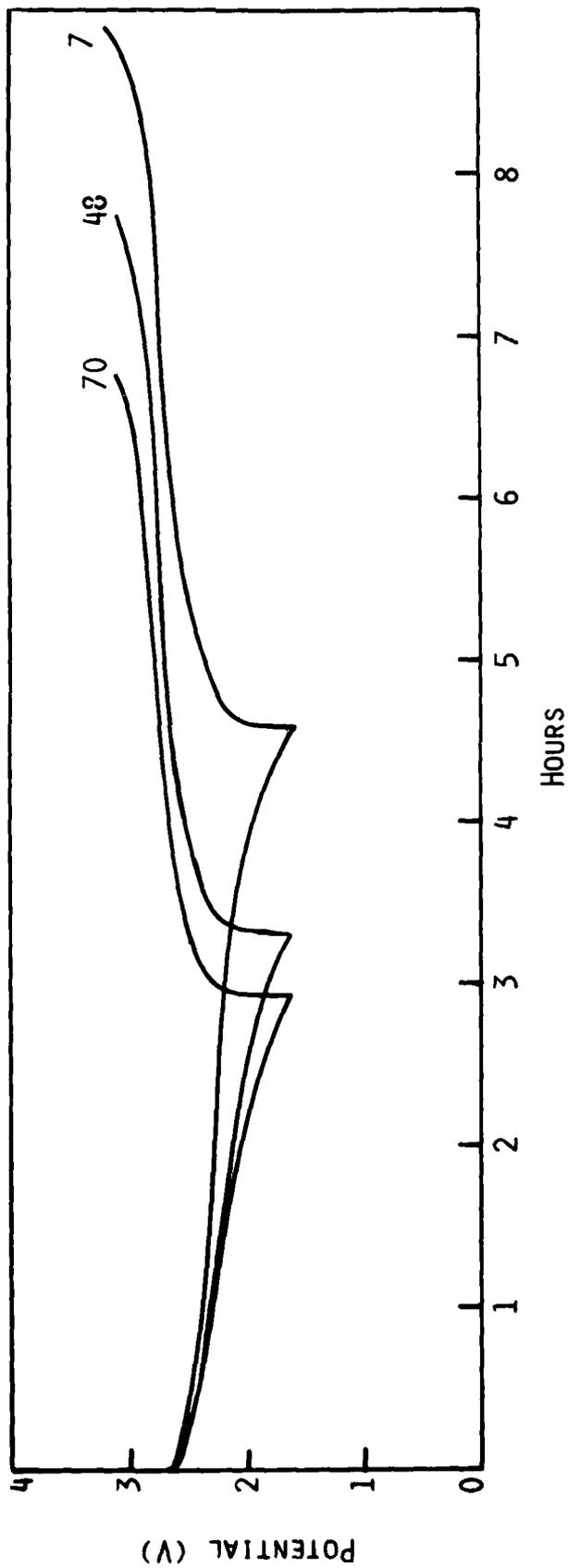
Fig. 29. Typical cycles for Cell TB-22-CVS. Cycle 7, id = ic = 2 mA/cm^2, voltage limits = 1.6-3.2V; for cycles 48 and 70, id = 2 mA/cm^2, ic = 1.5 mA/cm^2, voltage limits = 1.6-3.1V.

50th and 70th cycles respectively. The cycling behavior exhibited by this cell is not significantly different from that shown by cells containing 20 w/o C in the cathode. On the average, the utilization in the cell is about 5% lower than in cells containing 20 w/o C. In order to establish, beyond doubt, the beneficial effect of TiS_2 further work would be necessary. Therefore, all further studies in the present program have been limited to cathodes with 20 w/o C, 10 w/o T and 70 w/o $Cr_{0.5}V_{0.5}S_2$.

3.4.5 Cycling of Cells at Less than 100% Depth of Discharge

Two cells, TB-25-CVS and TB-26-CVS, both with a cathode composition of 70 w/o $Cr_{0.5}V_{0.5}S_2$, 20 w/o C and 10 w/o Teflon and containing 2Me-THF/ $LiAsF_6(1.4M)$, have cycled at a current density of 1 mA/cm^2. The depth of discharge (DOD) in TB-25-CVS was 30% of the theoretical and that in TB-26-CVS was 60% of the theoretical. After every 20 cycles, the cell's capacity corresponding to 100% DOD was determined by discharging it to 1.6V at 0.5 mA/cm^2. Figure 30 depicts the data for Cell TB-25-CVS. The figure displays the 100% DOD capacity obtained after every 20, 30% DOD cycles. Note that the 100% DOD capacity, which is ~ 0.9 e$^-$/$Cr_{0.5}V_{0.5}S_2$ initially, levels off to ~ 0.75 e$^-$/$Cr_{0.5}V_{0.5}S_2$ by the 50th cycle and diminishes to ~ 0.7 e$^-$/ $Cr_{0.5}V_{0.5}S_2$ by the 150th cycle. This behavior is not significantly different from that seen in cells continuously cycled at 100% DOD. In TB-26-CVS, cycled at 60% DOD, the full cathode capacity after 50 cycles was 0.68e$^-$/$Cr_{0.5}V_{0.5}S_2$, while the full cathode capacity in TB-25-CVS after an equivalent number of cycles was 0.75 e$^-$/$Cr_{0.5}V_{0.5}S_2$. The difference is relatively small.

The above data indicate that in low to moderate rate cycling, the capacity fade rate seen in these cells is more or less independent of the depth of discharge.

3.5 Analysis of Cycled Cells

Some of the cells have been opened after cycling and analyzed in order to assess cathode integrity and extent of electrolyte degradation. Analytical results of cells which have been subjected to overdischarge and overcharge are discussed in the next section.

The X-ray data for cathodes from cells TB-19-CVS (see Fig. 20) and TB-20-CVS (see Fig. 23) are given in Table 9. Both cells had been terminated at the end of a charge at a low rate. The lines observed at ~ 8.7 and 4.9 Å in both of the cathodes are the strongest lines due to Shawinigan carbon. The line at 2.32 Å in the cathode from TB-19-CVS appears to be due to LiF. The LiF lines have been found in forced overdischarged cathodes also (see below).

The rest of the lines in the pattern of TB-19-CVS are due to $Cr_{0.5}V_{0.5}S_2$. The pattern of TB-20-CVS can be assigned to a mixture of $Cr_{0.5}V_{0.5}S_2$ and $Li_xCr_{0.5}V_{0.5}S_2$.
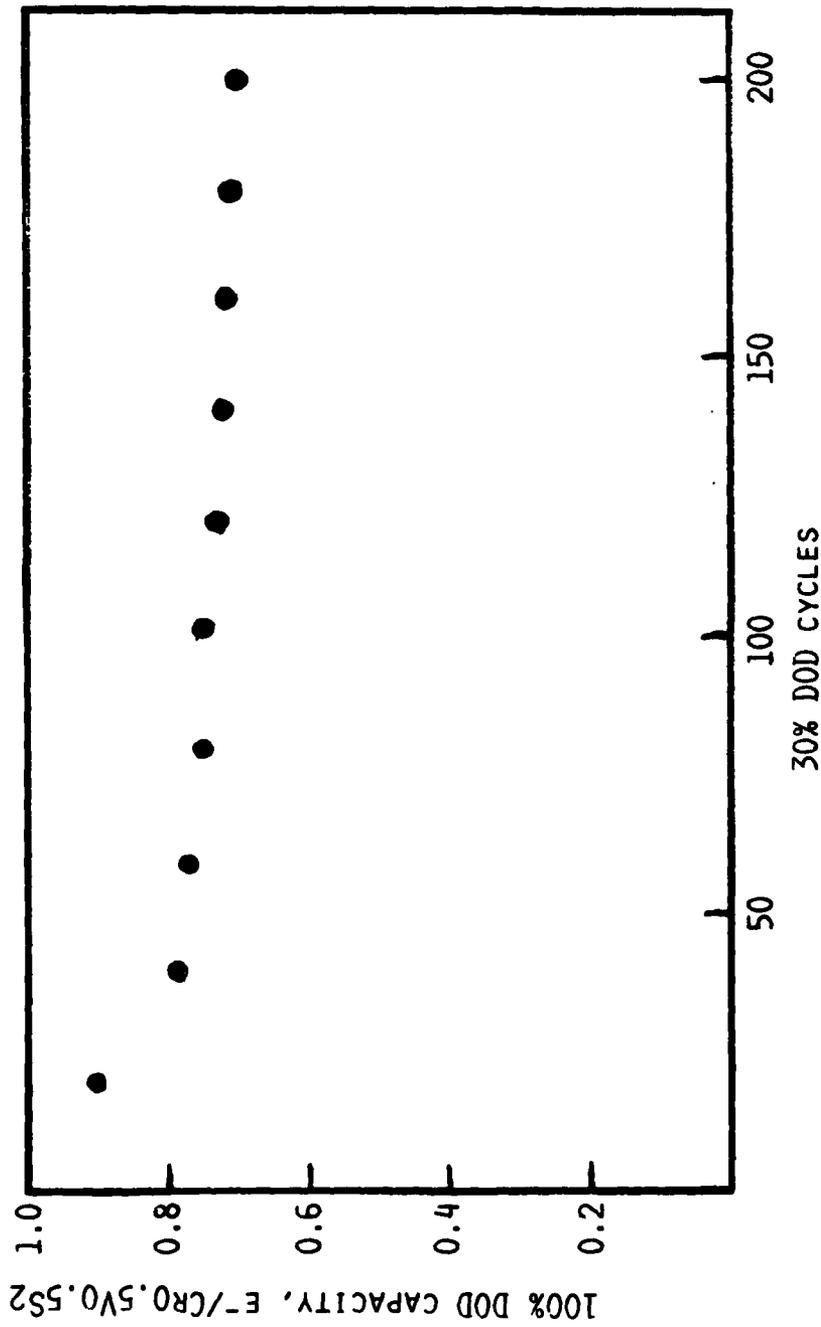
Fig. 30. The 100% DOD capacity of TB-25-CVS as a function of the 30% DOD cycles.

51

Table 9

X-Ray Data of Cycled Cathodes from Cells TB-19-CVS and TB-20-CVS

Cathode from TB-19-CVS		Cathode From TB-20-CVS		Shawinigan C	
d(Å)	$I_{(obs)}$	d(Å)	$I_{(obs)}$	d(Å)	$I_{(obs)}$
8.7	30	8.5	50	8.8	(diffuse)
5.64	80	5.86	100		
4.87	20	4.92	20	4.90	VS*
2.78	10	2.88	10	3.46	S,Vbr*
2.51	100	2.79	10		
2.32	40**	2.60	100		
2.00	90**	2.51	100		
1.64	10	2.06	50		
1.57	10	1.99	60		
1.42	20	1.61	40		
		1.57	20		
		1.54	10		
		1.42	10		
		1.35	10		
		1.25	10		

*VS, very strong, Vbr, very broad; S, strong.
**Also strongest lines of LiF. See Table 11.

The X-ray data show that the chemical integrity of $Cr_{0.5}V_{0.5}S_2$ does not change with extended cycling. Thus, for example, the X-ray data of none of the cycled cathodes showed any evidence for a reduction of $Cr_{0.5}V_{0.5}S_2$ forming Li_2S. The fact that the cycled TB-20-CVS cathode contains both $Cr_{0.5}V_{0.5}S_2$ and $Li_xCr_{0.5}V_{0.5}S_2$ suggests physical isolation of some of the discharged cathode material in the electrode matrix, eventually loosing contact with the bulk of the material. This is in agreement with the cycling data which suggest that a major reason for capacity fading with extended cycling is the difficulty in recharging a fraction of the discharged material.

The presence of LiF in TB-19-CVS probably has come from the reduction of $LiAsF_6$. It thus appears that some eduction of $LiAsF_6$ probably occurs during extended cycling. Since there is no evidence for LiF in TB-20-CVS, cycled essentially the same extent, it appears that this reduction is a minor process. It is noteworthy that in Cell TB-19-CVS, the electrolyte was 50:50 THF/2Me-THF/$LiAsF_6$. The conductivity of the electrolyte recovered from the various cells, shown in Table 10, indicates very little change from fresh solutions.

The UV-visible spectrum of the electrolyte from TB-20-CVS, is shown in Figure 31. The adsorptions at about 280 nm are due to electrolyte degradation products. Fresh 2Me-THF/$LiAsF_6$ solutions do not have any adsorptions at wavelengths higher than 250 nm.

3.6   Effects of Overcharge and Overdischarge on Cycle Performance

3.6.1   Overcharge

The effect of overcharge on cell cycle performance was evaluated with Cells TB-18-CVS and TB-22-CVS. Figures 20 and 28, respectively, depict the cycling history of these cells prior to the overcharge experiments.

3.6.1.1   Cell TB-18-CVS

Overcharge of TB-18-CVS began with cycle 102. Thirteen cycles were obtained at the voltage limits of 1.6-3.5 volts. The discharge current was 40 mA (2 mA/cm^2) and the charge current was 30 mA (1.5 mA/cm^2). A typical charge curve to 3.5V is shown by the 102nd charge given in Figure 32. The charge beyond 3.1V is characterized by a sloping region followed by a very small plateau at ~3.45V indicative of the onset of a second electrochemical process. What is interesting is that the capacity in the 13 cycles remained at about the same value as obtained with the 3.1V charge limit. It appears that the 3.5V charge limit does not have a deleterious effect on cell performance.

Table 10

Conductivity of Electrolyte Recovered from Cycled Cells

Cell Number	Specific Conductivity of Electrolyte $(\Omega cm)^{-1}$	Charge Passed/ml of Electrolyte (Ah)[1]
TB-19-CVS[2]	8.8×10^{-3}	4.1
TB-20-CVS	3.34×10^{-3}	~3.8
TB-21-CVS[3]	4.1×10^{-3}	~1.7
TB-22-CVS[3]	3.62×10^{-3}	~2.4

[1]Cathodic + anodic charge.

[2]1:1 THF/2Me-THF/LiAsF$_6$(1.5M), all others 2Me-THF/LiAsF$_6$(1.3M).

[3]Discussion of these cells are presented in the next section.
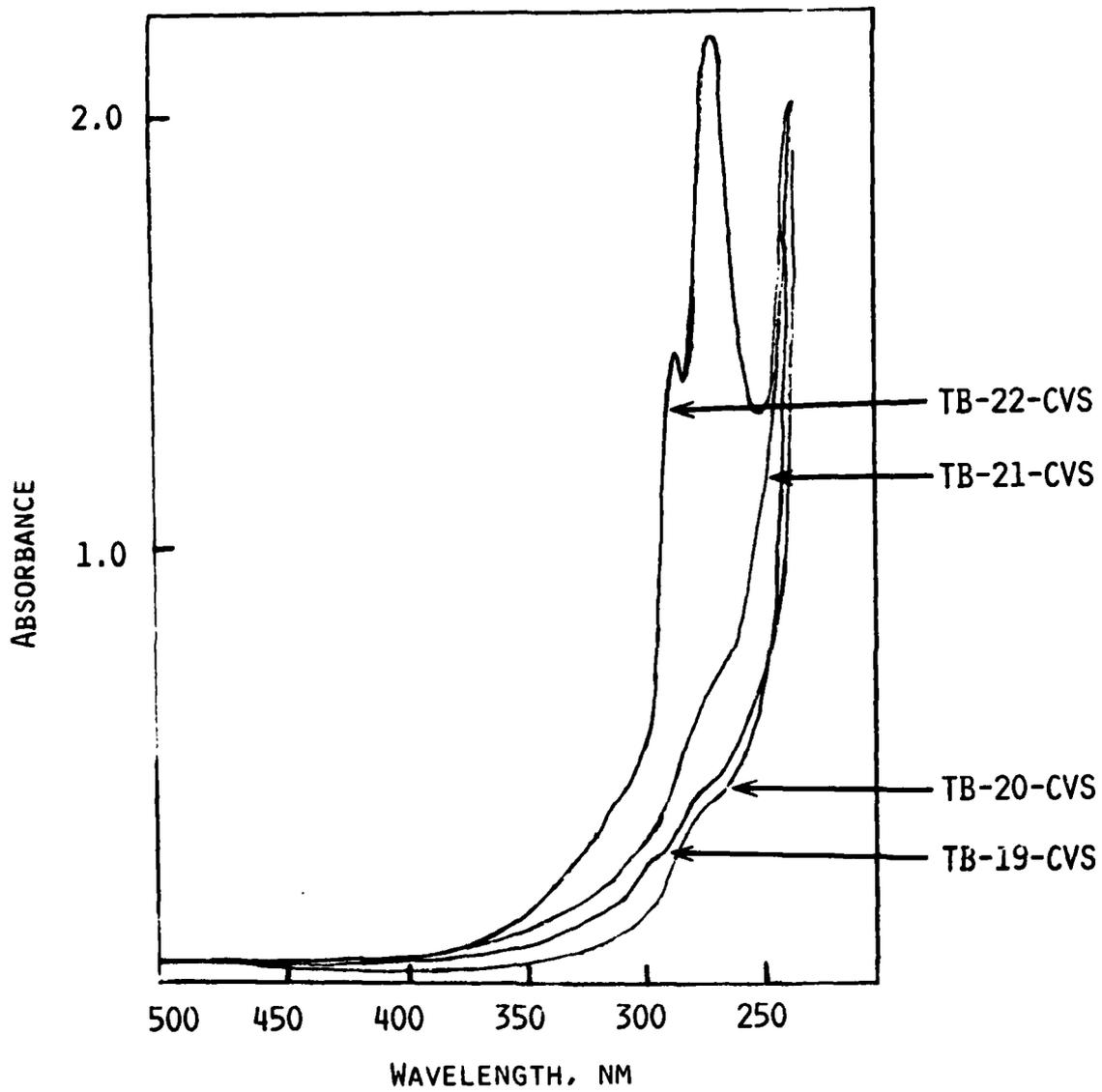
Fig. 31. UV-visible spectra of electrolyte from cycled cells.

Beginning with the 115th charge, the charge limit was increased to 4V. As seen in Figure 32, a substantial charge capacity was obtained between 3.5 and 4V. A portion of this charge capacity is most probably due to electrolyte oxidation. However, some oxidation of the sulfide may also occur. This is indicated by a change in the shape of the following discharge curve which does not have the curvature seen in the earlier discharges. Instead, the discharge exhibits a linear voltage profile with a larger slope. There was also an increase in the capacity of the discharge tol.6V. Five cycles were obtained with this charge limit. The cell did not fail. Rather, it showed a tendency to perform better. The utilization increased to greater than 60% by the 121st discharge. It should be noted that potential profiles of the portion of the charge between 3.5 and 4V showed significant changes on going from the 115th to 121st cycle.

3.6.1.2 Cell TB-22-CVS

Overcharge of TB-22-CVS began with cycle 71. Typical cycles corresponding to the various overcharge regions are given in Figure 33. Cycles 71 to 78 were performed with a charge limit of 3.5V and a discharge limit of 1.6V. The current densities were 2 mA/cm^2 for discharge and 1.5 mA/cm^2 for charge. The utilization remained at a relatively constant 55% in the seven cycles from 72-78. The data reinforce the findings in Cell TB-18-CVS that a charge limit of 3.5V *does* not have a deleterious effect on the performance of the cell.

Cycles 79 to 87 were performed with a charge limit of 3.7V and a discharge limit of 1.6V. The current densities were, again, 2 and 1.5 mA/cm^2 for discharge and charge respectively. Again, there was no adverse effect of the higher charge limit on cell performance. The utilization was a nearly constant 55% up to the 87th discharge.

Between cycles 88 and 103, the charge limit was maintained at 4V. The other parameters were the same as in the above cases. The capacity showed a gradual increase, reaching nearly 0.7e$^-$/Cr$_{0.5}$V$_{0.5}$S$_2$ (70% of the theoretical) by the 92nd cycled. Thereafter, the utilization remained relatively constant such that it was still 67% at the 103rd discharge. It appears that a charge limit of 4V does not have an immediate adverse effect on cell performance.

Cycles 104 to 107 were performed with a charge limit of 4.5V. Again, there was not any immediately noticeable adverse effect of the higher voltage limit on cell performance.

The results of the overcharge experiments indicate that Li/Cr$_{0.5}$V$_{0.5}$S$_2$ cells with 2Me-THF/LiAsF$_6$ can be overcharged without an immediate adverse effect on the cell's cycling performance.
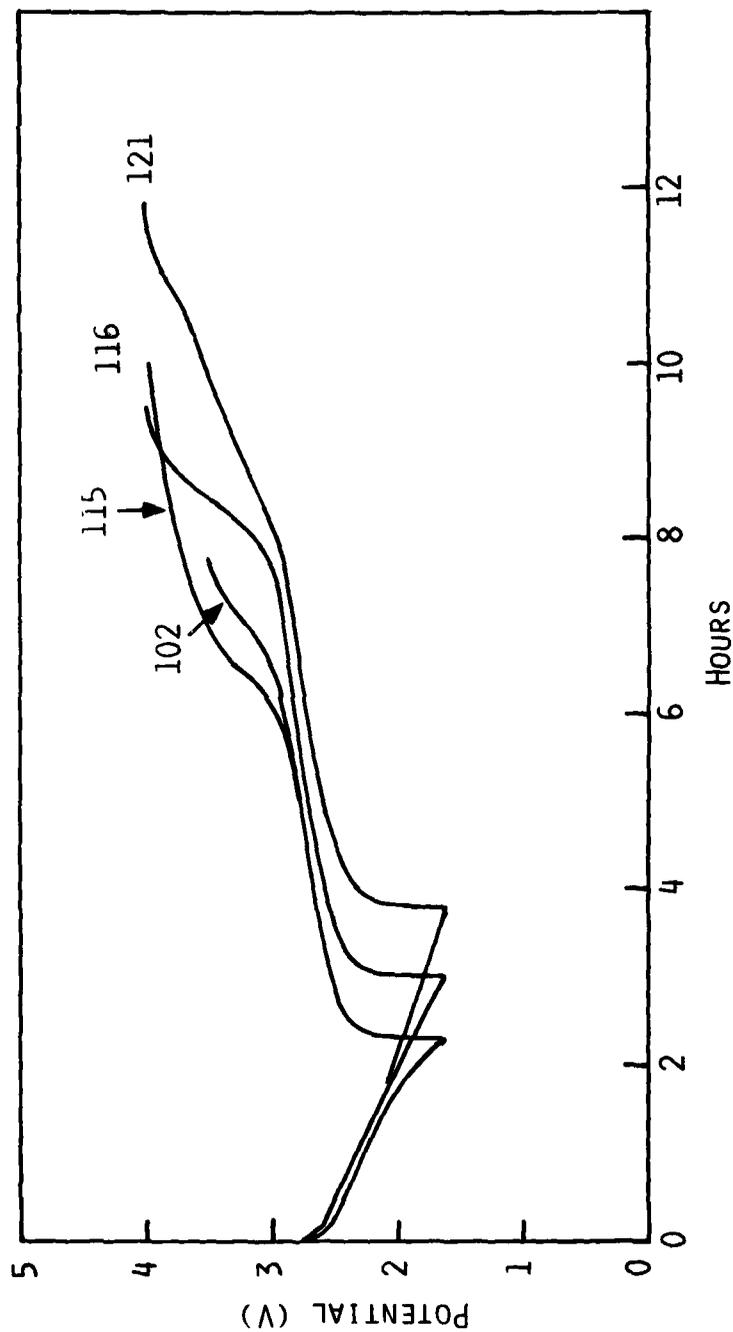
Fig. 32. Typical overcharge cycles for cell number TB-18-CVS. Current: i_d = 2 mA/cm^2 (40 mA); i_c = 1.5 mA/cm^2 (30 mA).

Cycle No.: 102, 1.6-3.5V - 1st cycle charged to 3.5V
115, 1.6-4.0V - 1st cycle charged to 4.0V
116, 1.6-4.0V - 2nd cycle charged to 4.0V
121, 1.6-4.0V - 7th cycle charged to 4.0V
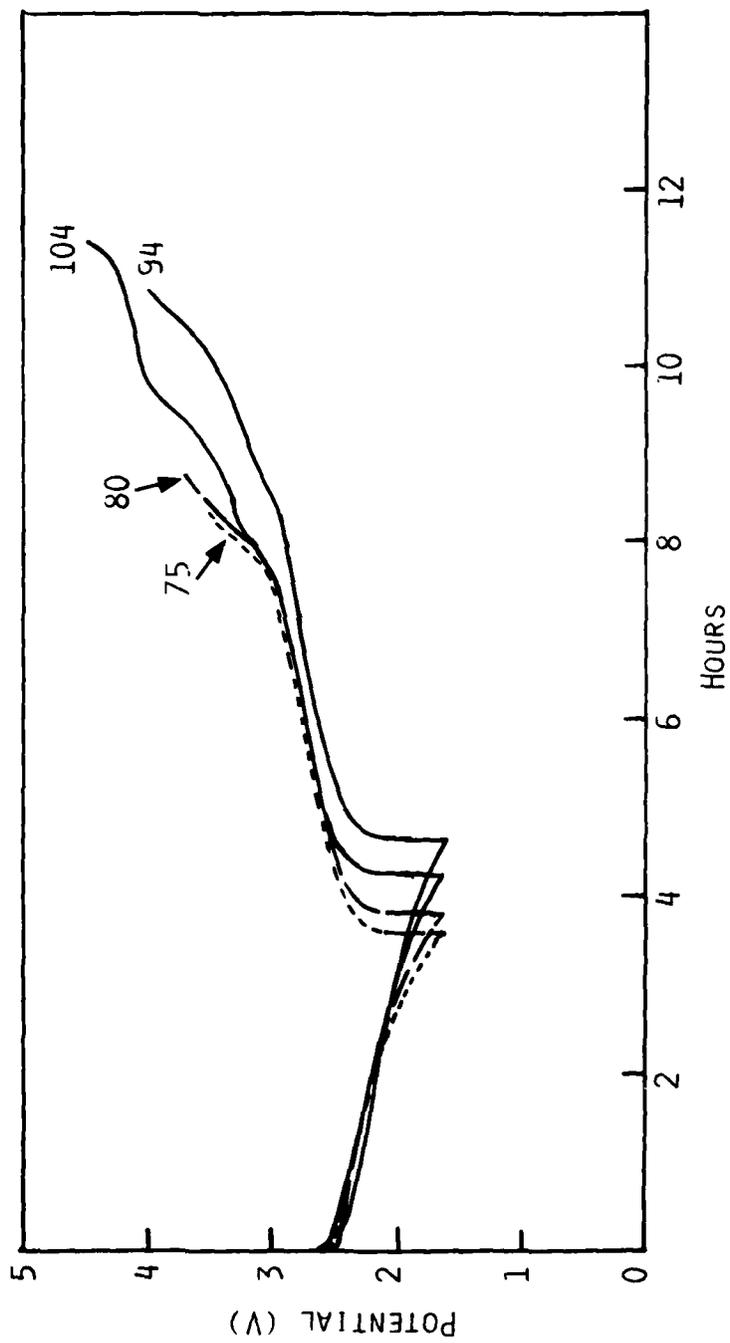
Fig. 33. Typical overcharge cycles for cell number TB-22-CVS.
id = 2 mA/cm^2, ic = 1.5 mA/cm^2.

58

3.6.2 Analysis of Overcharged Cells

The UV-visible spectrum of the electrolyte from the repeatedly over-charged Cell TB-22-CVS, shown in Figure 31, indicates that the overcharge leads to extensive electrolyte degradation. Despite this degradation, the overcharge does not have an immediate adverse effect on the cell's performance. It is noteworthy that the conductivity of the electrolyte (Table 10), recovered from Cell TB-22-CVS is nearly identical to that of fresh solutions.

3.6.3 Overdischarge

The effect of a discharge below the normal cutoff of 1.6V on the performance of the cell was evaluated in Cell TB-21-CVS. The data for the first 67 cycles of the cell was given in Figure 27. In the 68th discharge, the discharge voltage limit was lowered to 1.0V. The discharge is shown in Figure 34. It is characterized by an additional plateau beginning at ~1.5V. The adverse effect of the overdischarge on the cell's cycling ability is clearly indicated by the immediate failure of the cell. The results indicate that $Li/Cr_{0.5}V_{0.5}S_2$ cells with $2Me-THF/LiAsF_6$ should not be dis-charged below ~1.5V.

3.6.4 Analysis of Overdischarged Cells

The conductivity of the electrolyte, recovered from Cell TB-21-CVS indicates that the electrolyte conductivity has changed very little due to the overdischarge. Similarly, the UV-visible spectrum, shown in Figure 31, is identical to that of electrolytes from cells which have been extensively cycled between the limits of 1.6 and 3.1 volts.

The X-ray diffraction pattern of the cathode from Cell TB-21-CVS is more informative with respect to the processes which occur during over-discharge. The X-ray pattern is shown in Table 11. The cathode had been washed with diethyl ether to remove any adhering $LiAsF_6$. As mentioned earlier, the lines at 4.90 and 8.5 Å are most probably due to the Shawini-gan carbon. Among others, all lines except those at 2.32 and 2.01 Å are due to $LiCr_{0.5}V_{0.5}S_2$. The lines at 2.32 and 2.01 Å are the strongest lines in the pattern of LiF (see Table 11). The X-ray data show no evidence for Li_2S.

It appears that a predominant process in the overdischarge between 1.5 and 1.0V is the reduction of the salt, producing LiF. The relatively small change in the conductivity of the solution is probably due to the fact that the coulombic capacity of the overdischarge is relatively small in comparison to the amount of electrolyte present in the cell. The X-ray data seem to suggest that the cathode irreversibility after the overdis-charge may have been due to filming of or deposition on the electrode of insoluble LiF.
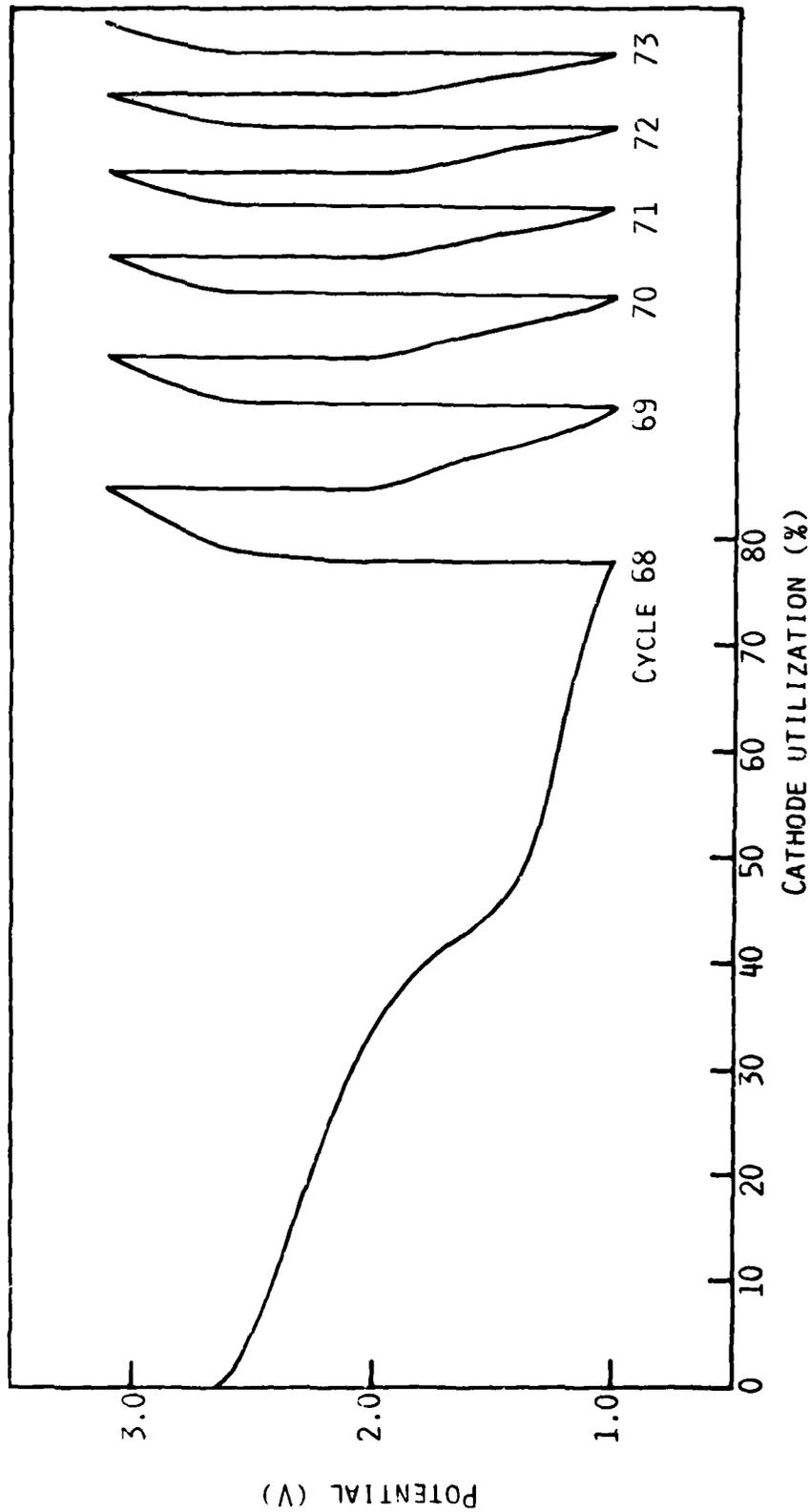
Fig. 34. Effect of overdischarge on Cell TB-21-CVS. Cycle limits = 1.0–3.1V. $i_d = i_c = 2$ mA/cm².

Table 11

X-Ray Diffraction Data of Cathode from TB-21-CVS

Cathode from TB-21-CVS		LiF	
d(Å)	I(obs)	d(Å)	I(obs)
8.5	30		
5.98	100		
4.90	40		
2.96	20		
2.64	100		
2.48	20		
2.32	10	2.32	95
2.11	90		
2.01	10	2.01	100
1.71	40		
1.66	30		
1.44	10	1.42	48
1.33	10		
1.19	10	1.22	10
1.13	10	1.16	11

3.7   Electrolytes with Improved Low Temperature Performance

It is apparent from the data presented in Section 3.3.2 that the low temperature performance of cells with 2Me-THF/LiAsF$_6$ is very poor. The results from Cell TB-19-CVS indicate that the low temperature of the cells can be improved by blending 2Me-THF/LiAsF$_6$(1.4M) with THF. Further studies of 2Me-THF/LiAsF$_6$ solutions blended with THF, as well as THF and 1,2-dimethoxy ethane (DME) have been carried out.

3.7.1   Conductivity Studies of 2Me-THF/THF/LiAsF$_6$ Solutions

Specific conductivities have been measured at 25, 0 and -20°C for 2Me-THF/THF/LiAsF$_6$(1.5M) solutions as a function of the amount (volume percent) of 2Me-THF. The data are presented in Figure 35. The conductivity at room temperature decreases in a linear fashion on going from 100% THF to 100% 2Me-THF. A similar behavior is seen also at 0 and -20°C. However, at -20°C, the solutions containing <10 volume-percent THF freeze. This freezing of the solution, more aptly termed crystallization of LiAsF$_6 \cdot$(solvent)$_n$ solvates, explains the rather poor low temperature performance of cells with 2Me-THF/LiAsF$_6$.

At each temperature, the 50:50 THF/2Me-THF/LiAsF$_6$(1.5M) solution has about twice the conductivity of 2Me-THF/LiAsF$_6$(1.5M). Furthermore, the -20°C conductivity of the 50:50 solution is slightly better than the room temperature conductivity of 2Me-THF/LiAsF$_6$(1.5M). Practical implications of the results are obvious.

We have also measured the specific conductivity of the 50:50 THF/2Me-THF/LiAsF$_6$ solutions as a function of the concentration of LiAsF$_6$. The data are depicted in Figure 36. The room temperature conductivities of THF and 2Me-THF solutions are included for comparison. The highest conductivity in the 50:50 blend at room temperature is observed at a LiAsF$_6$ concentration of 1.5M. It is interesting to note that the solutions in the 50:50 blend with LiAsF$_6$ concentrations $\leq$1M do not freeze even at -40°C. Furthermore, the -40°C conductivity of the 1M LiAsF$_6$ solution in the 50:50 blend is practically identical to that of the room temperature conductivity of the 2Me-THF/LiAsF$_6$(1-1.2M) solutions.

3.7.2   Conductivity Studies of THF/2Me-THF/DME/LiAsF$_6$ Ternary Solutions

Conductivity measurements of three ternary electrolyte solutions, THF(50 v/o):2Me-THF(40 v/o):DME(10 v/o)/1.5M LiAsF$_6$, THF(50 v/o):2Me-THF(30 v/o):DME(20 v/o)/1.5M LiAsF$_6$, and THF(50 v/o):2Me-THF(20 v/o):DME(30 v/o)/1.5M LiAsF$_6$ have been carried out over the temperature range of -40 to 25°C. The data are plotted in Figure 37. The conductivities of THF(50 v/o):2Me-THF(50 v/o)/1.5M LiAsF$_6$ measured over the same temperature range are included

Fig. 35. Specific conductivity vs volume percent of 2Me-THF in 2Me-THF/THF/1.5M LiAsF$_6$ electrolyte at various temperatures.

63
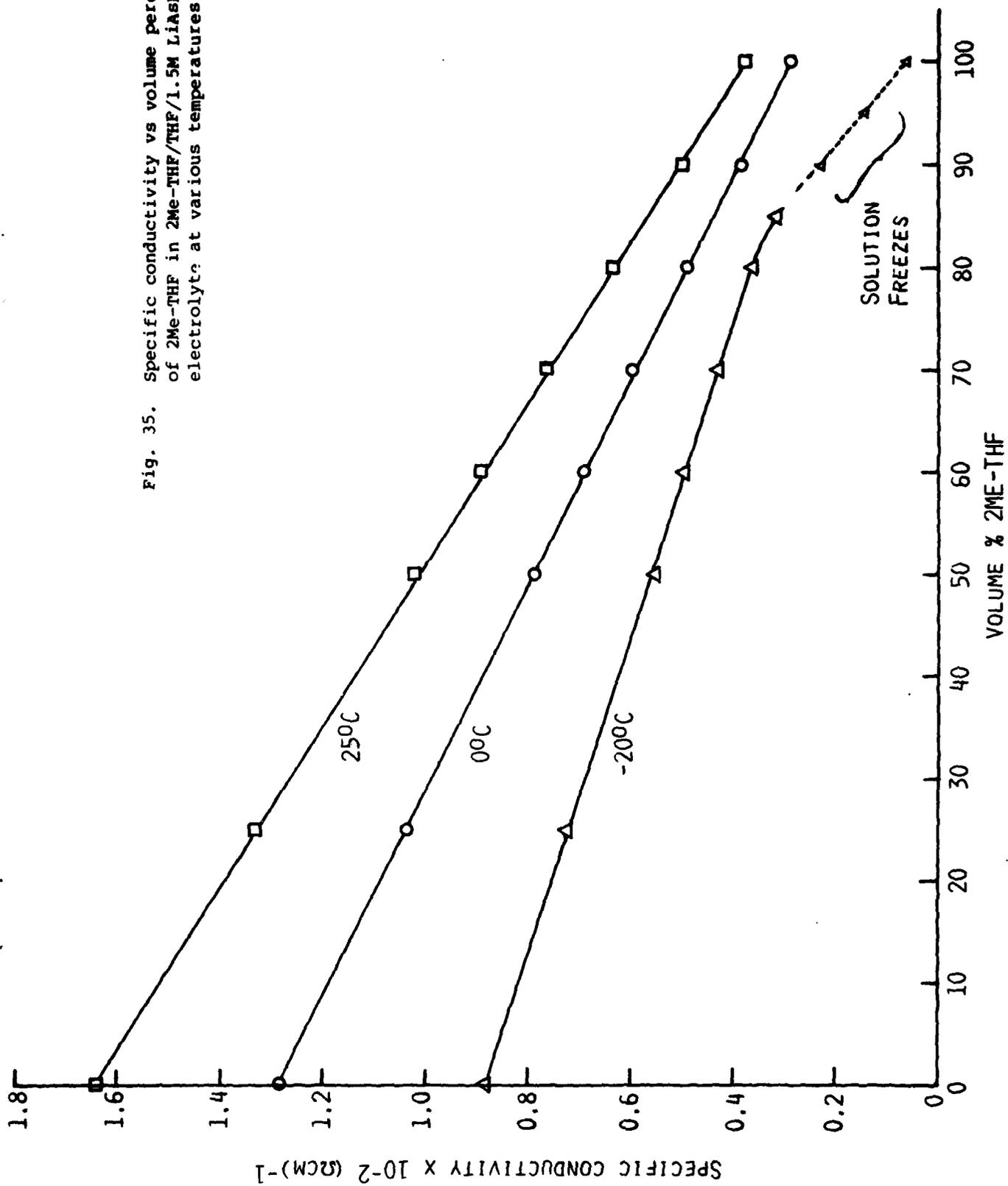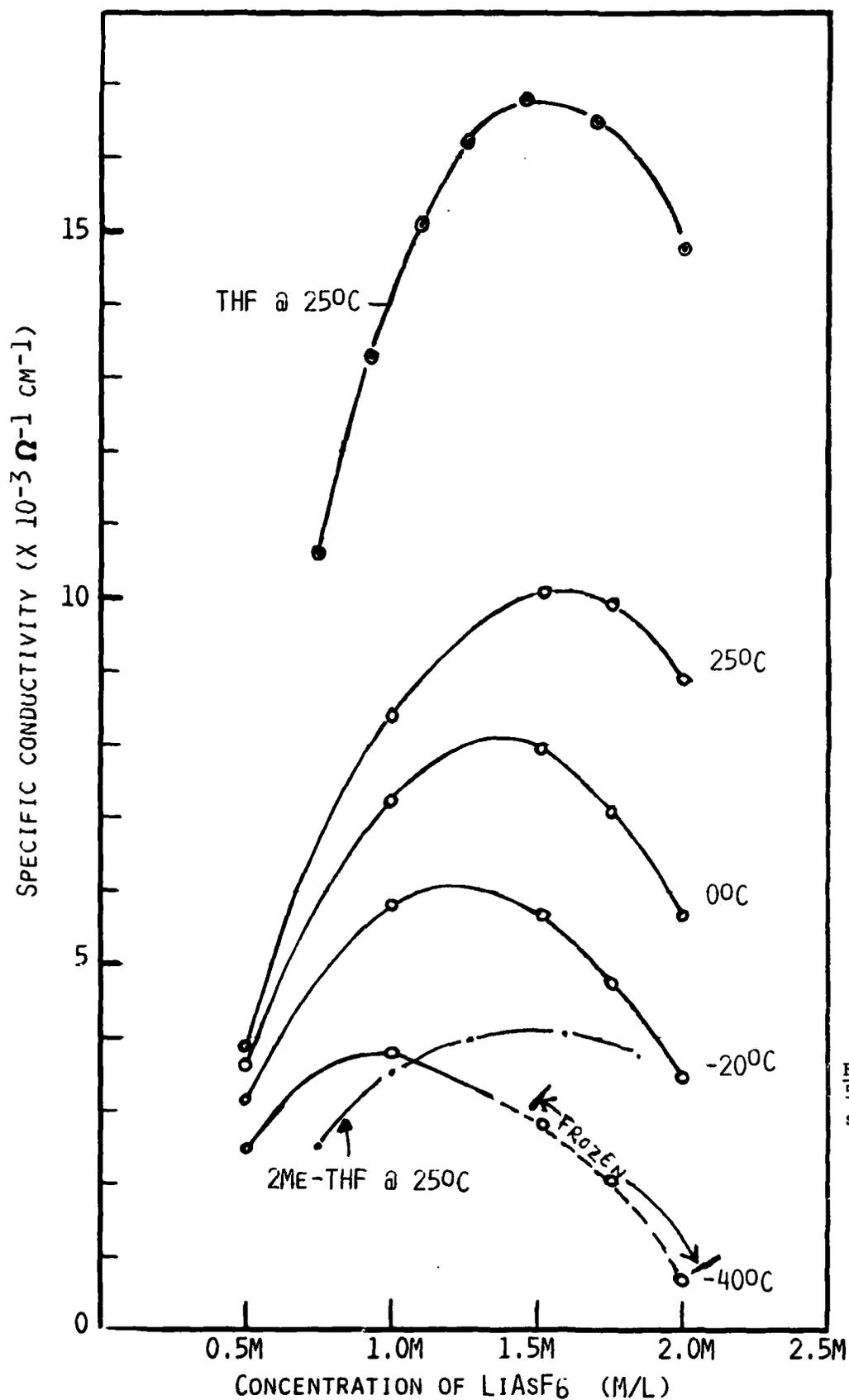
Fig. 36. Conductivity of 50:50 2Me-THF/THF (LiAsF$_6$) solutions.
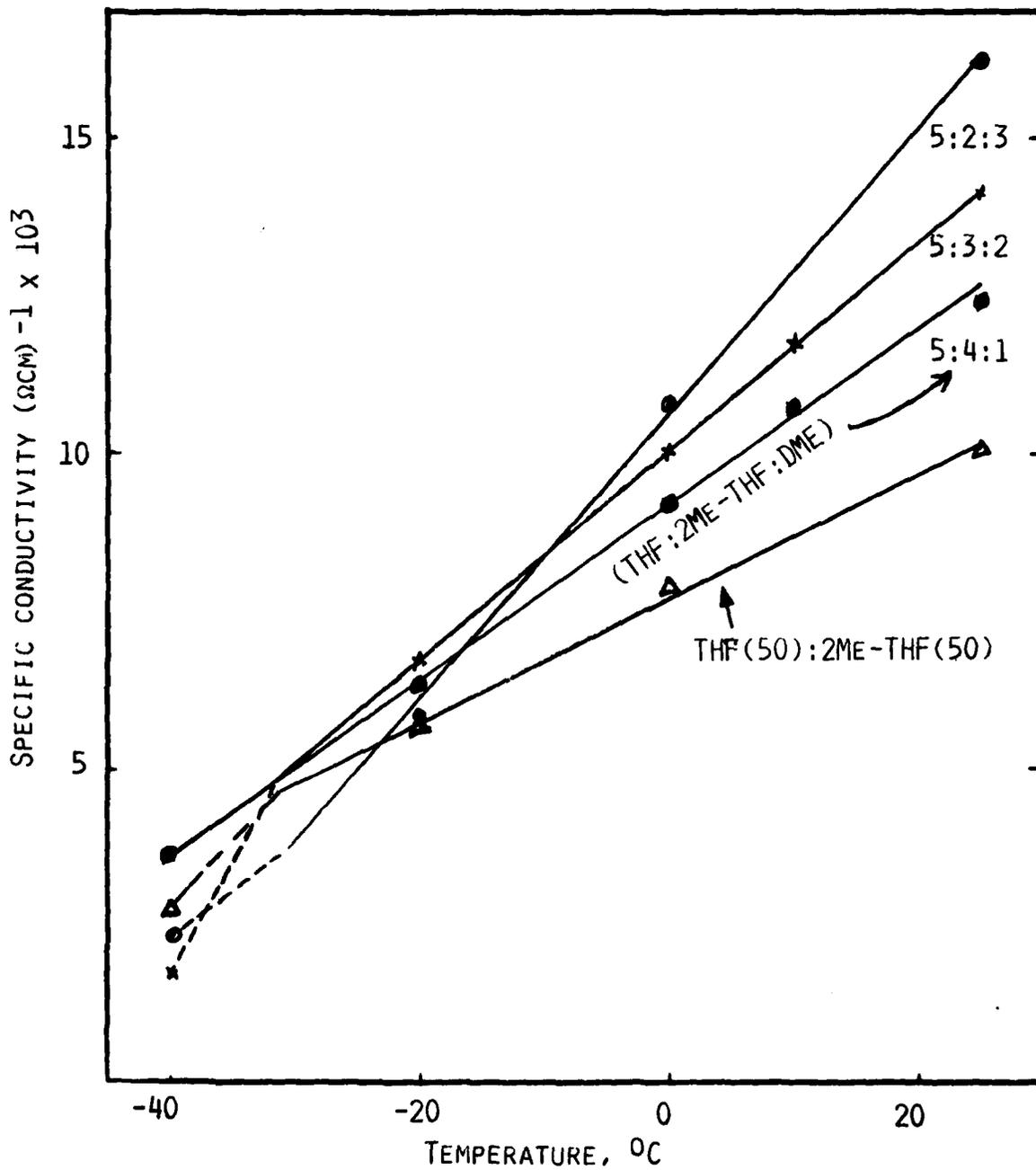
Fig. 37.   Conductivity of ternary electrolytes versus temperature.
All solutions 1.5M in LiAsF₆.

65

for comparison. The dotted lines indicate, approximately, the temperature regions where some of the solutions freeze. The THF(50 v/o):2Me-THF(40 v/o):DME(10 v/o)/1.5M LiAsF$_6$ solution remains a fluid even at -40°C. Its conductivity at -40°C is practically identical to that of 2Me-THF/1.5M LiAsF$_6$ at 25°C. The conductivity data show that the solution worthy of further consideration is THF(50 v/o):2Me-THF(40 v/o):DME(10 v/o)/1.5M LiAsF$_6$. This solution will hereafter be referred to as TMD/LiAsF$_6$(1.5M).

3.7.3 Cell Studies in Blended Solutions

The significant effect expected with the blended solutions is improved low temperature performance. However, in order for the solutions to be useful in practical cells, the Li electrode must cycle with acceptable cycling efficiencies.

3.7.3.1 Low Temperature Performance of Cells

The improved low temperature performance of cells with the 50:50 2Me-THF/THF/LiAsF$_6$(1.5M) solution has already been discussed (see Fig. 15). Cell TB-19-CVS at -10°C exhibited a capacity nearly 70% of the theoretical at current densities of 1 and 2 mA/cm^2. In contrast, the capacity of the 2Me-THF/LiAsF$_6$(1.4M) cell at -10°C and 2 mA/cm^2 is only ~14% of the theoretical cell capacity.

The rate-capacity characteristics of a cell with TMD/LiAsF$_6$(1.5M) are shown in Figure 38. The -30°C behavior of this cell is similar to that of the cell with 50:50 THF/2Me-THF/LiAsF$_6$(1.5M) (see Fig. 15). A cathode utilization of ~80% of the theoretical capacity is obtained in the present cell at -30°C with a discharge rate of 0.25 mA/cm^2. At -20°C, utilizations greater than 60% have been obtained at current densities of 0.5, 1 and 2 mA/cm^2. Clearly, this is a significant improvement over 2Me-THF/LiAsF$_6$(1.4M).

3.7.3.2 Li Electrode Cycling Efficiencies

The Li electrode cycling efficiency in 50:50 THF/2Me-THF/LiAsF$_6$(1.5M) has been calculated from the data in Figure 20, obtained with TB-19-CVS. The cycling efficiency is 93% (Figure of Merit, FOM$_{Li}$ = 14). This is to be compared with the typical FOM$_{Li}$ of 30-40 in 2Me-THF/LiAsF$_6$(1.4M). Clearly, there is a substantial reduction of Li cycling efficiency in the blended solution. However, the significantly improved low temperature performance of the cells would make this solution desirable for applications where some cycle life of the cell could be sacrificed for better low temperature performance.

The room temperature cycling behavior of a cell with TMD/LiAsF$_6$(1.5M) is depicted in Figure 39. Typical cycling curves are shown in Figure 40. This cell is to be compared with TB-19-CVS (Fig. 20). Note that the capacity in this cell faded to less than 50% of the theoretical by the 50th cycle
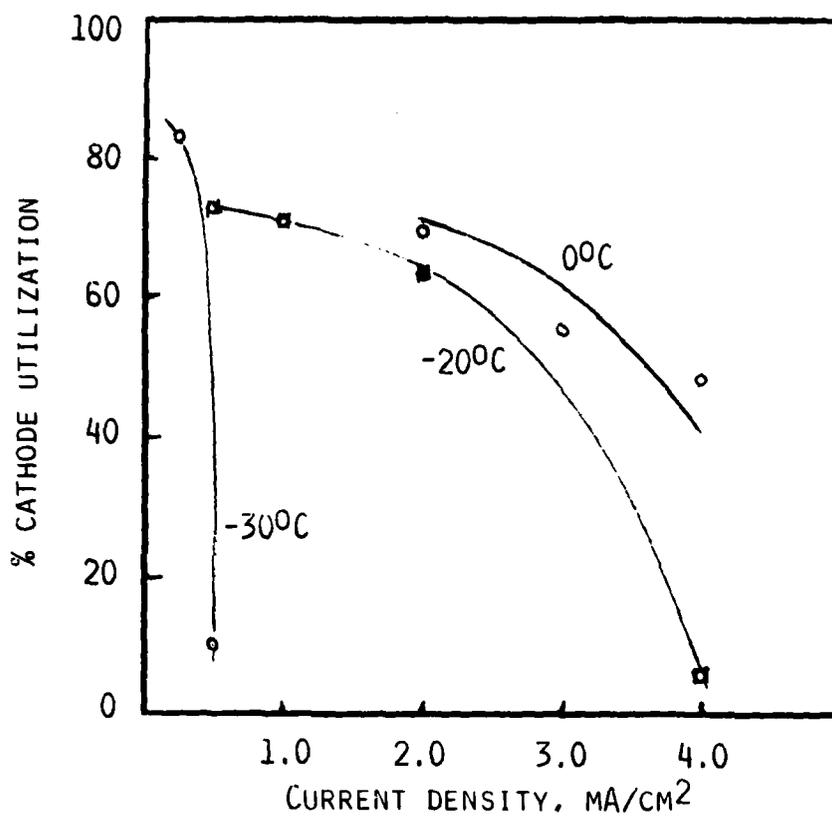
Fig. 38.   Cathode utilization (%) versus current density
for a Li/Cr$_{0.5}$V$_{0.5}$S$_2$ cell at -30, -20 and 0°C.
The electrolyte is TMD/1.5M LiAsF$_6$.
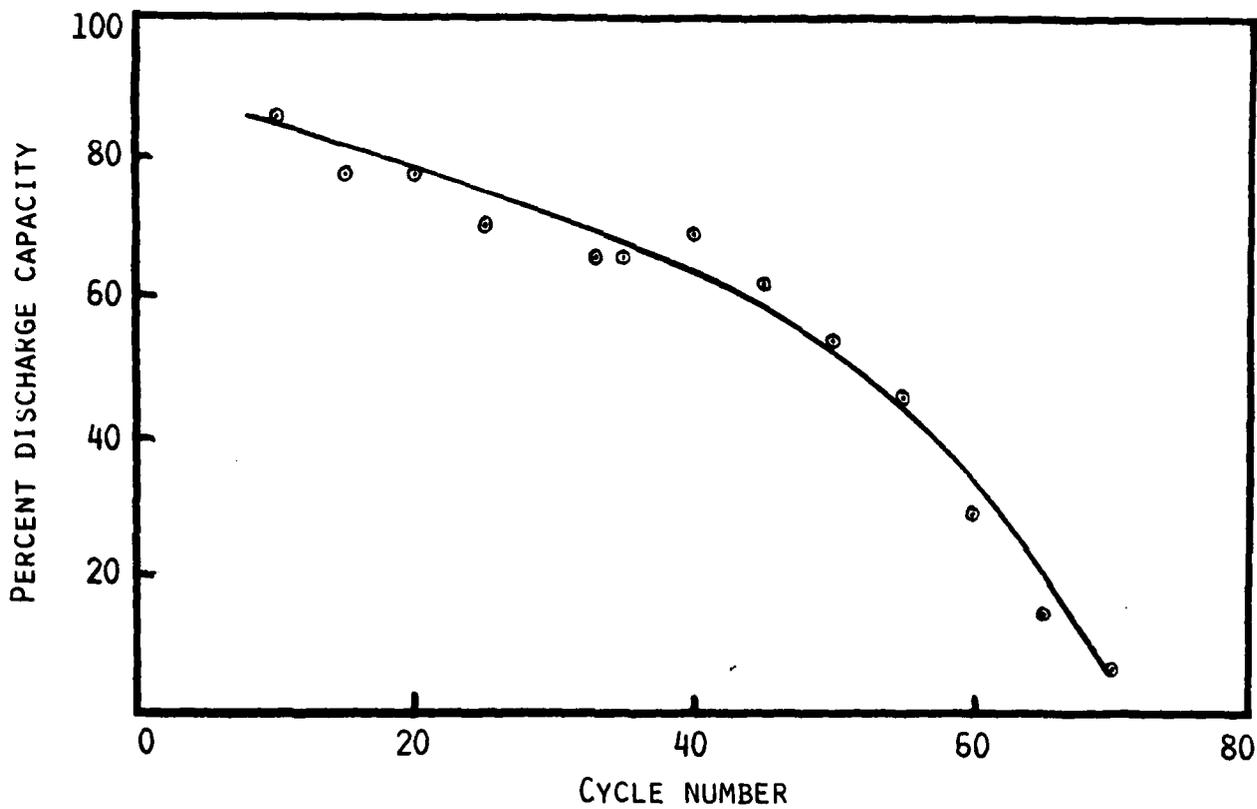
Fig. 39. Capacity versus cycle number for a $Li/Cr_{0.5}V_{0.5}S_2$ cell with $TMD/LiAsF_6(1.5M)$.
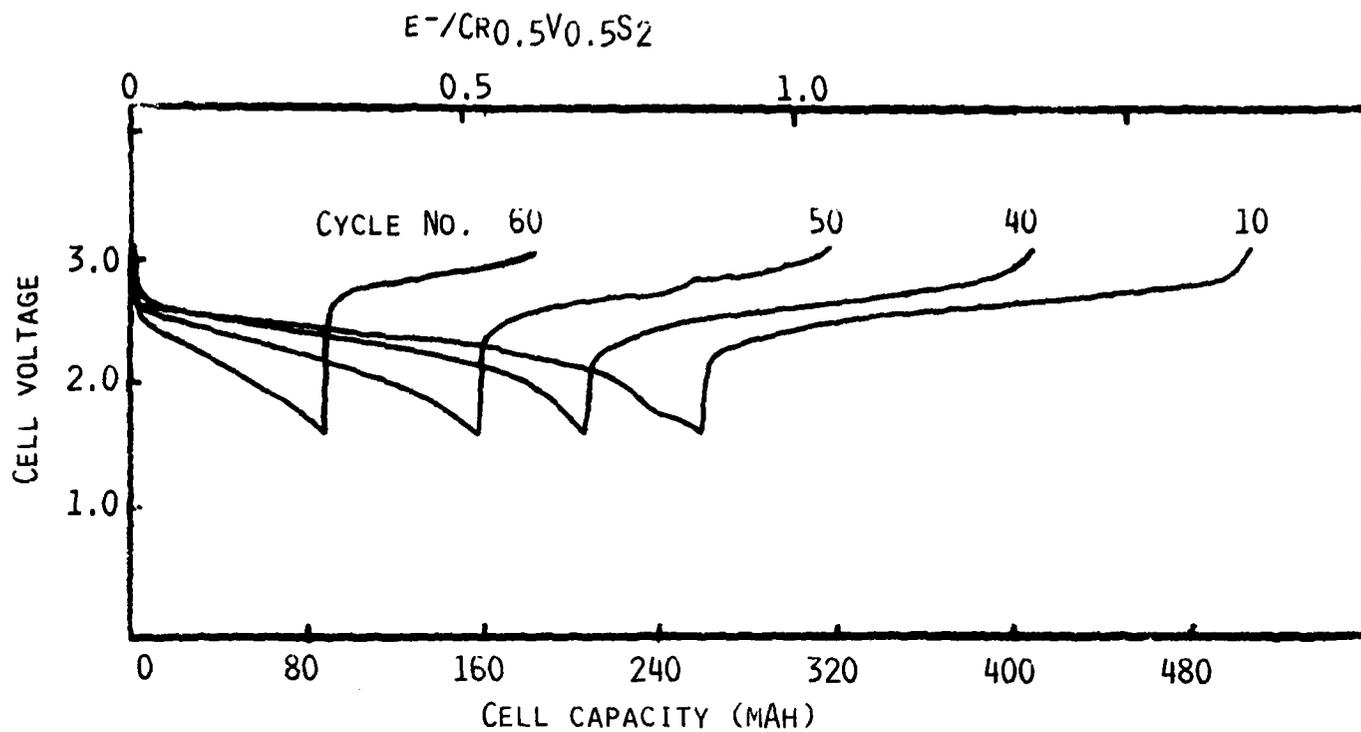
Fig. 40. Typical cycling curves of a $Li/Cr_{0.5}V_{0.5}S_2$ cell with TMD/$LiAsF_6$(1.5M). Current density, 1 mA/cm^2.

and the cell failed completely by the 70th cycle. The cycling efficiency of the Li electrode corresponds to only ~80% (FOM_{Li} = ~5).

In conclusion, the limited amount of work carried out in this program has shown that the low temperature performance of cells with 2Me-THF/$LiAsF_6$ solutions can be improved by judiciously blending the electrolyte with a second ether component such as THF. The 50:50 THF/2Me-THF/$LiAsF_6$(1.5M) solution appears to be suitable for limited cycle life cells. However, much further work is needed to fully explore this field.

4.0 CONSTRUCTION AND TESTING OF HERMETICALLY SEALED HIGH CAPACITY CELLS

Hermetically sealed, flat plate cells with approximately 10 and 20 Ah theoretical capacities (based on 1 $Li/Cr_{0.5}V_{0.5}S_2$) have been constructed. Both of these cells have the same electrode dimensions; they differ only in the number of electrode plates. Two of each type have been built. The 20 Ah cells have been cycled once at EIC and then sent to ERADCOM for further evaluation. The two 10 Ah cells have been cycled at EIC.

4.1 Cell Features

A schematic of the cell design is shown in Figure 41. The cells have been fabricated in a commercially available stainless steel can (Hudson Tool and Die Company, Inc., Can No. 76401). A readily available can off-the-shelf was chosen because of the limited number of cells being produced. The cans therefore are heavier (wall thickness, 36 mil) than would be desirable in cells for field applications. A can with its largest face open (that is the face parallel to the electrode face) was chosen primarily because placement of the electrode package in the can is facilitated since compression of the package is accomplished after rather than during placement in the can. Another advantage is that the cell capacity can be changed without changing the electrode dimensions by cutting the can to the proper depth.

4.1.1 Cathodes

Each cathode has an area of 9.96 x 9.25 cm = 92.13 cm^2/side. The electrode thickness ranges from 0.875 to 1.0 mm. The cathode composition is 70 w/o $Cr_{0.5}V_{0.5}S_2$, 20 w/o C (Shawinigan 50% compressed) and 10 w/o Teflon. The cathodes have been fabricated by pasting a slurry of the cathode mix in decane on either side of a 1 mil thick pierced nickel foil. The decane from the electrode was removed by prolonged pumping in vacuum until the electrodes attained constant weight. A photograph of the finished electrode is shown in Figure 42.

4.1.2 Anodes

Anodes were prepared by pressing 15 mil Li foil onto each side of an expanded Ni screen. The tab consisted of 1 mil thick, 0.2 inch wide Ni strips welded on one edge of the screen and extending to the length of the grid.

4.1.3 Assembly

Anodes and cathodes were heat-sealed in bags of Celgard 2400 separator. They were alternatively stacked into the cell case. The latter contained a layer of a FEP membrane insulator. The electrode tabs were

71
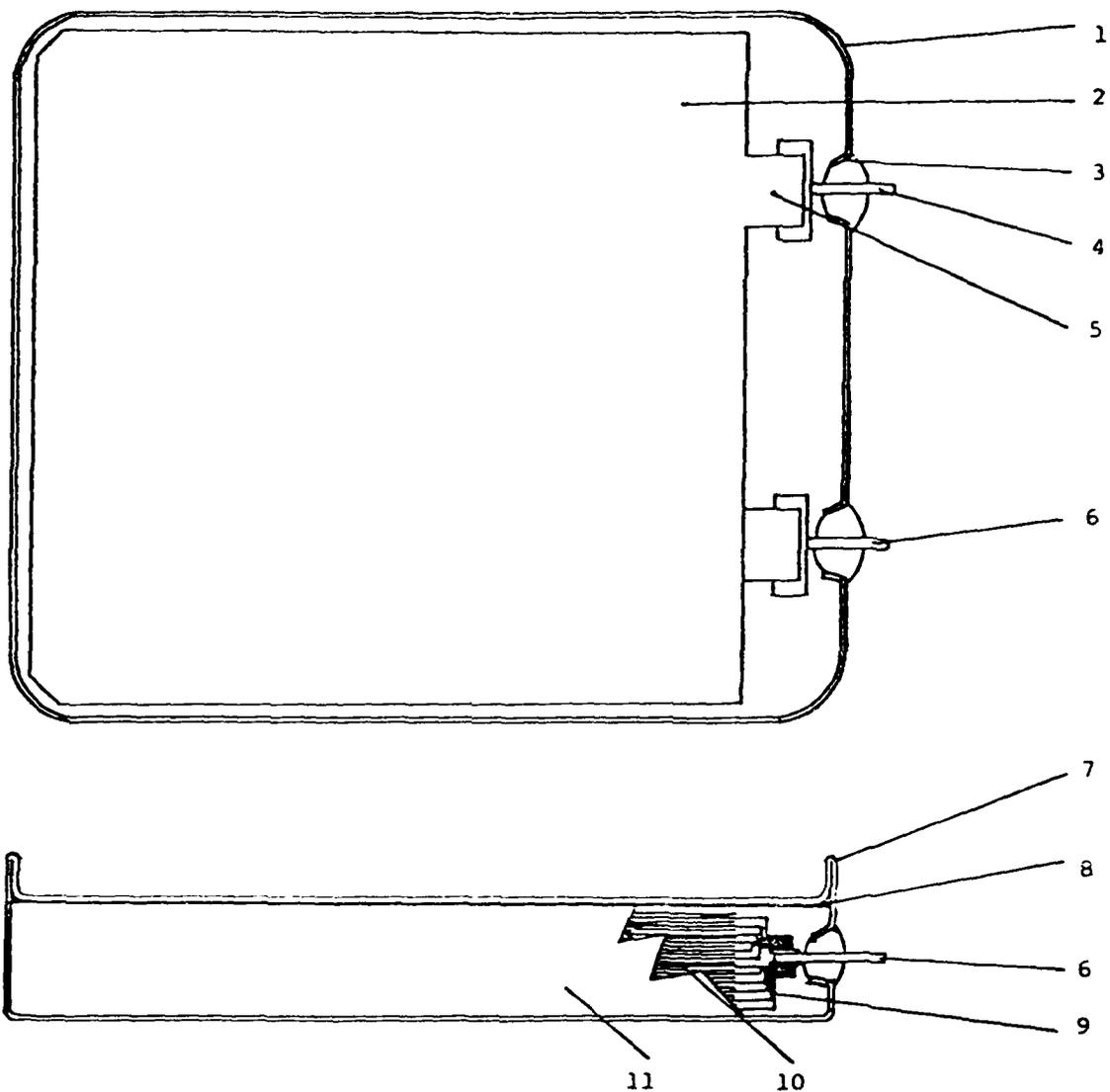
1. Hudson can No. 7640
2. Negative electrode
3. Glass to metal seal
4. Negative terminal
5. Lead to negative terminal
6. Positive terminal

7. Can-cover weld
8. PTFE sheet
9. Leads to positive terminal
10. Alternating electrodes with Celgard 2400 between each pair
11. Celgard 2400

Fig. 41.   Schematic of flat plate secondary Li battery.
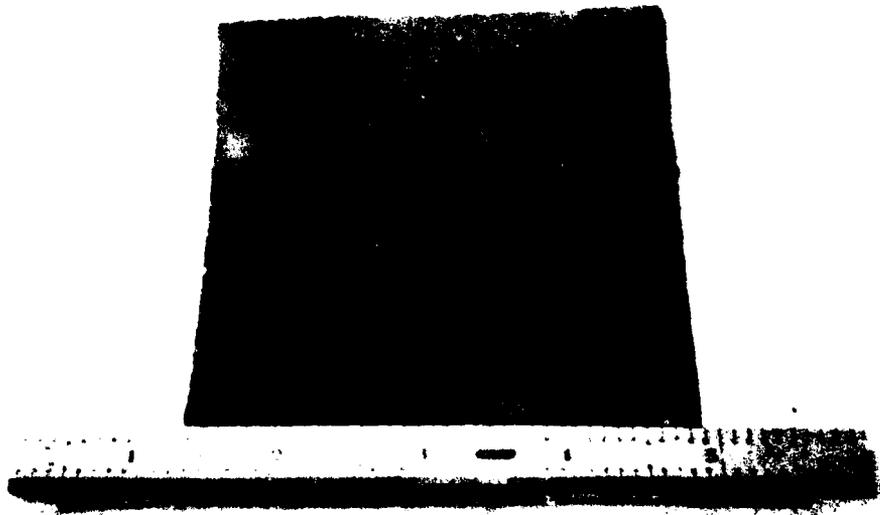
Fig. 42. Photograph of a finished cathode for 20 Ah cell.

joined to the bus bar comb by TIG welding. The completed electrode stack assembly was compressed, the cover secured by spot welds and subsequently hermetically sealed by TIG welding. The cells were filled with electrolyte after evacuation. Subsequently, the fill holes were hermetically sealed by TIG welding. A picture of the assembled cell without the cover is shown in Figure 43. The finished cell is shown in Figure 44.

4.2   The 20 Ah Cells

Each cell comprises 14 cathode and 15 anode plates. The theoretical cell capacity is $\sim$20 Ah based on $1e^-/Cr_{0.5}V_{0.5}S_2$. The cell is rated for 15 Ah or 75% of the theoretical capacity. The specifications of the 20 Ah cells, Cell 285-011 and 285-013, are listed in Table 12. One cell was filled with 2Me-THF/LiAsF$_6$(1.4M). The other cell was filled with the high rate solution, 50:50 THF/2Me-THF/LiAsF$_6$(1.5M).

4.2.1   Performance of the 20 Ah Cells

Both cf the cells were cycled once at 1A (0.39 mA/cm^2) between voltage limits of 1.6V and 3.1V. The cells delivered 19.7 Ah and 18.5 Ah respectively. The cycling curves are given in Figures 45A and 45B. The realized capacities correspond to >92% of the theoretical cathode capacities.

4.2.2   Further Evaluation of 20 Ah Cells

The two cells have been sent to ERADCOM for further evaluation.

4.3   The 10 Ah Cells

The specifications of the 10 Ah cells are shown in Table 13. Cell No. 285-014 was filled with 2Me-THF/LiAsF$_6$(1.4M) and Cell No. 285-015 was filled with 50:50 2Me-THF/THF/LiAsF$_6$(1.5M).

4.3.1   Cycling of 10 Ah Cells

Initially, the cells were cycled at room temperature between voltage limits of 1.6 and 3.1 with 1A total current (0.54 mA/cm^2). Both of the cells were subsequently cycled at 0°C. Cell No. 285-015 with 50:50 THF/2Me-THF/LiAsF$_6$(1.5M) was cycled at -20°C also. After the low temperature rate/capacity evaluation, both of the cells were subjected to extended cycling at room temperature with a total current of 1A between limits of 1.6 and 3.1 volts.

The data corresponding to the early cycles at various temperatures are summarized in Tables 14 and 15. The cycles of Cell No. 285-015 at 0°C and -20°C are depicted in Figures 46 and 47.
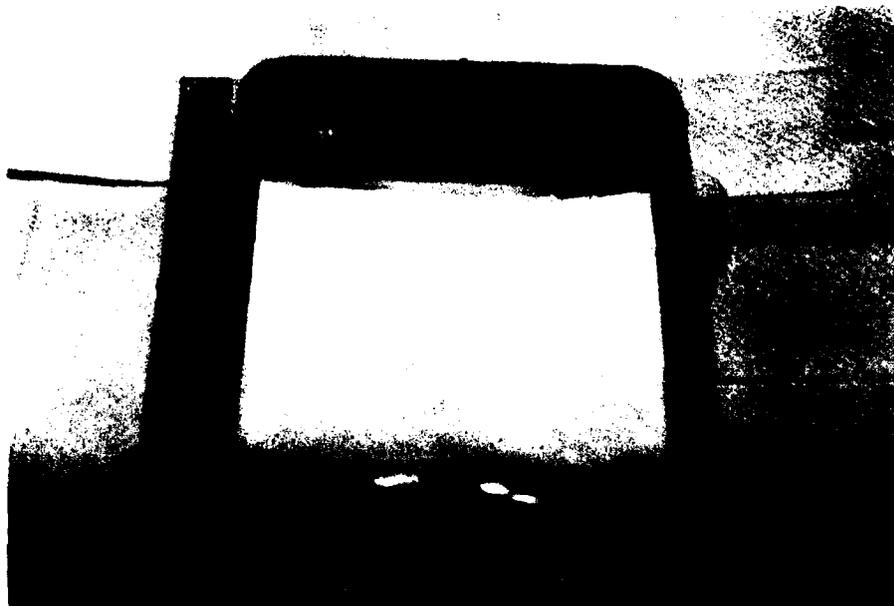
Fig. 43.   Photograph of the cell without the cover.
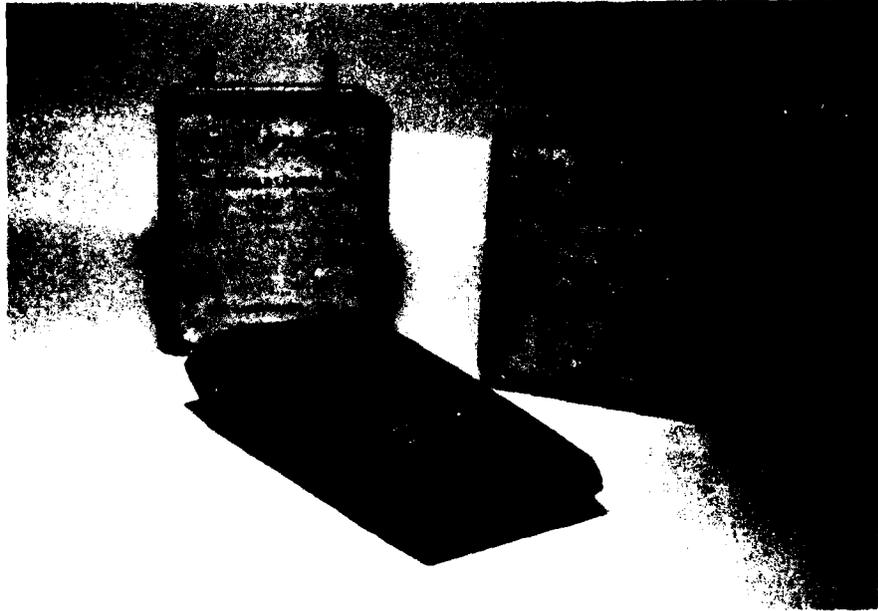
Fig. 44. Photograph of the finished 20 Ah cell.

Table 12

Specifications of Prismatic 20 Ah $Li/Cr_{0.5}V_{0.5}S_2$ Cells

Cell Parameters	Cell 285-75-011	Cell 285-75-013
Cathode[a]	125.5g (70% CVS, 20% C, 10% PTFE)	124.5g (70% CVS, 20% C, 10% PTFE)
Theoretical Cathode Capacity	20.4 Ah	20.2 Ah
Average Cathode Thickness/Electrode	37 mils	37 mils
Electrolyte	1.5M $LiAsF_6$ in THF/2Me-THF (1:1) (144 ml)	1.4M $LiAsF_6$ in 2Me-THF (148 ml)
Separator	Celgard 2400	Celgard 2400
Li Electrode Capacity[b]	219 Ah (57.2g)[c]	219 Ah (57.2 Ah)
Total Volume due to Cathode	123 ml	123 ml
Total Volume due to Anode	105 ml	105 ml
Volume due to Separator	20 ml	20 ml
Total Volume of Cell Package	248 ml	248 ml
Total Weight of Cell Package including Electrolyte	405g	410g
Cell Resistance[d]	~15 mΩ	~20 mΩ
Observed Capacity in First Discharge at 1.0A (0.3 mA/cm^2)	19.7 Ah	18.5 Ah
Observed Capacity in First Charge at 1.0A (0.3 mA/cm^2)	18.6 Ah	17.7 Ah

[a] Fourteen per cell, each is 9.96 x 9.25 cm.

[b] Fifteen per cell, each with same dimensions as cathodes.

[c] Designed for >300 cycles of 95% Li cycling efficiency.

[d] Measured by high frequency galvanostatic pulse.
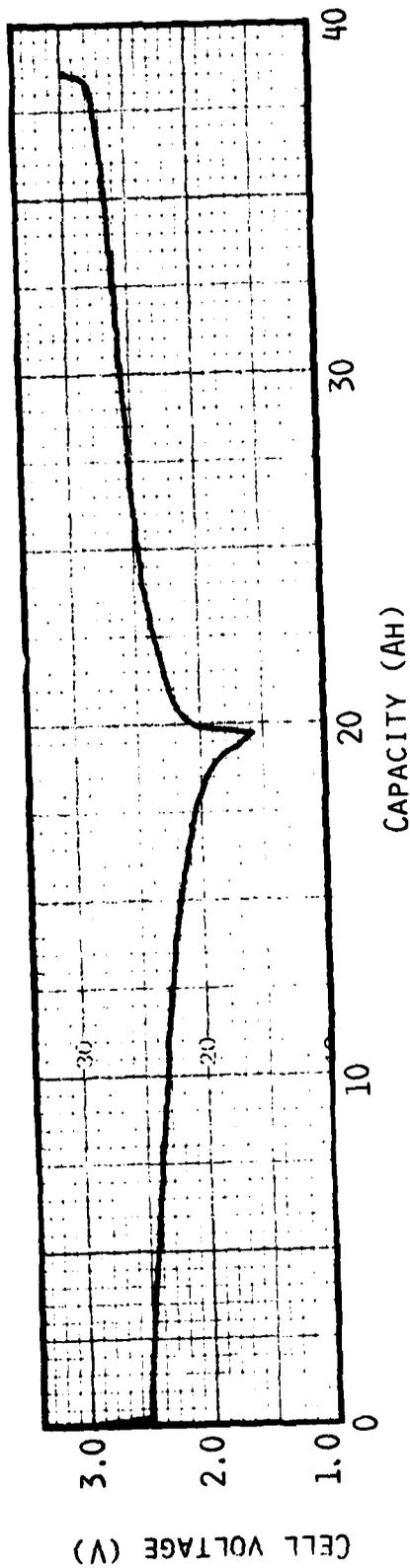
Fig. 45-A. First cycle of Cell 285-75-011
id = ic = 1.0A (0.3 mA·cm^{-2}).
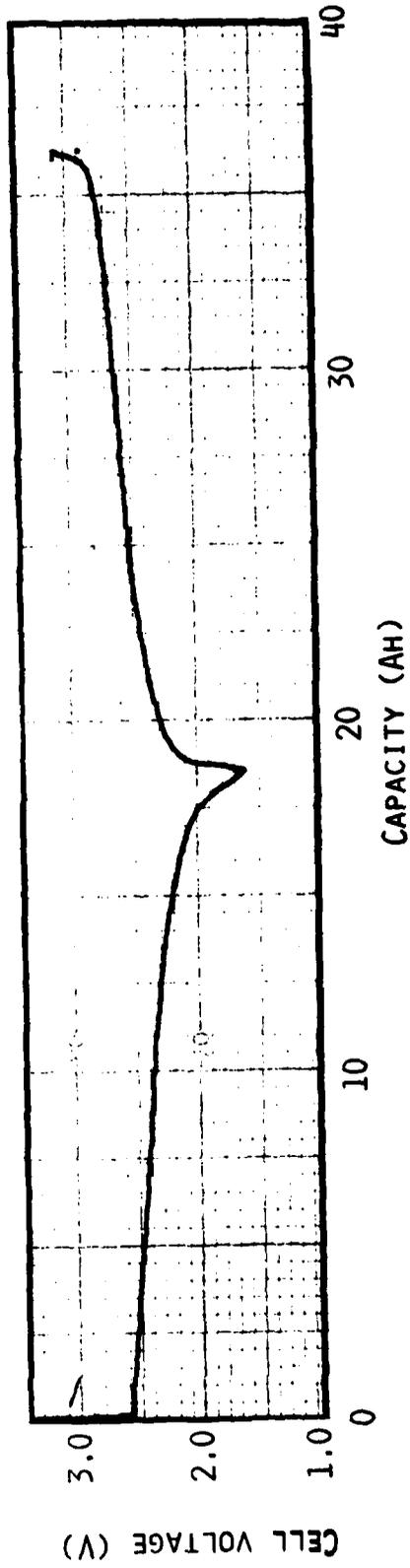
Fig. 45-B. First cycle of Cell 285-75-013
id = ic = 1.0A (0.3 mA·cm^{-2}).

Table 13

Specifications of the 10 Ah Li/Cr$_{0.5}$V$_{0.5}$S$_2$ Cells

Cell Parameters	Cell 285-014	Cell 285-015
Cathode	72g (70% CVS, 20% C, 10% PTFE. Total 10 Electrodes. Theoretical Capacity: 11.7 Ah	73.4g (70% CVS, 20% C, 10% PTFE. Total 10 Electrodes. Theoretical Capacity: 11.9 Ah
Average Cathode Thickness	31 mils	32 mils
Total Cathode Volume	72.5 cm^3	74.9 cm^3
Electrolyte	2Me-THF/LiAsF$_6$(1.4M)	50:50 THF/2Me-THF/LiAsF$_6$(1.5M)
Cell Resistance	~45 mΩ	~33 mΩ

79

Table 14

Test Results of 10 Ah Cell No. 285-014 with 2Me-THF/LiAsF$_6$(1.4M)

	Cycle No.	Discharge			Charge	
		Current (A)	Capacity (Ah)	Mid-Discharge Voltage	Current (A)	Capacity (Ah)
25°C	1	1.0	10.88	2.35	1.0	10.32
0°C	2	1.0	4.08	2.00	1.0	2.80
	3	0.5	8.16	2.14	0.5	9.20
-20°C	4	1.0	8.48	2.34	1.0	10.04
	5	1.0	9.92	2.35	1.0	9.96

Table 15

Test Results of 10 Ah Cell No. 285-015 with 50:50 THF/2Me-LiAsF$_6$(1.5M)

|		Discharge			Charge	
	Cycle No.	Current (A)	Capacity (Ah)	Mid-Discharge Voltage	Current (A)	Capacity (Ah)
25°C	1	1.0	10.4	2.40	1.0	10.64
0°C	2	1.0	10.0	2.21	1.0	9.44
	3	0.5	9.88	2.37	0.5	10.16
-20°C	4	0.5	8.80	2.09	0.5	8.32
	5	1.0	7.88	2.00	1.0	7.60
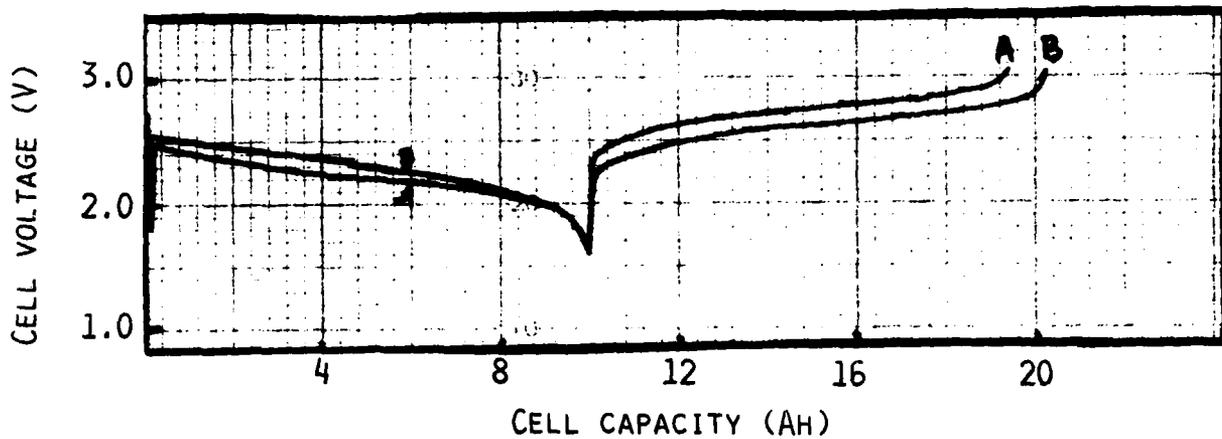
Fig. 46. Cycle curves for Cell 285-015 at 0°C containing 1.5M LiAsF$_6$ in THF/2Me-THF.

Cycle A: id = ic = 1.0A; Cycle B: id = ic = 0.5A
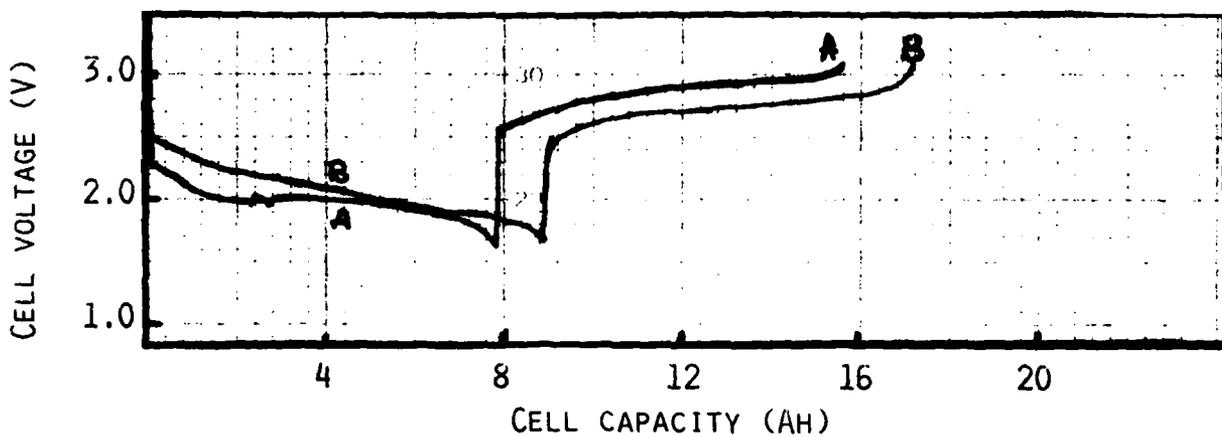

Fig. 47. Cycle curves for Cell 285-015 at -20°C.

Cycle A: id = ic = 1.0A;
Cycle B: id = ic = 0.5A.

ell No. 285-015 with 50:50 THF/2Me-THF/LiAsF$_6$(1.5M) exhibited excellent discharge behavior at all the three temperatures of 25, 0 and -20°C. Even at -20°C, the cell yielded a capacity of 7.88 Ah at the 1A rate which is 66% of the theoretical. Cell No. 285-014 with 2Me-THF/LiAsF$_6$(1.4M) yielded a capacity of only 4.08 Ah at 0°C at the 1A rate.

Both of the cells exhibited excellent utilizations in the long-term cycling following the low temperature tests. The data are given in Figures 48 and 49. Typical cycles are in Figures 50 and 51. As maintained, the cycling was performed with a total current of 1A. Although this is roughly equivalent to a C/10 rate, the current density is only 0.54 mA/cm^2. The electrodes in these cells have an average thickness of 30-32 mils as opposed to 45-50 mils in many of the laboratory test cells. It appears that with thinner electrodes and maintaining a low current density, high utilizations can be obtained in $Cr_{0.5}V_{0.5}S_2$ cells over a large number of cycles. In Cell No. 285-014 with 2Me-THF/LiAsF$_6$(1.4M), the capacity in the 100th cycle is 8.16 Ah which is 70% of the capacity in the first discharge. Cycling of this cell is continuing. Cell No. 285-015 with 50:50 2Me-THF/THF/LiAsF$_6$(1.5M) showed signs of failure by the 60th cycle and more or less completely failed by the 70th cycle. Failure of this cell has occurred due to the limited cycling ability of the Li electrode in the blended solution.

From the cycling data of these two cells it has been possible to demonstrate the excellent performance of $Cr_{0.5}V_{0.5}S_2$ in large capacity cells, as well as to compare the capabilities of the two major electrolytes investigated in this program.
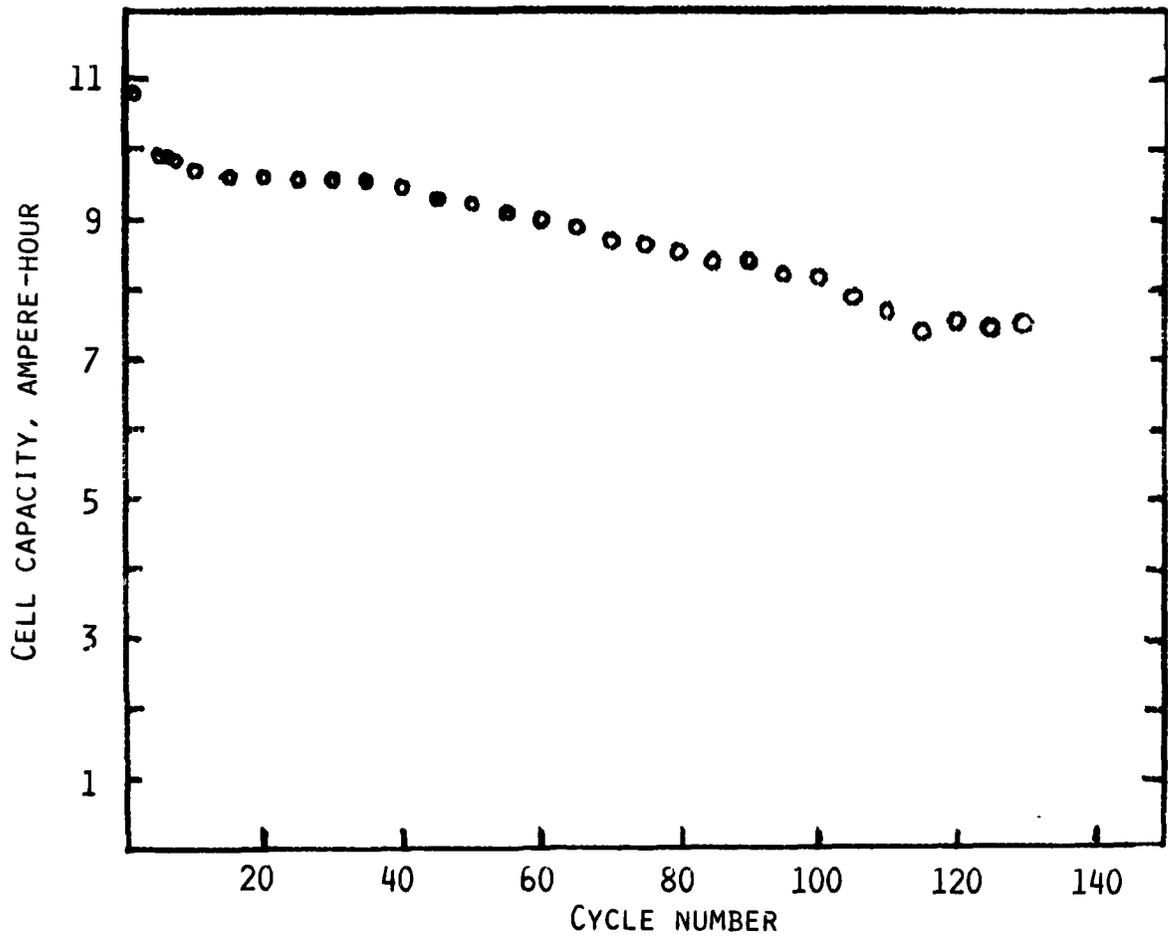
Fig. 48. Cell capacity versus cycle number in prismatic Cell No. 285-014.
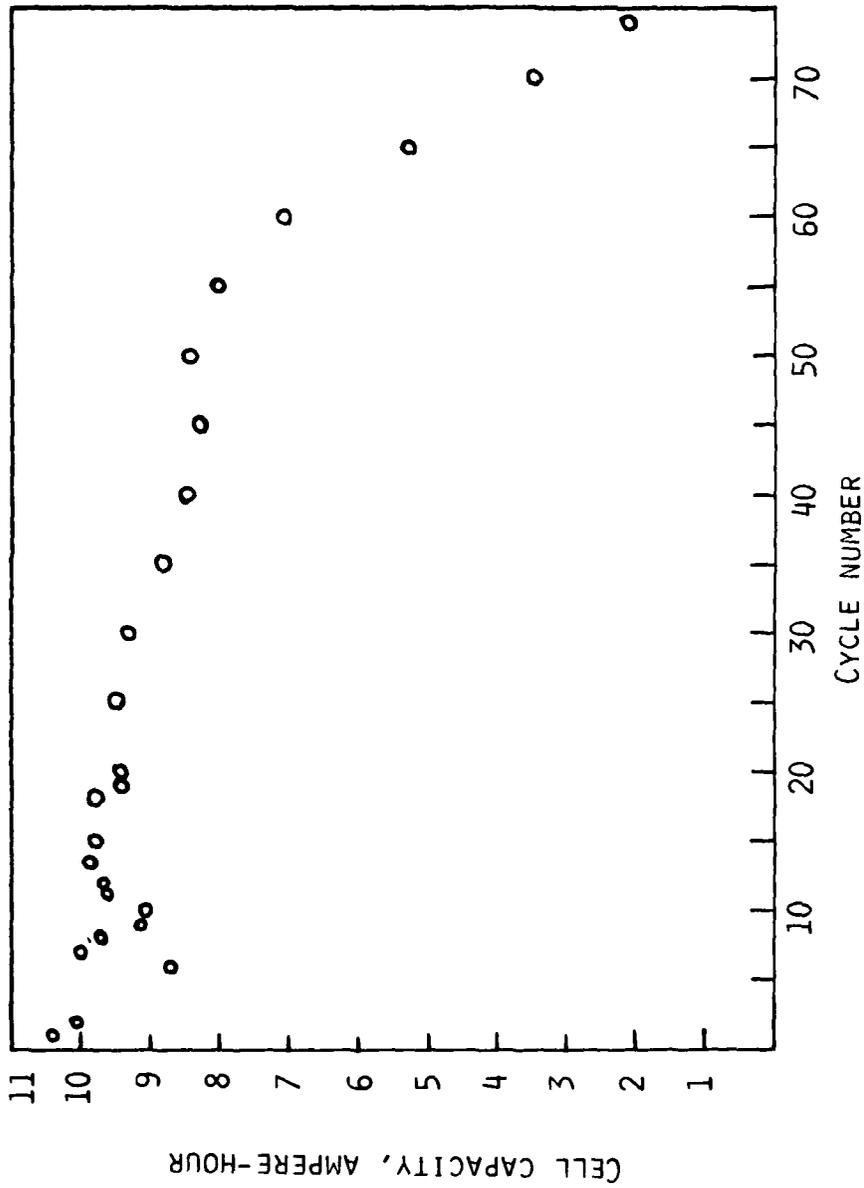
Fig. 49. Cell capacity versus cycle number in prismatic Cell No. 285-015.

85
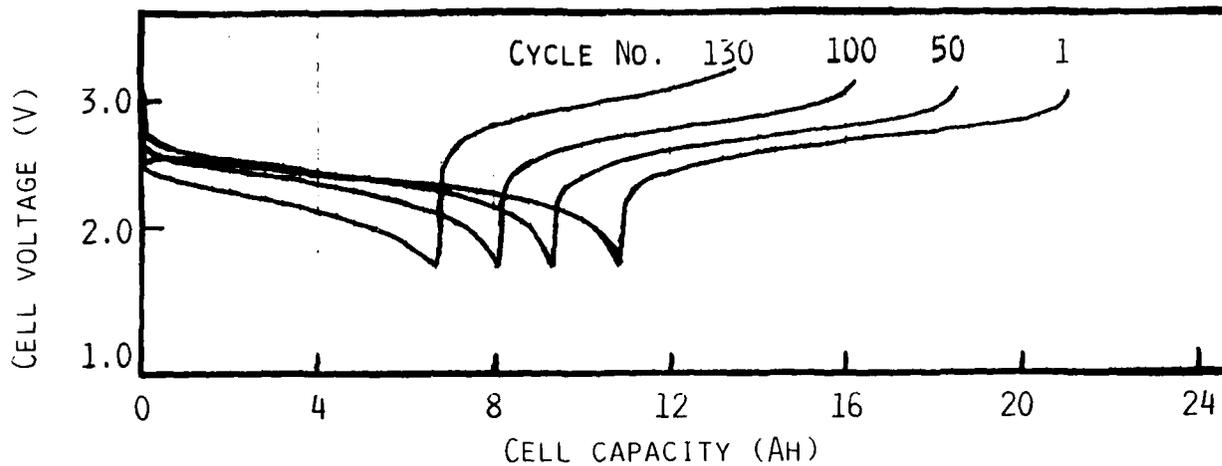
Fig. 50. Typical discharge-charge curves for Cell 285-014 with 2Me-THF/ LiAsF$_6$(1.4M). Current: id = ic = 1.0A; voltage limits; 1.6- 3.1.
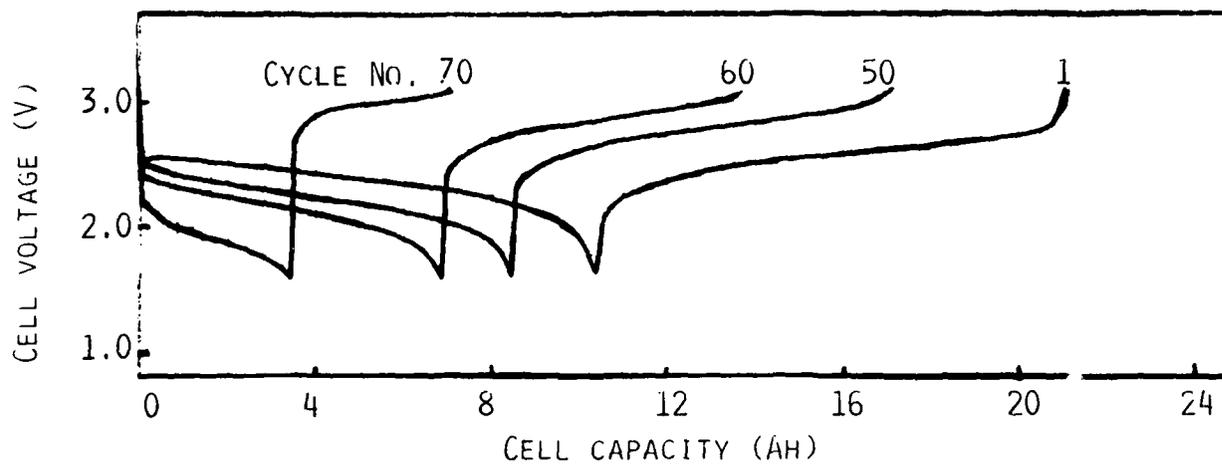

Fig. 51. Typical discharge-charge curves for Cell 285-015 with 50:50 2Me-THF/THF/LiAsF$_6$(1.5M). Current; id = ic = 1.0A; voltage limits: 1.6-3.1.

5.0 CONCLUSIONS

$Cr_{0.5}V_{0.5}S_2$ has been characterized as a useful cathode material for rechargeable Li cells. It yields a discharge capacity equivalent to nearly $1e^-/Cr_{0.5}V_{0.5}S_2$ in early cycles at low rates. The capacity which could be realized in long-term cycling was found to be $0.7-0.8e^-/Cr_{0.5}V_{0.5}S_2$. Laboratory cells exceeded 200 deep discharge cycles. Although $Cr_{0.5}V_{0.5}S_2$ and its Li intercalates have been characterized as good electronic conductors, 15-20 weight-percent carbon in the electrode matrix was found to be necessary for optimum rate and rechargeability of $Li/Cr_{0.5}V_{0.5}S_2$ cells. Because of this much amount of carbon in the cathode, the volumetric energy density achieved in cells has been significantly lower than what was anticipated at the outset of the program. It now appears that $Cr_{0.5}V_{0.5}S_2$ may not offer any particular advantage over TiS_2. However, $Cr_{0.5}V_{0.5}S_2$ provides higher cell voltages. The mid-discharge voltage of $Li/Cr_{0.5}V_{0.5}S_2$ cells is 2.3V; while that of Li/TiS_2 cells is 2.1V.

A major objective of the program has been development of a technology base for the construction of large flat-plate rechargeable Li cells. This has been accomplished. Cells with theoretical capacities of 10 and 20 Ah have been constructed and tested.

Preliminary work carried out on this program has shown that the low temperature performance of $2Me-THF/LiAsF_6(1.4M)$ could be improved by blending this electrolyte with ethers such as THF. A particularly useful electrolyte appears to be $THF(50 \text{ v/o}):2Me-THF(50 \text{ v/o})/LiAsF_6(1.5M)$. However, much more work remains to be done in order to realize the practical potential of this new area of study.

6.0 REFERENCES

1. K. M. Abraham and S. B. Brummer, in "Lithium Batteries", J. P. Gabano, ed., Academic Press (in print).

2. V. R. Koch, J. Power Sources 6, 357 (1981).

3. K. M. Abraham, J. Power Sources 7, 1 (1981/82).

4. J. L. Goldman, R. M. Mank, J. H. Young and V. R. Koch, J. Electrochem. Soc. 127, 1461 (1980).

5. K. M. Abraham, J. L. Goldman and M. D. Dempsey, J. Electrochem. Soc. 128, 2493 (1981).

6. K. M. Abraham, J. L. Goldman and D. L. Natwig, J. Electrochem. Soc., submitted for publication.

7. G. L. Holleck, K. M. Abraham and S. B. Brummer, in Power Sources for Biomedical Implantable Applications and Ambient Temperature Lithium Batteries, The Electrochemical Society Softbound Proceedings Series, B. B. Owens and N. Margalit, eds. (1980).

8. G. L. Holleck, K. M. Abraham, P. B. Harris, J. L. Goldman, J. Avery, M. Rupich and S. B. Brummer, Proceedings of the 30th Power Sources Symposium, Atlantic City, NJ (1982).

9. R. A. Rizzo, in Lithium Batteries, The Electrochemical Society Softbound Proceedings Series, H. V. Venkatasetty, ed. (1981).

10. M. S. Whittingham and A. J. Jacobson, J. Electrochem. Soc., 128, 485 (1981).

DISTRIBUTION LIST

Defense Technical Information Center (12)
Attn: DTIC-TCA
Cameron Station (Building 5)
Alexandria, VA 22314

Commander
Naval Surface Weapons Center (1)
White Oak Laboratory
Attn: Library, Code WX-21
Silver Spring, MD 20910

Commandant, Marine Corps (1)
Headquarter, US Marine Corps
Attn: Code LMC, INTS (In Turn)
Washington, DC 20380

Rome Air Development Center (1)
Attn: Documents Library (TSLD)
Griffiss AFB, NY 13441

AFGL/SULL (1)
S-29
Hanscom Air Force Base, MA 01731

Headquarter (1)
(DAMA-ARZ-D/Dr. F. D. Verderame)
Washington, DC 20310

Commander (1)
Harry Diamond Laboratories
Attn: Library
2800 Powder Mill Road
Adelphi, MD 20783

Director (1)
US Material System Anal. Actv
Attn: DRXSY-T
Aberdeen Proving Ground, MD 21005

Commander
USA Signals Warfare Laboratory (1)
Attn: DELSW-OS
Vint Hill Farms Station
Warrenton, VA 22186

Commander (1)
USA Mobility Equipment Research
and Development Command
Attn: DRDME-R
Fort Belvoir, VA 22060

Commander (1)
Harry Diamond Laboratories
Attn: DELHD-CO, TD (In Turn)
2800 Powder Mill Road
Adelphi, MD 20783

Commander (1)
US Army Electronics R&D Command
Fort Monmouth, NJ 07703

Attn: DELET-DD

Commander (1)
US Army Electronics R&D Command
Fort Monmouth, NJ 07703

Attn: DELET-DT

Commander (1)
US Army Electronics R&D Command
Fort Monmouth, NJ 07703

Attn: DELSD-L (Library)

Commander (2)
US Army Electronics R&D Command
Fort Monmouth, NJ 07703

Attn: DELSD-L-S (Stinfo)

Commander (10)
US Army Electronics R&D Command
Fort Monmouth, NJ 07703

Attn: DELET-PR (H. Hunger)

NASA Scientific & Tech Information (1)
Facility
Baltimore/Washington Int'l Airport
P. O. Box 8757, MD 21240

(1)

Honeywell, Inc. (1)
104 Rock Road
Horsham, PA 19044

Attn: Dr. D. Chuah

Eagle Picher Industries, Inc. (1)
Electronics Division
P. O. Box 47
Joplin, Missouri 64801

Attn: Mr. Robert L. Higgins

Yardney Electric Company (1)
82 Mechanic Street
Pawcatuck, CT 06379

Attn: Technical Library

Duracell International, Inc. (1)
Northwest Industrial Park
Burlington, MA 08103

Attn: Dr. A. N. Dey

Exxon Research & Engineering Company (1)
Corporate Research Laboratory
Linden, NJ 07036

Attn: Dr. R. Hamlen

Argonne National Laboratories (1)
9700 South Cass Avenue
Argonne, IL 60439

Attn: Dr. E. C. Gay

GTE Sylvania/SSD (1)
520 Winter Street
Waltham, MA 02154

Attn: Dr. Robert McDonald

General Motors Corporation (1)
Research Laboratories
General Motors Technical Center
12 Mile and Mounds Road
Warren, MI 48090

Attn: Dr. J. L. Hartman

Union Carbide Corporation (1)
Parma Research Center
P. O. Box 6116
Cleveland, OH 44101

Duracell, USA (1)
South Broadway
Tarrytown, NY 10591

Attn: J. Dalfonso

North American Rockwell Corporation (1)
Atomics International Division
P. O. Box 309
Canoga Park, CA 91304

Attn: Dr. L. Heredy

General Electric R&D Center (1)
P. O. Box 8
Schenectady, NY 12301

Attn: Dr. Stefan Mitoff

University of California (1)
Department of Science & Research
Santa Barbara, CA 93100

Attn: Dr. J. Kennedy

Gulton Industries, Inc. (1)
Metuchen, NJ 08840

Attn: Mr. S. Charlip

INCO Research & Development Center (1)
Sterling Forest
Suffern, NY 10901

Attn: Nehemia Margalit

Director (1)
Propulsion and Power Division
Mail Code EP5
NASA-Johnson Space Center
Houston, Texas 77058

Attn: Mr. B. J. Bragg

GTE Laboratories, Inc.   (1)
40 Sylvan Road
Waltham, MA 02254

Attn: Dr. Carl Schlaikjer

Electrochimica   (1)
2485 Charleston Road
Mountain View, CA 94040

Attn: Dr. Eisenberg

Energy Storage & Conversion Dept.   (1)
TRW Systems
One Space Park
Redondo Beach, CA 90278

Attn: Dr. H. P. Silverman

Power Conversion, Inc.   (1)
495 Boulevard
Elmwood Park, NJ 07407

Attn: Stuart Chodosh

G207   (1)
SRI
Menlo Park, CA 94025
Attn: Dr. Leonard Nanis

Bell Laboratories   (1)
600 Mountain Avenue
Murray Hill, NJ 07974

Attn: Dr. J. J. Auborn
       Room 1A-317

Jet Propulsion Laboratory   (1)
4800 Oak Grove Drive
Pasadena, CA 91103

Attn: Mr. Harvey Frank
       Mail Stop 198-220

Naval Surface Weapons Center   (1)
White Oak Laboratory
Code R-33 (M/S A026)
Silver Spring, MD 20910

Attn: Dr. D. Ernst

Energy Conversion Branch   (1)
  Code 3642
Naval Underwater Systems Center
Newport Laboratory
Newport, RI 02840

Attn: Mr. J. R. Modem

NASA Lewis Research Center   (1)
Mail Stop 6-1
21000 Brookpark Road
Cleveland, OH 44135

Attn: Dr. Stuart Fordyce

Altus Corporation   (1)
440 Page Mill Road
Palo Alto, CA 94306

Attn: Douglas Glader

Mail Stop 488   (1)
NASA Langley Research Center
Hampton, VA 23665

Attn: J. Bene

Boeing Aerospace Company   (1)
Mail Stop 8C-62
P. O. Box 3999
Seattle, WA 98124

Attn: Mr. Sidney Gross

Honeywell Technology Center   (1)
10701 Lyndale Avenue, South
Bloomington, MN 55420

Attn: Dr. H. V. Venkatasetty

Jet Propulsion Laboratory   (1)
Mail Stop 198-200
4800 Oak Grove Drive
Pasadena, CA 91103

Attn: Mr. Aiji Uchiyama

Naval Surface Weapons Center   (1)
White Oak Laboratory
Code R-33
Silver Spring, MD 20910

Attn: Dr. Frank Bis

D
FI
'O'